DELFT UNIVERSITY OF TECHNOLOGY

MASTER OF SCIENCE

Excess pore pressures near a slurry tunnel boring machine: modelling and measurements

Author:
S.P. Steeneken

Supervisors:
Prof. dr. M.A. Hicks
Prof. dr. ir. A. Bezuijen
dr. ir. W. Broere
dr. ir. K.J. Bakker
ir. drs. R.E.P. de Nijs
ir. J.A.T. Ruigrok

January 8, 2016

"Tunnelling is not boring."

Koen Rijnen

Acknowledgments

The list of people to acknowledge is quite long, hopefully I have not forgotten anybody. First of all, I would like to thank ir. drs. Richard de Nijs for the opportunity to conduct my graduation thesis at Witteveen+Bos. Richard, together with ir. Jan Ruigrok, you have been of great value in discussions on-topic and fun off-topic during the coffee breaks. Thank you both for the amazing period at the office in Amsterdam. As my daily supervisor from the University of Technology Delft, dr. ir. Wout Broere, you are a real specialist on this topic and you were of great help in finishing this thesis. Also a specialist on this topic is prof. dr. ir. Adam Bezuijen from Ghent University, Belgium. It was of great value to have you in my graduation committee. The same holds for dr. ir. Klaas Jan Bakker, thank you for putting things in perspective during our sessions. Last but not least, the chairman of the committee prof. dr. Michael Hicks. Despite of the incredibly busy schedule as head of the section you have found time to attend the meetings and give valuable input. It applies to all the members of the committee that I highly appreciate the amount of time that was available for discussions and meetings during my graduation period.

During the preparation of my laboratory work Dianne den Hamer from Deltares has been of great assistance. Also, Han de Visser and Arno Mulder have been of great help during the actual laboratory work and I have learned a lot from their years of experience. The German company IMERYS provided the bentonite for the experiments for free, thank you very much mister Jean-Marie Nachtigal. I have made some great friends within the Master Geo-Engineering, thank you all for a pleasant two years and for your support. Special thanks to Alex for preparing me for committee meetings and the critical questions on my work.

Dear Titus, Janine and Lisa, thank you for all your support during my years of study in Delft, I am very fortunate to have you as a family. The last words are for Ilse, you are simply the best.

Summary

In this thesis an investigation is performed into the rise of excess pore pressures in front of a slurry tunnel boring machine (TBM) during boring. Accurate prediction of excess pore pressures is particularly important when boring close to foundation piles or when boring with a small overburden. The existence of this phenomenon has been known for approximately two decades and several groundwater flow models have been derived since. Laboratory experiments are conducted to investigate the applicability of laboratory results as input for the existing groundwater flow models. Furthermore, a new relation to calculate excess pore pressures at the tunnel face is derived. The discharge from the tunnel face during boring is investigated as well. Calculations considering the cutter wheel configuration are compared with calculations considering a mean slurry infiltration time and show similar results. This research originated from the North/South (N/S) metro line in Amsterdam, at which excess pore pressures presented a real challenge in crossing a historical bridge. Data from the Green Heart Tunnel (GHT) is also used in this research to serve as validation.

Tunnel face stability calculations made with a wedge shaped failure mechanism are widely used in engineering practices [4, 13, 25, 39]. Excess pore pressures result in a less effective face support on the triangle soil column. To keep the tunnel face stable under these conditions, the minimal allowable face pressure should be increased significantly [11, 18]. Slurry infiltration is a transient process [4, 18] and the infiltration-excavation cycle during boring is the driving force behind the excess pore pressures in front of a slurry TBM.

The slurry infiltration formulas from Broere [18], Bezuijen [10], Huisman [26] and Talmon [36] are compared. At least one parameter in each relation is determined in a column infiltration test. A sensitivity analysis with the formulas of Broere [18] is conducted, resulting in a wide range of possible slurry infiltration depths (45 - 625 mm). In order to provide a deeper understanding of the slurry infiltration processes of the N/S line project, laboratory experiments have been conducted. The laboratory results provided vital information for this research.

Sand originating from the project location (Third Sand Layer, Amsterdam) was not available and therefore manually composed sand is used in the laboratory experiments. A similar column infiltration apparatus to that in existing literature is used. Thirteen column infiltration tests have been performed and the slurry infiltration depth in time shows good resemblance with existing literature. A clear transition between slurry infiltration (mud spurt) and plastering (external filter cake formation) is distinguished. The maximum slurry infiltration depth, x_{max}, is approximately 50 mm. The slurry infiltration formulas of Broere [18] and Huisman [26] can be accurately applied to the average laboratory results.

In order to accurately calculate the discharge from the tunnel face into the soil, an accurate value of a (time to reach half x_{max}) needs to be determined. The value of a determined with laboratory experiments is 11 s. This value is compared with field data. The drop in piezometric head at stop boring is used to determine the value of a for the TBM. In boring the Third Sand Layer a has a value of 136 s. Therefore, the value of a determined in the laboratory cannot be used directly in the groundwater flow models. The reason for this is the difference in flow in the infiltration column compared to the TBM. A relation is derived to determine the value of a for the TBM combining laboratory results and a relation provided by Bezuijen [13]. This relation incorporates 1-dimensional flow resistance and a contribution of the yield stress of the slurry, and depends on laboratory parameters, TBM specific parameters and field parameters. An accurate fit with the determined value of a in the field is seen. Although the value of a from

laboratory experiments cannot be used directly in the groundwater flow models, laboratory experiments are valuable in determining the value of a specific for the TBM.

In the case of the N/S line, mud spurt is present in front of the tunnel face during boring. The measured pore pressure is lower than the excess face pressure, indicating that mud spurt causes the pressure drop. The measured pore pressure is called the piezometric head at the far side of the mud spurt, indicated with φ_{ms}. The cutter wheel configuration and the mean infiltration time are used in determining the value of φ_{ms} using the 1-dimensional flow model of Bezuijen [10] and both show similar results as measured in the field.

A relation is derived to determine the excess pore pressure at the tunnel face, incorporating the TBM specifications and the parameters of the soil in front of the tunnel. For more or less homogeneous soil conditions the relation provides accurate results. To ensure an excess pore pressure lower than the excess face pressure during boring, the pore water velocity should be greater than the velocity of the TBM. This relation should be validated in future projects.

The transient flow model can be used to predict excess pore pressures in front of a TBM, which is in accordance with existing literature [18]. At a distance of approximately 5 to 10 meters from the tunnel face a fine prediction is seen. Close to the tunnel face the excess pore pressure is underestimated. The calculated discharge specific for the cutter wheel is compared to the discharge calculated with the mean infiltration time and shows similar results. The model is especially sensitive to the permeability and the specific storage of the aquifer.

Laboratory experiments in combination with TBM data and measured pore pressures provided an excellent and indispensable source of information for this research. For future research it is therefore highly recommended that pore pressure sensors are installed at future projects and that laboratory experiments are conducted.

Several remarks regarding this research should be made at this stage. The laboratory experiments could not be conducted at the excess pressure normative for the N/S line due to limitations of the laboratory equipment. Extrapolation with laboratory data from Krause [30] is performed to provide a value of the maximum slurry infiltration depth x_{max}. It is recommended that the excess pressure used in the laboratory experiments should be equal to the excess face pressure used during boring.. The relation derived to determine the excess pore pressures at the tunnel face is validated with the N/S line and the GHT. It is recommended that this relation should be validated with future projects. The same statement applies to the determination of a specific for the TBM, calculated with laboratory results and the relation incorporating 1-dimensional flow resistance and a contribution of the yield stress of the slurry. In this research the calculated discharges that consider the cutter wheel configuration and the mean infiltration time are similar. This also requires further validation with future projects.

Contents

List of Figures

List of Tables

List of Abbreviations

DUT	**D**eflt **U**niversity of **T**echnology
GHT	**G**reen **H**eart **T**unnel
NI	**N**umerical **I**ntegration
N/S	**N**orth/**S**outh metro line
TBM	**T**unnel **B**oring **M**achine
W+B	**W**itteveen+**B**os

List of Symbols

a	timespan to reach half $x_{max;Broere}$ or x_{max}	s
a_{BTL}	timespan to reach half $x_{max;BTL}$	s
A_{cw}	surface area cutter wheel	m^2
A_i	partial surface area cutter wheel	m^2
A_{IC}	surface area infiltration column	mm^2
$\tilde{c}$	hydraulic resistance aquitard, $d_{aquitard}/k_{aquitard}$	s
D	diameter of the cutter wheel	m
D_h	characteristic hydraulic pore diameter, BTL-report 32	m
d_{10}	characteristic grain diameter	m
$d_{aquitard}$	layer thickness aquitard	m
g	acceleration of gravity	m/s^2
H	thickness aquifer	m
h_{pw}	height of displaced pore water in the infiltration column	cm
h_{sample}	height of sand sample in the infiltration column	cm
Δh_{sl}	difference in slurry height before and after the test	cm
i	hydraulic gradient	$-$
I_E	maximum infiltration distance	cm
k	permeability	$m\,s^{-1}$
k_s	permeability of the sand in front of the tunnel	$m\,s^{-1}$
k_{ws}	permeability of the consolidated slurry	$m\,s^{-1}$
k_{start}	permeability at start of column infiltration test	$m\,s^{-1}$
k_{after}	permeability after slurry infiltration in column infiltration test	$m\,s^{-1}$
l_{cut}	cutting depth per one rotation of the cutter wheel	m
$l_{i;cut}$	cutting depth for t_i	m
L	total height of sample in the infiltration column, = $L_s + L_v$	m
L_s	height of sand sample in the infiltration column	m
L_v	height of valve to the sample in the infiltration column	m
m_v	compressibility modulus	Pa^{-1}
n	porosity	$-$
p_0	initial pore pressure	kPa
Δp	excess pressure	Pa
Δp_{air}	excess air pressure used in column infiltration test	Pa
q	specific discharge	$m\,s^{-1}$
q_{av}	average specific discharge over entire tunnel face	$m\,s^{-1}$
$q_{f;0}$	initial specific discharge, BTL-report 32	$m\,s^{-1}$
q_{cw}	specific discharge for the cutter wheel	$m\,s^{-1}$
Q	discharge per unit width of the aquifer	m^2/s
Q_{cw}	discharge from the cutter wheel	m^3/s
R	radius cutter wheel	m
s	face pressure	kPa
Δs	excess face pressure, $s - p_0$	kPa
S_s	specific storage aquifer	m^{-1}
t	time	s
t_{boring}	time required to bore one ring of distance w_{ring}	s
t_{cut}	cutting time, equals t_r	s
t_r	time required for one full rotation of the cutter wheel	s
t_F	average slurry infiltration time	s
t_i	maximum infiltration time per rotation cutter wheel	s

$t_{i;period}$	slurry infiltration period	s
v_{av}	average slurry infiltration velocity over entire tunnel face	$\mathrm{m\,s^{-1}}$
v_{slurry}	slurry infiltration velocity	$\mathrm{m\,s^{-1}}$
$v_{p;Darcy}$	pore water velocity (Darcy's law)	$\mathrm{m\,s^{-1}}$
V_{pw}	volume of displaced volume in column infiltration apparatus	$\mathrm{mm^3}$
v_{TBM}	TBM velocity	$\mathrm{m\,s^{-1}}$
w_{ring}	ring width	m
x	distance from tunnel face / slurry infiltration distance	m
$x(t)$	slurry infiltration depth in time	m
$x_{Broere}(t)$	slurry infiltration depth in time, Broere	m
$x_{BTL}(t)$	slurry infiltration depth in time, BTL-report 32	m
x_{max}	max slurry infiltration depth	m
$x_{max;Broere}$	max slurry infiltration depth from Broere	m
$x_{max;BTL}$	max slurry infiltration depth from BTL-report 32	m
x_{ms}	mud spurt depth	m
$x_{ms;max}$	max mud spurt depth	m
x_{sensor}	distance infiltration front to pore pressure sensor (Laboratory)	m
YP	yield point of slurry	Pa
α	fitting parameter in formula of $x_{max;Broere}$	$-$
α_{BTL}	constant depending on geometry of pore channels, BTL-report 32	$-$
α^*	factor describing which part of $\varphi_{ex;face}$ is φ_0	$-$
β	compressibility of water, 4.6E-10	$\mathrm{Pa^{-1}}$
γ_w	specific weight of water	$\mathrm{kN/m^3}$
Γ	ratio $\Delta p/x_{max}$ from column infiltration test	$-$
θ	angle of the column infiltration apparatus from the horizontal	$^\circ$
σ	total stress	kPa
σ'	effective stress	kPa
σ'_h	horizontal effective stress	kPa
σ'_v	vertical effective stress	kPa
τ	yield strength	Pa
τ_F	dynamic shear strength slurry	Pa
τ_y	static yield strength slurry	Pa
λ	leakage length	m
ν	dynamic viscosity of slurry	Pa s
ρ_s	density of slurry	$\mathrm{kg/m^3}$
ρ_w	density of water	$\mathrm{kg/m^3}$
φ	piezometric head in aquifer	m
$\Delta\varphi$	excess piezometric head	m
φ_0	excess piezometric head at the tunnel face	m
φ_∞	piezometric head in aquifer at $x \to \infty$	m
$\varphi_{ex;face}$	excess face pressure, calculated in piezometric head	m
φ_{ms}	piezometric head at far side of the mud spurt	m
ψ	one-dimensional flow resistance aquifer	$\mathrm{s^{-1}}$

Chapter 1

Introduction

In April 2003 the construction of the North/South (N/S) metro line started. Within the trajectory different types of tunnels are constructed, but this thesis is focused on the bored part. It consists of two tunnels with a total length of 3.8 kilometers. The tunnel boring machine (TBM) used is of a slurry type due to the non-cohesive soils present in the subsurface of Amsterdam. The trajectory of the N/S line and the area of interest are visualized in figure 1.1.

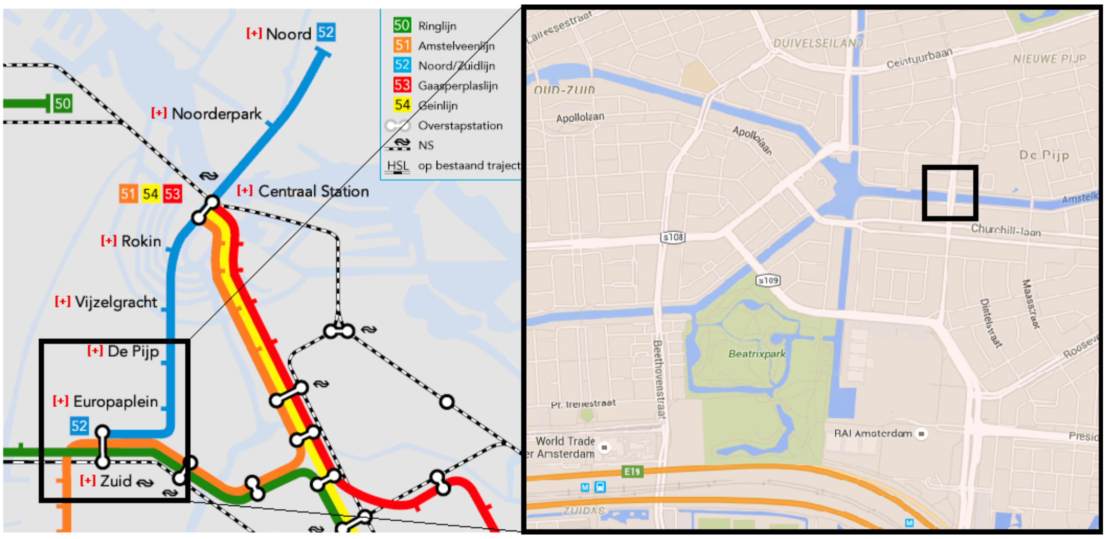

FIGURE 1.1: North/South line trajectory in blue (metro 52) and the location of Bridge 404 [2].

1.1 Motivation

To secure the tunnel face stability during boring and to limit surface settlements a certain excess face pressure is used. As a result slurry infiltrates into the pores of the soil, initiating a flow of pore water in the direction of boring. The area in which slurry has infiltrated is called the mud spurt. The excess face pressure is transferred to the soil skeleton via the mud spurt and a larger mud spurt results in a greater transfer of pressure. The pressure that is *not* transferred to the soil skeleton is called the excess pore pressure. As the pore pressure increases, the effective stress of the soil decreases, resulting in lower strength of the soil. If foundations are present in the soil this could lead to settlements, resulting in structural damages.

Due to the vertical alignment of station *Ceintuurbaan* the tunnels have a different depth configuration from station *Europaplein* to *Ceintuurbaar (De Pijp)*. The shallow tunnel passes the foundation of an historical bridge at approximately 1.5 meters, visualized in figure 1.2. It is therefore important to consider the excess pore pressures that occur during boring. The occurrence of this phenomenon has been known for two decades [18], but this effect has not been incorporated into the standards yet [7, 28]. To calculate the excess pore pressure for the shallow tunnel a back-calculation with measured field data from the deep tunnel has been conducted [28, 35]. The pore pressures are recorded with piezometers. A back-calculation is not always possible, however. If one tunnel is considered in the design, measured data at the critical passage is not available. It is therefore interesting to investigate the possibility to predict excess pore pressures prior to construction.

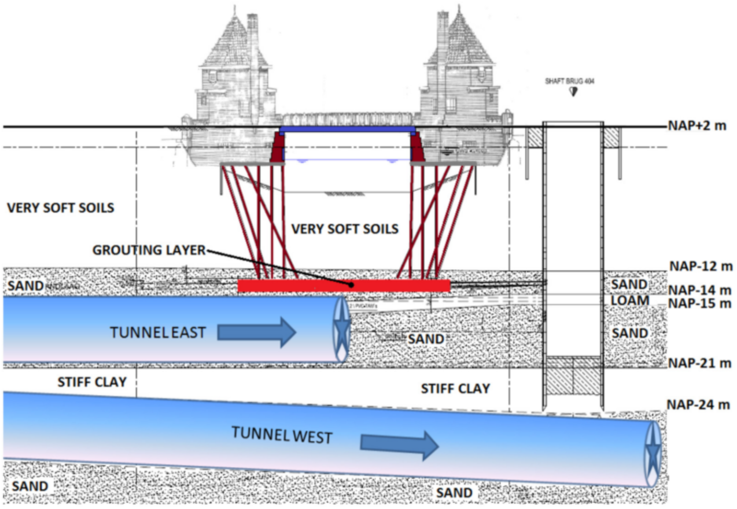

FIGURE 1.2: Depth configuration West and East tunnel at Bridge 404, from [28].

1.2 Research goal

The goal of this thesis is to predict the excess pore pressures during boring with a slurry TBM. The following approach is followed:

- Evaluate existing slurry infiltration formulas and groundwater flow models;
- Conduct a series of laboratory experiments specific for the North/South line and fit slurry infiltration formulas on the results;
- Determine whether the laboratory results are applicable as input for the existing groundwater flow models;
- Derive a new relation to predict the excess pore pressure at the tunnel face;
- Use existing groundwater flow models to predict excess pore pressures taking into account the cutter wheel configuration of the N/S line and compare the results with the current calculation method;
- Use existing field data from the North/South line project and the Green Heart Tunnel to validate both the new relation and the existing groundwater flow models;

1.3 Thesis outline

This thesis starts with a literature review in Chapter 2. The conducted laboratory experiments are presented in Chapter 3. The excess pore pressure calculations with groundwater flow models are discussed in Chapter 4. The report is completed with a discussion in Chapter 5 and conclusions and recommendations in Chapter 6.

Chapter 2

Literature Review

In this section the existing literature is reviewed. First, the working of slurry tunnel boring machine is discussed. After that, the slurry infiltration processes are discussed and this is followed by an elaboration of the slurry infiltration formulas presented in existing literature. Thereafter, a sensitivity analysis regarding the slurry infiltration formulas is conducted. Then, an overview is given of the different groundwater flow models. Next, averaging the infiltration depth over the entire cutter face is elaborated and a possible improvement is outlined. This chapter has a conclusion at the end.

2.1 Working of a slurry tunnel boring machine

A slurry tunnel boring machine (TBM) is widely used in saturated, non cohesive soils [22]. The supporting face uses a bentonite suspension (slurry) which is subjected to pressure to keep the bore front stable. A blow-out occurs when the slurry pressure is too high, and a cave-in (active failure towards the face) occurs when the slurry pressure is too low [14]. A sketch of a slurry TBM is shown in figure 2.1.

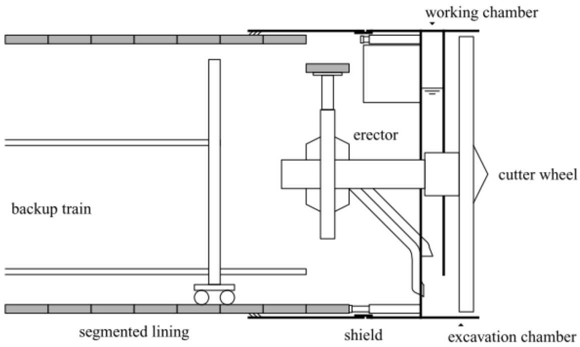

FIGURE 2.1: Sketch of a slurry TBM, from [18].

The most important parts of the slurry TBM regarding this research are the pressurized slurry in the excavation chamber, the cutter wheel, the cutter teeth and the velocity of the TBM. Pressurized slurry is the driving force in slurry infiltration into the sand in front of the TBM [18] and also provides stability of the tunnel face. Besides a stabilizing effect the slurry also serves as conveyance for transportation of the excavated soil [23]. During excavation the density of the slurry increases with depth, since the excavated material is mixed with the slurry and falls to the bottom of the excavation chamber [12, 21]. During boring and installation of a new ring slurry is renewed, resulting in a decrease of density [21]. Renewing of the slurry is necessary, since pumping of the slurry to the separation plant is only possible until a certain density of the slurry. In figure 2.1 the working and excavation chamber, respectively, are shown. The two chamber design of the shield makes the machine very flexible for inspection and repair works. Furthermore, the face pressure can be regulated easily by altering the air pressure at the top of the working chamber [23]. The geometry of the cutter wheel in combination with the configuration of the teeth are part of the excavation mechanism. Slurry infiltration is a transient process [4, 18] and the infiltration-excavation cycle is the driving force behind the creation of excess pore pressures. For more information regarding a slurry TBM, please see [5, 18, 31].

Tunnel face stability calculations with a wedge shaped failure mechanism are widely used in engineering practices [4, 13, 25, 39]. Excess pore pressures in front of the tunnel face due to boring have been measured by half a dozen project in the Netherlands alone [9, 10, 18, 35]. Considering no excess pore pressures during boring due to perfect (instantaneous) plastering of the tunnel face is proven to be incorrect [9, 18, 28, 35]. The influence of the excess pore pressure on the face stability is explained in figure 2.2.

In the figure a three dimensional plot of the failure surface is shown, according to the wedge shaped failure surface theory of Jancsecz [3, 27]. In the cross-sections two situations are presented. In both situations it is clear that the face support onto the soil column is less effective due to excess pore pressures. The first situation states that the area of excess pore pressure falls within the wedge width, indicating that the stability model by Jancsecz [27] is still valid, approximately [13]. In the second situation the excess pore pressure exceeds the width of the wedge, resulting in a decreased net force from the tunnel face on the triangle soil column. This clearly indicates a lower effective support pressure. On the other hand, a vertical gradient over the soil block results in a reduction of the force of this block onto the tunnel face [13]. To keep

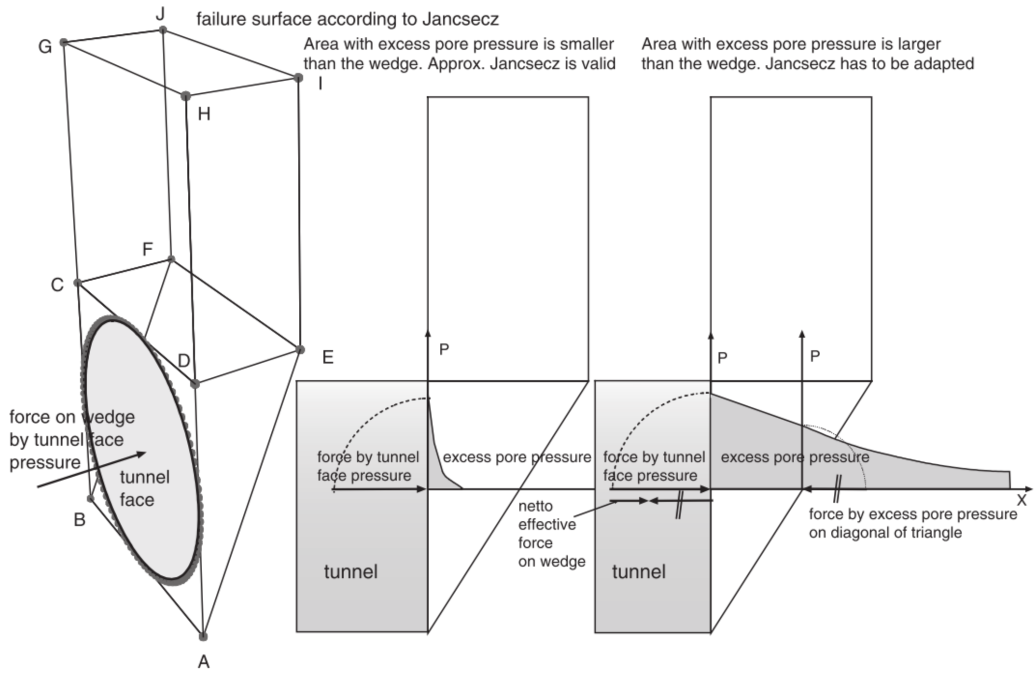

FIGURE 2.2: Influence of excess pore pressure on the stability of the tunnel face, from [13]

the tunnel face stable under these conditions the minimal allowable tunnel face pressure should be increase significantly [11, 18]. During boring of a critical passage this increase of face pressure could lead to settlements of the foundation piles situated above the tunnel or a blow-out of the tunnel face.

2.2 Slurry infiltration processes

Slurry consists of a mixture of bentonite and water. Bentonite is a type of clay that is formed by weathering of volcanic ash and it consists mainly of the clay mineral montmorillonite. A negative charge on the surface of the molecular layers is responsible for the capability of cation exchange (adsorption of Na- or Ca-cations). In the presence of water the cations can hydrate and the distance between the layer packs will widen. This mechanism gives the slurry some interesting properties [23]:

- High viscosity (depending on bentonite concentration);
- Formation of a yield point;
- Ability to stagnate, mainly in sandy soils.

A wide range of bentonite mixtures are available to cope with different geological conditions. It is also possible to use additives in the mixing process to make slurry tunnel boring in high permeable sands possible [23, 24, 29, 33].

It is important to define the pressures that influence the infiltration processes of the slurry, see figure 2.3. A theoretical equilibrium between the tunnel face and the soil skeleton exists when,

$$s = \sigma'_h + p_0, \tag{2.1}$$

in which s is the face pressure, σ'_h is the horizontal effective stress and p_0 is the initial pore water pressure, all in kPa [5, 23]. The excess face pressure Δs is defined in Eq. (2.2) and during boring $\Delta s > \sigma'_h$ [9, 18, 35].

$$\Delta s = s - p_0 \tag{2.2}$$

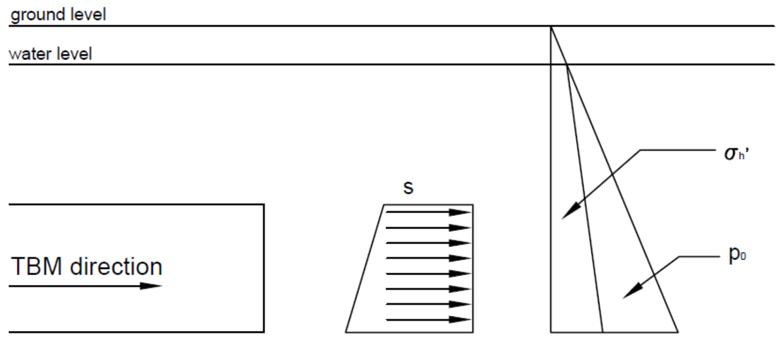

FIGURE 2.3: Definition of different pressures in front of a slurry TBM [5].

Slurry infiltration processes are described by several authors [18, 22, 30, 33, 36]. Krause [30] used an idealized pore channel, shown in figure 2.4 and this theory is adopted by Broere [18]. Pressurized slurry infiltrates in the soil and replaces the present pore water [9]. The slurry experiences increasing shear resistance τ from the sand grains, resulting in a maximum infiltration distance I_E at a given excess pressure Δp. Furthermore, the assumption is made that the hydraulic diameter is equal to the d_{10} of the infiltrated sand [30].

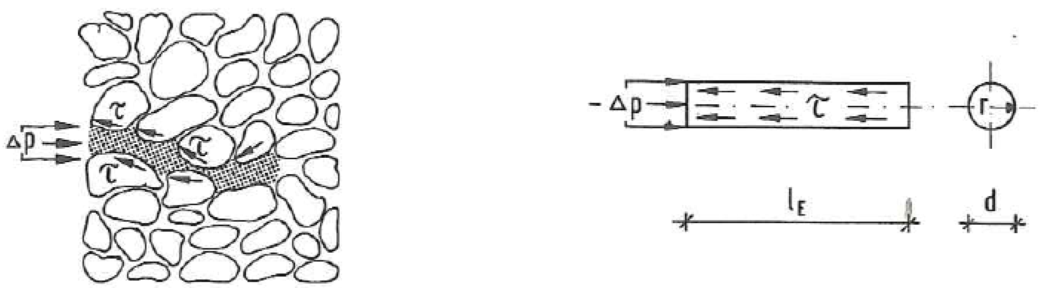

FIGURE 2.4: Slurry infiltration in an idealized pore channel, from [30].

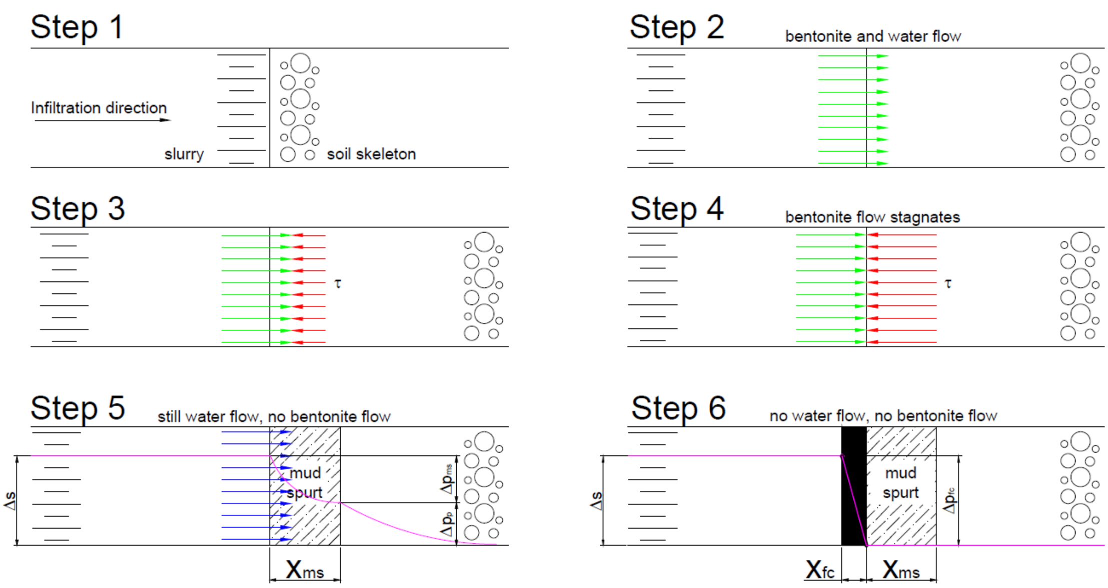

FIGURE 2.5: Slurry infiltration steps and theoretical pressure drop over the mud spurt and the external filter cake.

Figure 2.5 describes the slurry infiltration process in time. Step 1 indicates no infiltration. In step 2, slurry starts to infiltrate into the soil. The slurry encounters increasing resistance from the sand grains with infiltration distance in step 3 [4, 30, 36]. At a certain distance slurry infiltration stagnates, since the wall shear stresses from the sand grains are equal to the excess pressure, indicated in step 4 [36]. In step 5 the maximum mud spurt depth is reached and this area consists of slurry and sand [31]. Water still flows from the TBM through the mud spurt into the soil skeleton, because $\Delta s > p_0$. The flow velocity is smaller than at the start of infiltration due to a lower permeability of the mud spurt [12]. The water is squeezed out of the slurry, leaving bentonite particles consolidated at the face and an external filter cake is formed [12, 18, 31]. Due to consolidation of the slurry the permeability of the external filter cake is lower than the permeability of the mud spurt and the fresh soil, clearly visible in figure 3.4. This figure also indicates a constant permeability of the external filter cake due to the straight line in the square root of time. The formation of the external filter cake is shown in step 6.

2.3 Slurry infiltration formulas

In this section different slurry infiltration formulas are discussed. These formulas are the starting point in calculating the excess pore pressures during boring and it is therefore relevant to investigate which formulas can best be used in this research. Slurry infiltration formula presented by Broere [18], Bezuijen [9], Huisman [26] and Talmon [36] are discussed.

2.3.1 Broere

To determine the slurry infiltration depth in time Broere uses the theory of Krause [30] and Mohkam [34]. The slurry infiltration depth in time $x_{Broere}(t)$ is a hyperbolic function [18]. In Eq. (2.4) the maximum infiltration depth $x_{max;Broere}$ is calculated, and according to Broere, covers both the mud spurt and plastering processes [18].

$$x_{Broere}(t) = \frac{t}{a+t} x_{max;Broere} \tag{2.3}$$

$$x_{max;Broere} = \frac{\Delta p \, d_{10}}{\alpha \tau_F} \tag{2.4}$$

In Eqs. (2.3) and (2.4) t is the time in s, a is the timespan to reach half $x_{max;Broere}$ in s and is determined with column infiltration tests, Δp $(= \Delta s)$ is the excess pressure in Pa, d_{10} is the grain diameter for which 10% is finer than d_{10} in mm, α is a fitting factor determined with column infiltration test ($2 \leq \alpha \leq 4$) and τ_F is the yield strength of the slurry in Pa [17, 18]. Since the d_{10} of one sieve curve is considered, homogeneous soil conditions are assumed. It has to be noted that Eq. (2.3) does not take the flow in front of the TBM into account, which is preferable when considering slurry infiltration in front of the TBM. This relation is a result of extensive laboratory experiment and is therefore an empirical relation but is not derived from first principles. Due to the limit amount of parameters it is interesting to investigate if this relation can be used in determining slurry infiltration depth. Furthermore, in literature [18] this relation is used and provided accurate results.

Parameter t_r is introduced and is the time of one full rotation of the cutter wheel in s. In this case the assumption is made that the cutter teeth are equally distributed and positioned non-overlapping over the cutter wheel. Integrating Eq. (2.3) over t_r and equating this to the infiltration depth obtained with a mean infiltration time t_F establishes the mean infiltration time shown in Eq. (2.5). This t_F in s is used in Eq. (2.3) to estimate the mean slurry infiltration depth in time.

$$t_F = \frac{t_r}{ln(1 + t_r/a)} - a \tag{2.5}$$

This method is compared with taking the cutter wheel configuration into account. It is interesting to investigate the difference between the two methods and what effect the differences have on the calculation of the excess pore pressures during boring.

2.3.2 Bezuijen

To determine the slurry infiltration depth Bezuijen applies the theory that slurry cannot infiltrate faster than pore water can flow out the pores of the soil under a certain excess pressure [9]. To determine the pore water velocity at the tunnel face under a certain excess piezometric head, Bezuijen takes the derivative of Eq. (2.6) at $x = 0$, leading to Eq. (2.7).

$$\varphi = \varphi_0\left(\sqrt{1+\left(\frac{x}{R}\right)^2} - \frac{x}{R}\right), \tag{2.6}$$

$$i = \frac{\varphi_0}{R}, \tag{2.7}$$

In Eqs. (2.6) and (2.7) φ_0 is the excess piezometric head at the tunnel face in m, R is the radius of the cutter wheel in m, x the distance from the tunnel face in m, φ the excess pore pressure at distance x in m and i is the hydraulic gradient. Eq. (2.6) does not take (partial) plastering during boring into account. From field measurements at the North/South line it is seen that (partial) plastering is present [28, 35]. Therefore, it is preferred that this relation is altered such that the plastering processes during boring are taken into account. It is also possible to consider that boring 'stops' between subsequent cutting teeth passages and that slurry infiltration takes place within this timespan. Then, an alteration as mentioned might not be necessary.

Following Darcy's law the pore water velocity, v_p, can be written as in Eq. (2.8). In this equation k is the permeability of the soil in m/s and n the porosity of the soil which is dimensionless.

$$v_{p;Darcy} = \frac{ki}{n} \tag{2.8}$$

It is possible to derive the course of the pore pressure in the soil just in front of both the tunnel face and the mud spurt. Close to the tunnel face there is 1-dimensional flow and therefore the piezometric head in front of the tunnel due to the mud spurt can be written as [13, 26]

$$\varphi_{ms} = \frac{x\psi + nk_{ws} + k_s(\varphi_0 - \Gamma x)}{x\psi + nk_{ws} + k_s}, \tag{2.9}$$

in which φ_{ms} is the piezometric head at the far end of the mud spurt in m, φ_0 the piezometric head at the tunnel face in m, x the distance the slurry has infiltrated into the soil in m, k_{ws} the permeability of the consolidated slurry in m/s, k_s the permeability of the sand in front of the tunnel in m/s, Γ the ratio between applied piezometric head in m and the maximum slurry infiltration depth in m in a column infiltration test. ψ is the 1-dimensional flow resistance in s^{-1} in front of the tunnel (without considering the slurry, so groundwater flow only) defined as

$$q = \psi\varphi_{ms}, \tag{2.10}$$

in which q is the specific discharge in m/s. In Eq. (2.10) excess values are considered. Due to the small thickness of the mud spurt compared to the dimensions of the tunnel the mud spurt thickness is neglected in determining the value of the flow resistance [10]. Using Eq. (2.8) and Darcy's law the flow resistance is calculated as

$$\psi = \frac{k}{R}, \tag{2.11}$$

in which k is the permeability of the soil in front of the tunnel in m/s and R is the radius of the cutter wheel in m. The distance of infiltrated slurry varies with time and can be solved with Eq. (2.12).

$$\frac{dx}{dt} = k_s\left(\frac{\varphi_0 - \varphi_{ms}}{x} - \Gamma\right) \tag{2.12}$$

According to Bezuijen it is also possible to describe the relation above slightly different. The starting point is to consider that the infiltrated slurry is equal to the flow resistance and a contribution of the yield stress of the slurry. The contribution of the yield stress increases linearly over the slurry infiltration depth, as considered by Krause [30]. It is assumed that all the time dependency is caused by the mud spurt, so no distinction is made between mud spurt and external filter cake formation. The pressure difference between the excess piezometric head at the tunnel face, φ_0, and the piezometric head at the far side of the mud spurt, φ_{ms}, can be described with Eq. (2.13). In this equation x is the slurry infiltration depth in m.

$$\varphi_0 - \varphi_{ms} = \underbrace{(q/k_{ws})x}_{\text{Darcy's law}} + \underbrace{\beta x}_{\text{yield stress}} \tag{2.13}$$

Now, φ_{ms} is eliminated by rewriting Eq. (2.10) and equating in Eq. (2.13), resulting in

$$\varphi_0 = \frac{q}{k}R + \frac{q}{k_{ws}}x + \beta x. \tag{2.14}$$

Next, the specific discharge q is rewritten with Darcy's law as $q = (dx/dt)n$ leading to

$$\varphi_0 = \left(\frac{n}{k}R + \frac{n}{k_{ws}}x\right)\frac{dx}{dt} + \beta x. \tag{2.15}$$

When the slurry infiltration depth x reaches x_{max}, φ_{ms} is zero since all the piezometric head is transferred to the soil skeleton. As a result q is zero as well, since there is no flow. With these two known boundaries, the value of β is determined to be φ_0/x_{max}. Above can be rewritten to Eq. (2.16). The slurry infiltration depth can be determined with numerical integration.

$$\frac{dx}{dt} = \frac{\varphi_0 - \dfrac{\varphi_0}{x_{max}}x}{\dfrac{n}{k}R + \dfrac{n}{k_{ws}}x} \tag{2.16}$$

In Eq. (2.16) a combination of TBM specifications (R and φ_0), laboratory results (x_{max} and k_{ws}) and field data (n and k_s) is presented.

2.3.3 BTL-report 32

The *Boren Tunnels Leidingen* (BTL) reports (in Dutch) are the result of a wide range of studies regarding the boring of tunnels and pipes. The initiators were *Stichting Boren Tunnels en Leidingen* (BTL) and CUR [12, 26].

According to BTL-report 34 [12] the value of the initial infiltration velocity and the end value of the slurry infiltration depth ares calculated with Eq. (2.17) and Eq. (2.18), respectively.

$$q_{f;0} = \frac{k}{n}\left\{\frac{\Delta p}{\rho_w g L} + \left(1 + \frac{L_v}{L_s}\right)\sin(\theta)\right\} \tag{2.17}$$

$$x_{max;BTL} = \frac{\Delta p + \rho_w g L \sin(\theta)}{\dfrac{\tau_y}{\alpha_{BTL} D_h} + \rho_w g\left(1 - \dfrac{\rho_s}{\rho_w}\right)\sin(\theta)} \tag{2.18}$$

In which k is the permeability of the sand in m/s, n the porosity of the sand, Δp the excess pressure in Pa, ρ_w the density of water in kg/m^3, ρ_s the density of slurry in kg/m^3, L the distance from infiltration front to the position where atmospheric pressure is reached ($= L_s + L_v$) in m, L_s the length of the sand sample in m, L_v the length from the valve to the sample in the set-up in m, τ_y the yield strength in Pa, $\alpha = 8/75$ dependent on the geometry of the pore channels, D_h the characteristic hydraulic pore diameter in m and θ the angle of the test set-up from the horizontal in degrees. Several parameters need to be measured in laboratory experiments before they can be used in the formulas. It is problematic to use this formulas without available laboratory results and therefore the formulas are not suitable in calculating the slurry infiltration depth when no laboratory results are available. In this research the formulas are used to fit the laboratory results.

Also, a formula is presented to calculate the parameter a from Eq. (2.3),

$$a_{BTL} = \frac{x_{max;BTL}}{\frac{k}{n}\left\{\frac{\Delta p}{\rho_w g L} + \left(1 + \frac{L_v}{L_s}\right)\sin(\theta)\right\}} = \frac{x_{max;BTL}}{q_{f;0}}. \tag{2.19}$$

It is stated that the value of a_{BTL} is calculated with a determined value of $x_{max;BTL}$ retrieved from laboratory tests [12], and $q_{f;0}$ is the starting value of the infiltration velocity of the slurry. The slurry infiltration depth in time is calculated with

$$x_{BTL}(t) = \frac{t}{a_{BTL} + t} x_{max;BTL}. \tag{2.20}$$

2.3.4 Talmon

A publication by Talmon [36] provides a study under which conditions slurry infiltration (mud spurt) and filter cake formation (plastering) occur. Experimental and theoretical developments are compared with data from tunneling projects. It is stated that filter cake formation only occurs when the infiltration velocity falls below the Peclet criteria for undrained behaviour of the suspension [36]. Although the relations presented in this study are interesting, they are not used in this thesis. The reason is that in order to use the formula accurately the value of the consolidation coefficient c_v in m^2/s of the slurry should be known. This parameter could not be determined accurately in this research, due to the in-availability of a API filter test, and therefore the relations presented in this publication are not used in this thesis.

2.3.5 Summary of slurry infiltration formulas

Broere [18] provides slurry infiltration formulas which depend on few parameters. Each parameter, except a and α, can be determined quite easily. The parameters a and α need to be determined with column infiltration tests, but parameter ranges are presented in literature [18, 30]. The formulas are not derived from first principles, but have a solid experimental basis.

Bezuijen [13] provides a formula which combines laboratory results with parameters in the field in Eq. (2.9). The slurry infiltration depth in time is calculated with Eq. (2.12), assuming quasi-static conditions. This equation also incorporates a parameter Γ which follows directly from column infiltration tests. Therefore, it is not possible to use this equation to calculate the slurry infiltration depth without conducting column infiltration tests. Another relation is provided by Bezuijen in which the slurry infiltration depth is equal to the flow resistance and a contribution of the yield stress of the slurry, Eq. (2.16). This relation uses the maximum slurry infiltration depth x_{max}, which is determined with a column infiltration test.

Huisman [26] provides a relation for the maximum infiltration depth x_{max} and parameter a in BTL-report 32. The same equation to calculate the slurry infiltration depth in time as Broere are used. Unfortunately, the parameters to calculate x_{max} and a rely heavily on laboratory experiments, e.g. L, L_s and L_v. It is therefore difficult to calculate the slurry infiltration depth accurately without conducting laboratory experiments.

It is concluded that all the relation provided above have one or more parameters that are directly related to laboratory experiments. Therefore, it is concluded that column infiltration tests should be conducted within this research. In the next section a sensitivity analysis is done to investigate the possible range of slurry infiltration depths in time. The equations provided by Broere [18] are used for this sensitivity analysis, because few parameters are present in the equations and for each parameter a range of possible values is present in existing literature [18].

2.4 Sensitivity analysis of the slurry infiltration formulas

A sensitivity analysis is done with Eqs. (2.3) and (2.4) to investigate how sensitive the slurry infiltration formulas are to changing parameters. This study is done for the Second and Third Sand Layer, but only the results of the latter are presented in this section. For the results of the Second Sand Layer see Appendix B.1.2.

The sensitivity analysis consists of two parts. The first part aims to give insight in the effect of the different parameters on the slurry infiltration depth. In each case, four of the five parameters are kept constant and one parameter varies within a range. The second part aims to give insight in the maximum and minimum slurry infiltration depth by choosing the values of the parameters in such a way that a maximum and minimum slurry infiltration depth is achieved. Table 2.1 shows the values of the parameters used in the sensitivity analysis. Parameters d_{10} and τ_F are quite easy to determine from laboratory tests and Δp is the excess face pressure used during boring. The parameters to focus on are a and α. The value of a is particularly important to the speed of slurry infiltration and α influences the magnitude of the maximum slurry infiltration depth.

TABLE 2.1: Overview of parameters used in the sensitivity analysis of the slurry infiltration formulas for the Third Sand Layer.

Parameter	Value(s)	
	Fixed	*Range*
a [s]	180	[60, 100, 140, 180]
Δp [Pa]	25E+03	[10E+03, 15E+03, 20E+03, 25E+03]
d_{10} [mm]	0.135	[0.125, 0.145, 0.165, 0.185]
α [-]	3	[2, 2.5, 3, 3.5, 4]
τ_F [Pa]	5	[2.5, 5, 7.5, 10]

The values in table 2.1 are in agreement with existing literature and reference project in the Netherlands [18]. Parameter a varies from fine to coarse sand. The Third Sand Layer consists of moderately fine sand. The excess pressure is considered 25 kPa, which is a commonly used excess face pressure when boring with a slurry TBM. The value of d_{10} is retrieved from the sieve curve of the Third Sand Layer and the range is chosen such due to the possible variations in the soil. The parameter α varies between 2 and 4 [18]. The yield stress of the slurry, τ_F, is chosen with respect to reference projects [18].

The result of the first part of the sensitivity analysis is presented in Appendix A, figure B.1, and the physical behavior of the parameters is as expected. The result of the second part of the sensitivity study is presented in figure 2.6. The vertical line in the plots indicates the maximum slurry infiltration time per rotation of the cutter wheel. The slurry infiltration depth ranges between 45 and 625 mm. The maximum value is big compared to literature [26, 30]. It is concluded that the range of slurry infiltration depths is too great to make a decent estimation of the slurry infiltration depth for the N/S line project. This, in combination with the fact that all the slurry infiltration formulas presented in section 2.3 have a direct relation to column infiltration tests, it is concluded that laboratory experiments are required to provide a deeper insight into the slurry infiltration processes of the N/S line project.

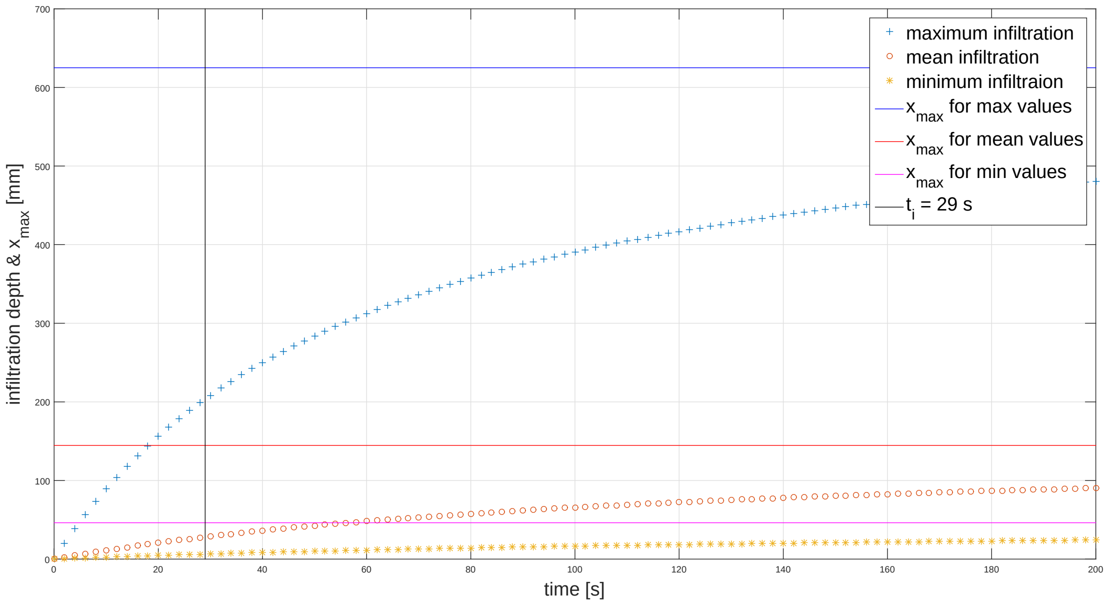

FIGURE 2.6: Sensitivity analysis of parameters on the maximum and minimum slurry infiltration depth for the Third Sand Layer.

2.5 Groundwater flow models

During infiltration the slurry replaces the present pore water, initiating a groundwater flow in the direction of boring. This groundwater flow causes the excess pore pressures [18]. Therefore, it is interesting to investigate the different groundwater flow models present in existing literature.

The applicability of the flow models depend heavily on the geological conditions. Mainly two different geological situations regarding aquifers are distinguished with respect to the N/S line project:

- Unconfined aquifer (Bezuijen);
- Semi-confined aquifer (Broere).

If an aquifer is not bounded by layers with a lower permeability than the aquifer, i.e. no retardation of flow in any direction, the aquifer is considered unconfined. A semi-confined aquifer is defined as an aquifer that is bounded by layers with a lower permeability than the aquifer (called aquitards), but despite a retardation of flow, the flow of water is possible through these layers [37, 38].

2.5.1 Unconfined aquifer

The model of Bezuijen focuses on homogeneous soil in an unconfined aquifer and assumes no plastering of the tunnel face during boring, a constant excess pore pressure at the tunnel face, no influence of the surface, evenly distributed flow over the entire tunnel face and quasi-static conditions [9, 10]. In quasi-static conditions there is change in time, but the change is small and therefore internal equilibrium is guaranteed. The actual 3D boundary problem reduces to a rather simple formula, see Eqs. (2.21) and (2.22).

$$\varphi = \varphi_0\left(\sqrt{1+\left(\frac{x}{R}\right)^2} - \frac{x}{R}\right) \tag{2.21}$$

$$\varphi = \frac{q}{k}(\sqrt{x^2+R^2} - x) \tag{2.22}$$

In the equations φ is the excess piezometric head above hydrostatic level in m at distance x in m, φ_0 is the excess piezometric head in m at $x = 0$ and R is the radius of the cutter wheel in m. In Eq. (2.22) the formula is written slightly different, including the permeability and porosity (incorporated in q). This model has provided fine results in predicting excess pore pressures at the tunnel face [9, 10].

The design team of Witteveen+Bos used Eq. (2.21) to back-calculate the excess pore pressures at the tunnel face for the shallow tunnel passing Bridge 404 [28, 35]. The formula fits good onto the field data, although close to the tunnel face the fit is slightly better. Bezuijen [10] states that the difference between the quasi-static model and the transient flow model of Broere is limited close to the tunnel face. Therefore it is possible to calculate the excess pore pressures close to the tunnel face with Eq. (2.21) in a semi-confined aquifer as well.

2.5.2 Semi-confined aquifer

Using transient groundwater flow models for the excavation period as well as for the stand-still between subsequent excavation periods, a time-dependent build-up and dissipation of excess pore pressures in front of the face can be calculated. Combined with a rough estimate of the discharge from the TBM, this model can be used to predict the excess pore pressures in layered soil conditions exceptionally well [16, 18].

In order to determine the rise of excess pore pressures with time, the discharge from the face into the soil needs to be determined. According to Broere [18] this can be done in two ways. The first option is to use the average infiltration velocity of slurry. Differentiating Eq. (2.3) to time and multiplying by the porosity leads to a specific discharge,

$$q = n\ v = n\left(\frac{a}{(a+t)^2}x_{max}\right). \tag{2.23}$$

The second option states that the amount of water displaced by the penetrating slurry for each full turn of the cutting wheel is equal to the amount of pore water in the excavated soil [34], which leads to a specific discharge of

$$q = \frac{l_{cut}}{t_{cut}}n, \tag{2.24}$$

in which l_{cut} is the cutting depth in m and t_{cut} is the time in s for a full turn of the cutting wheel and is equal to t_r [18]. It has to be noted that for Eq. (2.24) it is assumed that no external filter cake is formed. The calculated discharges can be used in Eq. (2.25) [19], which is a solution for transient flow in a semi-confined aquifer and is used to estimate the rise of excess pore pressure in front of the tunnel face [18].

$$\varphi = \varphi_\infty + \frac{Q\lambda}{4kH}\left[\text{erfc}\left(\frac{xu}{2\sqrt{t}} + \frac{\sqrt{t}}{u\lambda}\right)\exp\left(\frac{x}{\lambda}\right) - \text{erfc}\left(\frac{xu}{2\sqrt{t}} - \frac{\sqrt{t}}{u\lambda}\right)\exp\left(-\frac{x}{\lambda}\right)\right] \tag{2.25}$$

In Eq. (2.25) Q is the discharge per unit width of the aquifer in m^2/s, $u = \sqrt{S_s/k}$, $S_s = \rho g(m_v + n\beta)$ is the specific storage of the aquifer in m^{-1}, $\lambda = \sqrt{kH\tilde{c}}$ the leakage length in m, H the thickness of the aquifer in m, x is the distance from the tunnel face in m, t is the boring time in s and φ_∞ is the piezometeric head at $x \to \infty$ in m. Please note that Q is a negative value, since water is added to the aquifer instead of subtracted from the aquifer [15, 19].

When boring is stopped and assuming an impermeable external filter cake the time dependent pressure distribution in the aquifer is given by

$$\varphi = \varphi_\infty + \frac{\Delta\varphi}{2}\left[\operatorname{erfc}\left(-\frac{xu}{2\sqrt{t}} + \frac{\sqrt{t}}{u\lambda}\right)\exp\left(-\frac{x}{\lambda}\right) + \operatorname{erfc}\left(\frac{xu}{2\sqrt{t}} + \frac{\sqrt{t}}{u\lambda}\right)\exp\left(\frac{x}{\lambda}\right)\right], \tag{2.26}$$

in which $\Delta\varphi$ is the excess pore pressure in m. This equation is used to estimate the pressure drop in the aquifer between excavation periods or to estimate the remaining excess pore pressure at the start of a sequence if the excess pore pressures are not fully dissipated [18]. Both Eq. (2.25) and (2.26) are in good agreement with field measurements [15, 16, 18].

The shear strength τ_F used in formula described in Eq. (2.4) has been used without the influence of the shear velocity. So, implicitly the shear capacity is described by the static yield stress τ_y. The dynamic shear strength τ_F can be described by

$$\tau_F = \tau_y + \nu\left(\frac{8v}{d_{10}}\right), \tag{2.27}$$

in which ν is the dynamic viscosity and v the infiltration velocity of the slurry [18]. In this equation the characteristic grain size d_{10} has been equated to the characteristic hydraulic pore diameter for simplicity [18, 26]. It is shown that the slurry suffers from significant deterioration in shear strength when subjected to mechanical mixing, which can reach up to 60% of τ_y [34]. Also, slurry infiltration leads to shear strain and thus a lower shear strength of the slurry. Therefore, during boring the shear strength is expected to be lower than during standstill [18].

2.6 Cutter wheel configuration versus average infiltration

The slurry infiltration processes described in figure 2.5 assume a sharp transition between slurry and soil skeleton and an averaged slurry infiltration depth over the entire face. These assumptions are however not veracious due to the ordination of the cutting teeth and the rotational speed of the cutter wheel. Rather small zones are excavated by the cutter wheel and therefore the infiltration depth of the slurry varies over the entire face [12, 18]. Both Broere and Bezuijen average the infiltration depth of the slurry over the entire face to simplify the model. From Eq. (2.23) it is seen that the infiltration velocity decreases with time, which indicates that the velocity is greater at the start of the infiltration compared to the end of infiltration. If the cutter wheel has overlapping teeth, higher discharges occur more often, making the average infiltration time used by Broere and Bezuijen possibly inaccurate. The cutter wheel of the N/S line is presented in figure A.6.

2.7 Conclusions

A slurry tunnel boring machine (TBM) is widely used in saturated, non cohesive soils [22]. The supporting face uses a bentonite suspension (slurry) which is subjected to an excess pressure to keep the bore front stable [18]. Besides a stabilizing effect of the slurry, it also serves as conveyance of the excavated soil [23]. The geometry of the cutter wheel, in combination with the configuration of the cutter teeth, are part of the excavation mechanism. Pressurized slurry is the driving force in the slurry infiltration process during boring. Slurry infiltration is a transient process [4, 18] and the infiltration-excavation cycle during boring is the driving force behind the excess pore pressures in front of a slurry TBM.

Slurry consists of a mixture of bentonite and water. Bentonite is a type of clay that is formed by weathering of volcanic ash and it consists mainly of the clay mineral montmorillonite. In the presence of water a double layer is formed and the distance between the layer packs will widen. This gives the slurry a high viscosity (depending on bentonite concentration), a yield point and the ability to stagnate in sandy soils [23].

Tunnel face stability calculations made with a wedge shaped failure mechanism are widely used in engineering practices [4, 13, 25, 39]. Excess pore pressures in front of the tunnel face due to boring have been measured by half a dozen projects in the Netherlands alone [9, 10, 18, 35]. Considering no excess pore pressures during boring due to perfect (instantaneous) plastering of the tunnel face is proven to be incorrect [9, 18, 28, 35]. Excess pore pressures result in a less effective face support on the triangle soil column. Two situations are distinguish. First, the excess pore pressure falls within the wedge width, indicating that the stability calculations according to Jancsecz [27] are still valid, approximately [13]. The second situation is that the excess pore pressure exceeds the wedge width, resulting in a decreased net force from the tunnel face on the triangle soil column. This clearly indicates a lower effective support pressure. To keep the tunnel face stable under these conditions the minimal allowable face pressure should be increased significantly [11, 18].

An idealized pore channel is used in existing literature to model the slurry infiltration depth into the soil [18, 30]. Pressurized slurry infiltrates in the soil and replaces the present pore water. During infiltration the slurry experiences increasing shear resistance τ from the sand grains, resulting in a maximum infiltration distance at a given excess pressure Δp. This distance is called the mud spurt, $x_{ms;max}$, which only occurs in the soil in front of the cutter wheel. The external filter cake is formed due to consolidation (plastering) of the bentonite and is formed within the excavation chamber. The different processes of slurry infiltration, plastering and segregation can occur simultaneously [18] and result in a maximum slurry infiltration depth x_{max}.

Several slurry infiltration formulas are found in existing literature. Each relation relies on at least one parameter that should be determined in a column infiltration test. It is therefore concluded that laboratory experiments are required in this research to provide a deeper understanding of the slurry infiltration processes of the North/South (N/S) line project. A sensitivity analysis is done with the slurry infiltration formulas of Broere [18], because few parameters are present in the equations and for each parameter a range of possible values is present in existing literature.

To determine the slurry infiltration depth in time a hyperbolic function is defined by Broere [18] as,

$$x(t) = \frac{t}{a+t} x_{max}, \tag{2.28}$$

$$x_{max} = \frac{\Delta p \, d_{10}}{\alpha \tau_F}. \tag{2.29}$$

The slurry infiltration velocity is the derivative of Eq. (2.28) with respect to time and the infiltration velocity decreases in time [18]. As a result of the sensitivity analysis, the slurry infiltration depth has a minimum value of 45 mm and a maximum value of 625 mm. The range of solutions is too great to provide a solid basis for calculations, which highlights the necessity of laboratory experiments.

Groundwater flow models for an unconfined [10] and a semi-confined aquifer [18] are presented. Close to the tunnel face the groundwater flow model for an unconfined aquifer can also be used in the case of a semi-confined aquifer [10]. Both models require model input from the slurry infiltration formulas and therefore it is important to determine the slurry infiltration as accurate as possible.

In existing literature an average slurry infiltration depth is used to determine the discharge from the tunnel face as input for the groundwater flow models [9, 18]. It is also assumed that only one cutter tooth passes every rotation. This is not veracious for the N/S line project, because the cutter wheel is asymmetric and consists of areas with multiple cutter teeth passages per rotation. Since the slurry infiltration velocity decreases with time, the areas with multiple cutter teeth passages per rotation will experience higher slurry velocities more often, resulting in higher discharges in these areas. A comparison regarding the cutter wheel configuration and the mean infiltration time onto the excess pore pressures will be done in this research.

To validate the excess pore pressure prediction, data from the N/S line and the Green Heart Tunnel (GHT) is used. For both projects, TBM data and recorded pore pressures are available. The most important data of the TBM is the excess face pressure, which is the driving force of the slurry infiltration process. Also, the boring time and the position of the TBM with respect to the piezometer are important. The recorded pore pressures are used to check whether the excess pore pressures prediction with the groundwater flow models provide accurate results.

Chapter 3

Laboratory Experiments

In this section the laboratory experiments conducted in this research are elaborated. First, the goals are described. Then, an overview of the materials, the column infiltration apparatus and the preliminary tests is provided. Next, the results are presented and is followed by an overview of the limitations and remarks. After that, the slurry infiltration formulas are fitted on the laboratory results. Finally, the usability of the laboratory results as input for the groundwater flow models is discussed. This chapter has a conclusion at the end.

3.1 Goal

The goal of the laboratory experiments is to simulate the slurry infiltration into a sand configuration normative for the Third Sand Layer at N/S line project. The objectives are to:

- Measure the slurry infiltration depth and the outflow of pore water in time;
- Measure the pressure drop in time;
- Measure the porosity and permeability before starting the tests;
- Fit the slurry infiltration formulas on the laboratory results;
- Investigate the usability of the results as input for the groundwater flow models.

The tests have been conducted under the supervision of laboratory staff of the Delft University of Technology in a period of approximately six weeks.

3.2 Outline

3.2.1 Materials

In the laboratory experiments manually composed sand and IBECO B1 bentonite are used. The sieve curves of the Second and Third Sand Layer are shown in figure 3.1. The Third Sand Layer is used in the experiments, since the Second Sand Layer is too fine for the available filters at the laboratory, too fine to compile with dry sieving and such fine sand was not available at laboratory. The manually composed sand representing the Third Sand Layer consists of a mixture of five different sands, see Appendix B.2. The bentonite used is IBECO B1, since this is the material used in the N/S line project. To compile the slurry, 50 grams of bentonite is added to 1 liter of water. The bentonite and water are mixed in a Hobort mixer and stiffened for a several of hours. For more information about this process and a fact sheet of the bentonite see Appendix B.2.

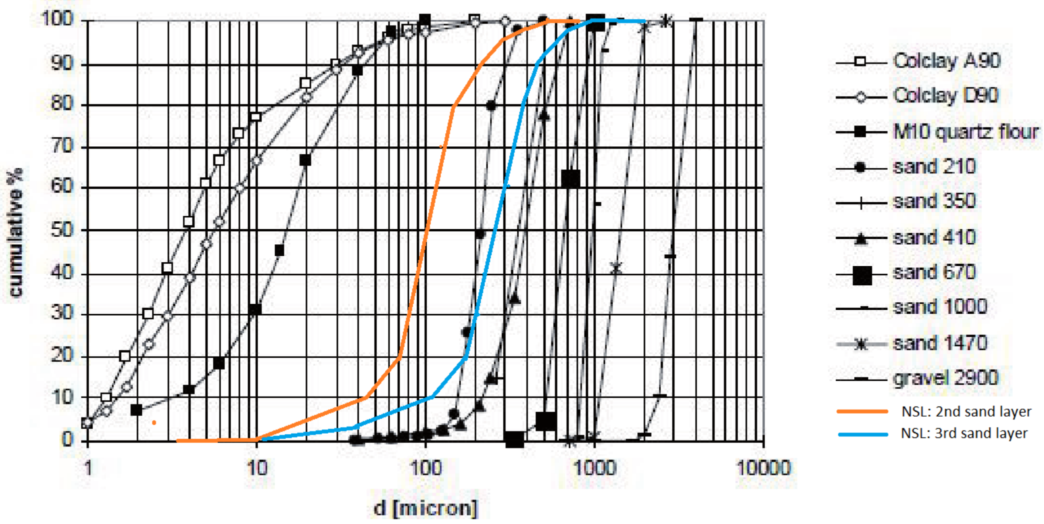

FIGURE 3.1: Sieve curves of the Second and Third Sand Layer close to the project site. Underlying figure adopted from [36].

3.2.2 Column infiltration apparatus

The column infiltration apparatus is shown in figure 3.2. Slurry is placed upon a saturated sand column and is pressurized with air. In this case the excess air pressure is approximately 25 kPa. When the valve at the bottom of the column is closed no infiltration can occur, because water cannot flow out of the apparatus. The slurry infiltration process starts when the valve at the bottom of the apparatus is opened. It has to be noted that the slurry infiltrates in fresh soil.

Three sensor positions are present in the column, but only two sensors are available at the laboratory. The majority of the tests are conducted with sensors situated in the bottom two openings, see figure 3.2a. A computer is used to record the pore water pressures, see figure 3.2b. In Appendix B.3 guidelines for preparing the infiltration column are presented.

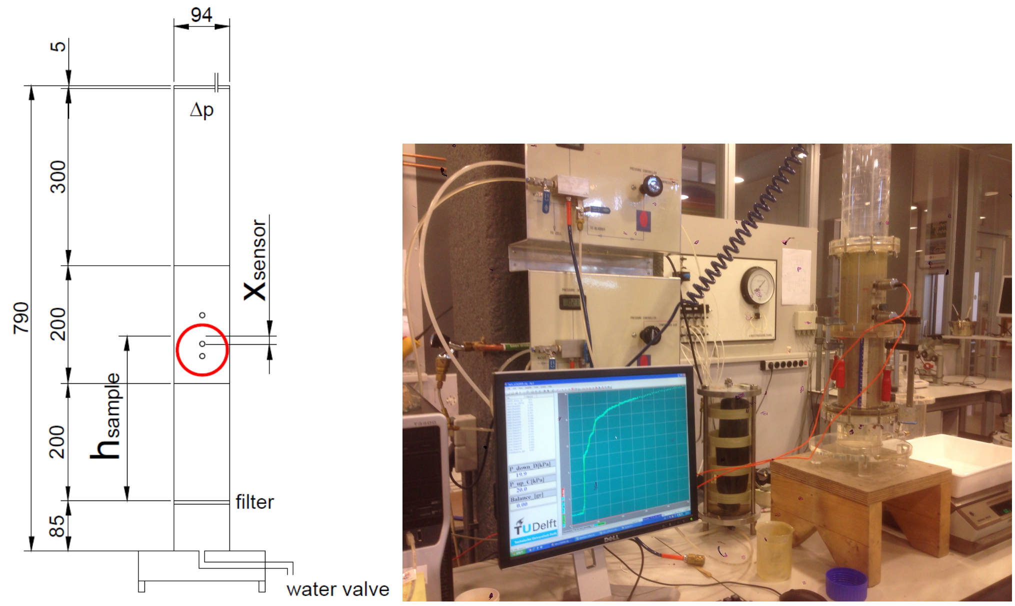

(A) (B)

FIGURE 3.2: Design of the column infiltration apparatus (A) and a photograph of the set-up in the laboratory (B).

3.2.3 Preliminary tests

Prior to each column infiltration test three preliminary tests are conducted. These tests are necessary to check whether the sand and the slurry sample are consistent. To check the consistency of the sand, the porosity and the permeability are measured. For every slurry mixture the yield point τ_y is measured with a Fann viscometer. The different formulas used in the preliminary tests are presented in Appendix B.3.

3.3 Results

3.3.1 Slurry infiltration depth in time

An overview of the relevant slurry infiltration test results are shown in figure 3.3 and shows remarkable similarities with existing literature, see figure 3.4 [22, 26, 30, 36]. The test results are used as a starting point in fitting the slurry infiltration formulas. The measured values for each test are summarized in table 3.1. The displaced volumes are greater in figure 3.4, since the sand used in these experiments is coarser. The gradient of the line in the consolidation area of the graph from the laboratory experiment is greater than in literature. This is due to the finer sand used in this laboratory experiment, which leads to a slower segregation of water and bentonite. Therefore, when the same time is considered, more water is segregated, which leads to a higher gradient. The similarities of both graphs give confidence that the laboratory results are veracious.

For all the tests a change in gradient is clearly visible. The change in gradient implies the transition from slurry infiltration (mud spurt) to plastering (external filter cake formation) [36]. Note that the x-axis of the graph is presented in $\sqrt{t}$, since this makes the change in the gradient easier to identify. On this $\sqrt{t}$-axis the straight line indicates a hyperbolic relation regarding the slurry infiltration, which is in accordance with literature [18]. The tests are coded as date conducted (e.g. "13-8" is August 13^{th}) and part of day (e.g. "m" is morning).

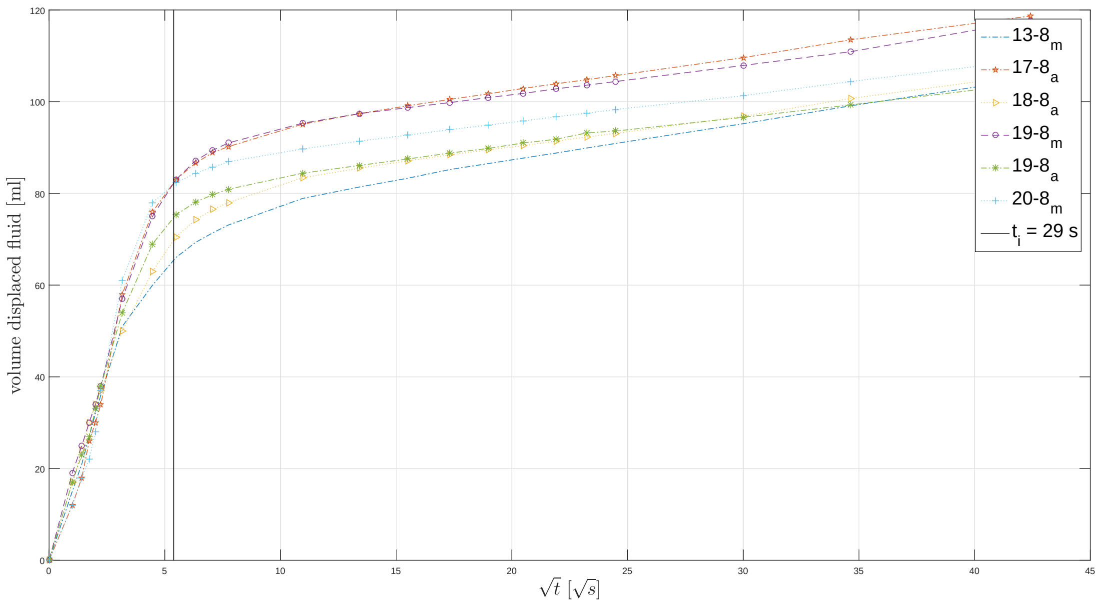

FIGURE 3.3: Volume of displaced fluid in time for the relevant column infiltration test results.

The differences in the results may be due to different yield strength of the slurries, local inhomogeneities, different permeabilities and errors during sample preparation. The values of the permeability are quite consistent, with the exception of the permeability of test 18-8_a, which is twice as high as the other tests. This could be due to a measurement error in determining the permeability or errors mentioned above. The difference between the lowest and highest value of the displaced fluid V_{pw} is approximately 14%, which is quite accurate.

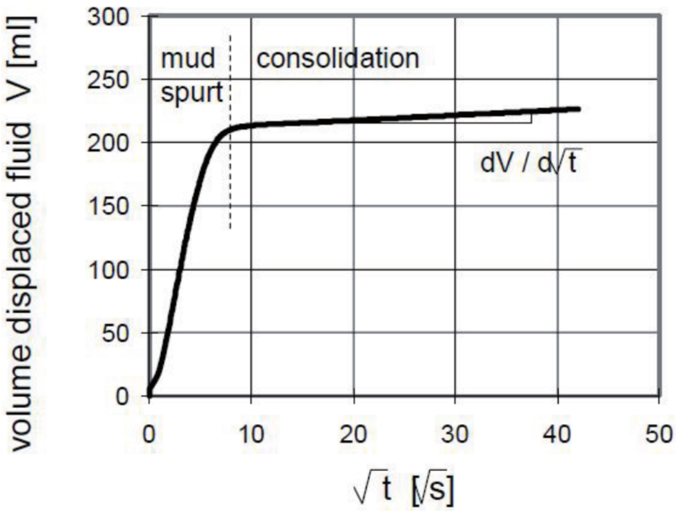

FIGURE 3.4: Volume of displaced fluid in time from existing literature [36].

TABLE 3.1: Measured and calculated parameters for the relevant column infiltration test results.

Test	h_{sample} [cm]	x_{sensor} [cm]	n [-]	k [m/s]	YP [Pa]	V_{pw} [ml]	h_{pw} [cm]
13-8$_m$	27.5	2.0	0.30	N/A	9.9	105	5.0
17-8$_a$	27.3	1.8	0.30	2.2E-04	7.1	119	5.7
18-8$_m$	26.0	0.5	0.30	5.8E-04	10.4	129$^{t=110min}$	6.3
19-8$_m$	26.3	0.8	0.30	2.3E-04	8.5	118	5.7
19-8$_a$	27.0	1.5	0.31	2.6E-04	9.0	104	4.9
20-8$_m$	26.8	1.3	0.30	2.7E-04	7.1	109	5.2

The distance of displaced pore water in the infiltration column is calculated as [18, 30],

$$h_{pw} = \frac{V_{pw}}{A_{IC} \cdot n} \tag{3.1}$$

with h_{pw} the height of displaced pore water in the column in mm, V_{pw} the volume of displaced fluid in mm^3, A_{IC} the surface area of the infiltration column in mm^2 and n the porosity [30]. For the relevant tests the distance of displaced pore water is plotted in time, see figure 3.5. The results are compared to figure 3.6 from literature [18]. Please note that the values on both the x-axis and y-axis are different. The differences in values on the y-axis is explained by the fact that different sands have been used. Krause [30] used sand with a higher d_{10} (0.3 to 0.7 mm) compared to the the d_{10} (0.11 mm) used in this research. A higher d_{10} indicates a coarser sand, which leads to a higher slurry infiltration depth according to Eq. (2.4). Krause [30] also used different excess pressures, ranging from 10 kPa up to 50 kPa, compared to the 25 kPa used in this research. Greater excess pressures also lead to higher slurry infiltration depths, according to Eq. (2.4). Another difference between figure 3.5 and 3.6 is the transition between mud spurt and plastering, which goes much faster in figure 3.5. This indicates a lower value of a, which means that the slurry infiltration processes goes faster. Due to lower values of d_{10} and Δp the maximum slurry infiltration depth is smaller for the column infiltration tests conducted in this research compared to Krause [30]. Lower values of a also indicate finer sands, which is in agreement with the sands used in this research compared to Krause [30].

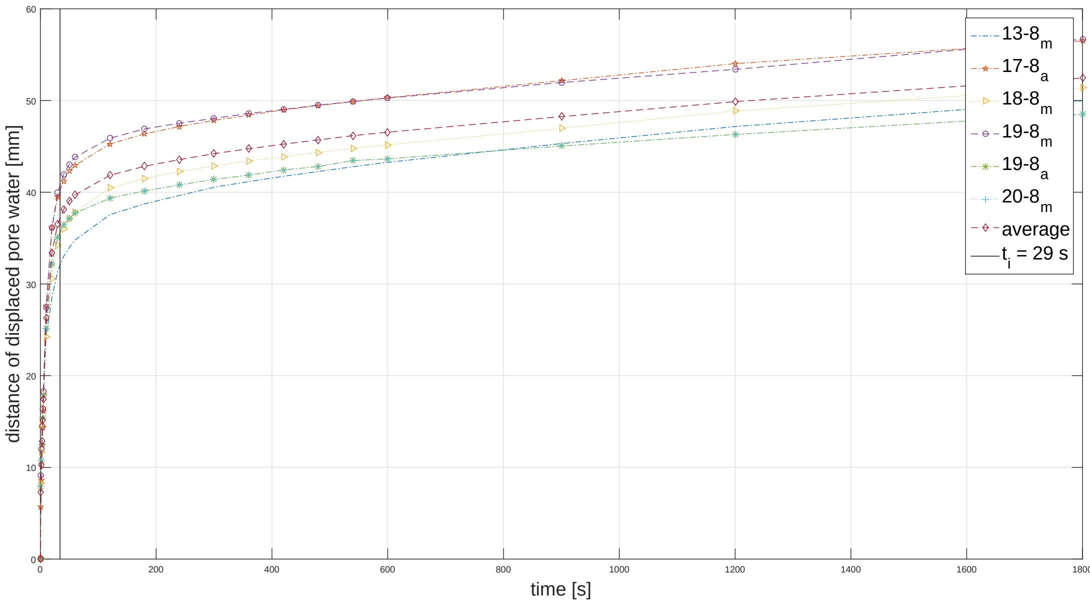

FIGURE 3.5: Distance of displaced pore water in the infiltration column in time for the relevant test results.

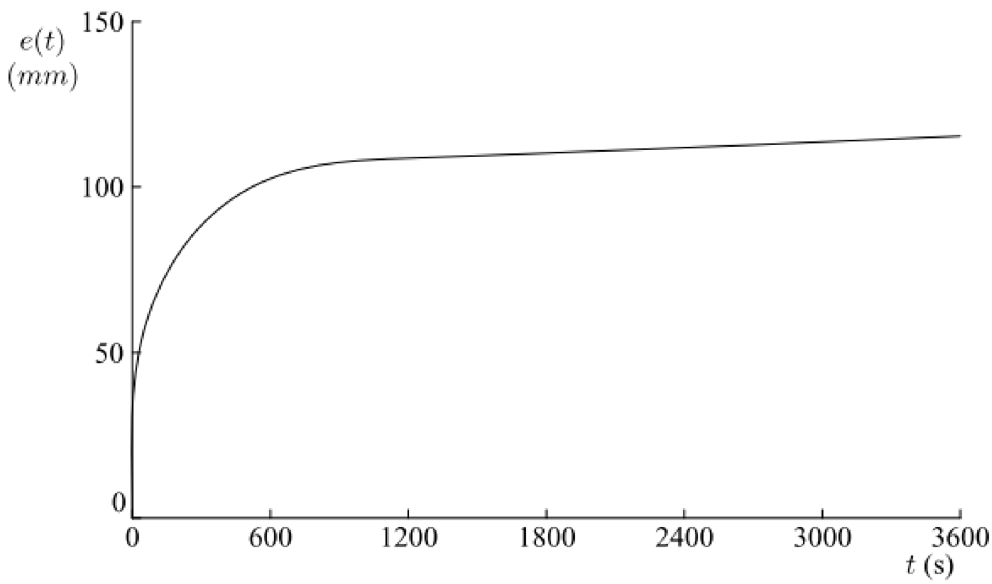

FIGURE 3.6: Distance of displaced pore water in the infiltration column in time with Δp = 50 kPa, d_{10} = 0.48 mm and 60 g/l bentonite concentration, from [18].

From figure 3.5 it is seen that the slurry infiltration depth is in the order of 30 to 40 mm after approximately 30 seconds. The visual measurement in figure 3.7 shows approximately 30 mm of mud spurt for test 13-8$_m$ and 20-8$_m$ after a period of 30 minutes. This is visual proof of both mud spurt and plastering processes and confirms the transition seen in figure 3.4. It is however not possible to give a decisive answer whether segregation processes are occurring in the first 30 seconds of infiltration.

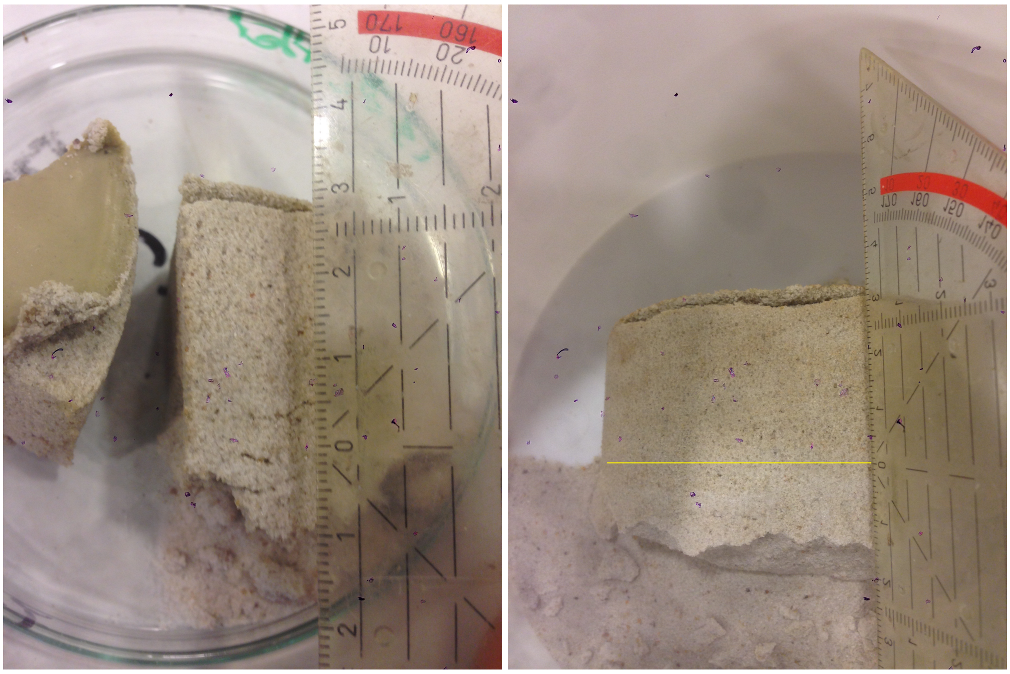

(A) (B)

FIGURE 3.7: Visibility of the mud spurt ($\approx 30\ mm$) and the external filter cake in test 13-8$_m$ (A) and 20-8$_m$ (B).

3.3.2 Pore pressure drop in time

The pore pressure drop in time is measured using two pore pressure sensors, see figure 3.8. A steep decrease of pore pressure is seen when the test is started. This is due to the fact that the pore pressure at the location of the valve decreases quickly when the valve is opened. The magnitude of the decrease is not the same for each test. A clear relation between the permeability of the sample and the pressure drop cannot be given. There is a clear relation between the disturbed sample 17-8$_m$ and the pressure drop. The volume pushed out of this sample is very small, which indicates fast and short slurry infiltration. Therefore, the pressure drops quickly in the first seconds of the test. The same is found in test 14-8$_m$, but less severe. As the total filter cake is formed (mud spurt and external filter cake) it is expected that the pore pressure sensors would record negative pressures due to suction. The value of the suction should be in the order of -2.5 kPa ($-(h_{sample} - x_{sensor}) \cdot \rho_w \cdot g = -0.25 \cdot 1000 \cdot 9.81 \approx -2500 Pa$). This suction is not seen in figure 3.8. This could be due to the measurement capacity of the sensors. The sensors can measure up to 10 bar (1,000 kPa) and the pressure that should be recorded is -2.5 kPa, which is 0.25% of the maximum capacity of the sensor. The laboratory staff did not know the error range of this particular sensor, but it is possible that these low pressure fall within the error range. Another reason could be that the sensors are not fully saturated with water and therefore no suction is recorded. An overview of the different parameters measured for the tests visualized in figure 3.8 can be found in table B.3

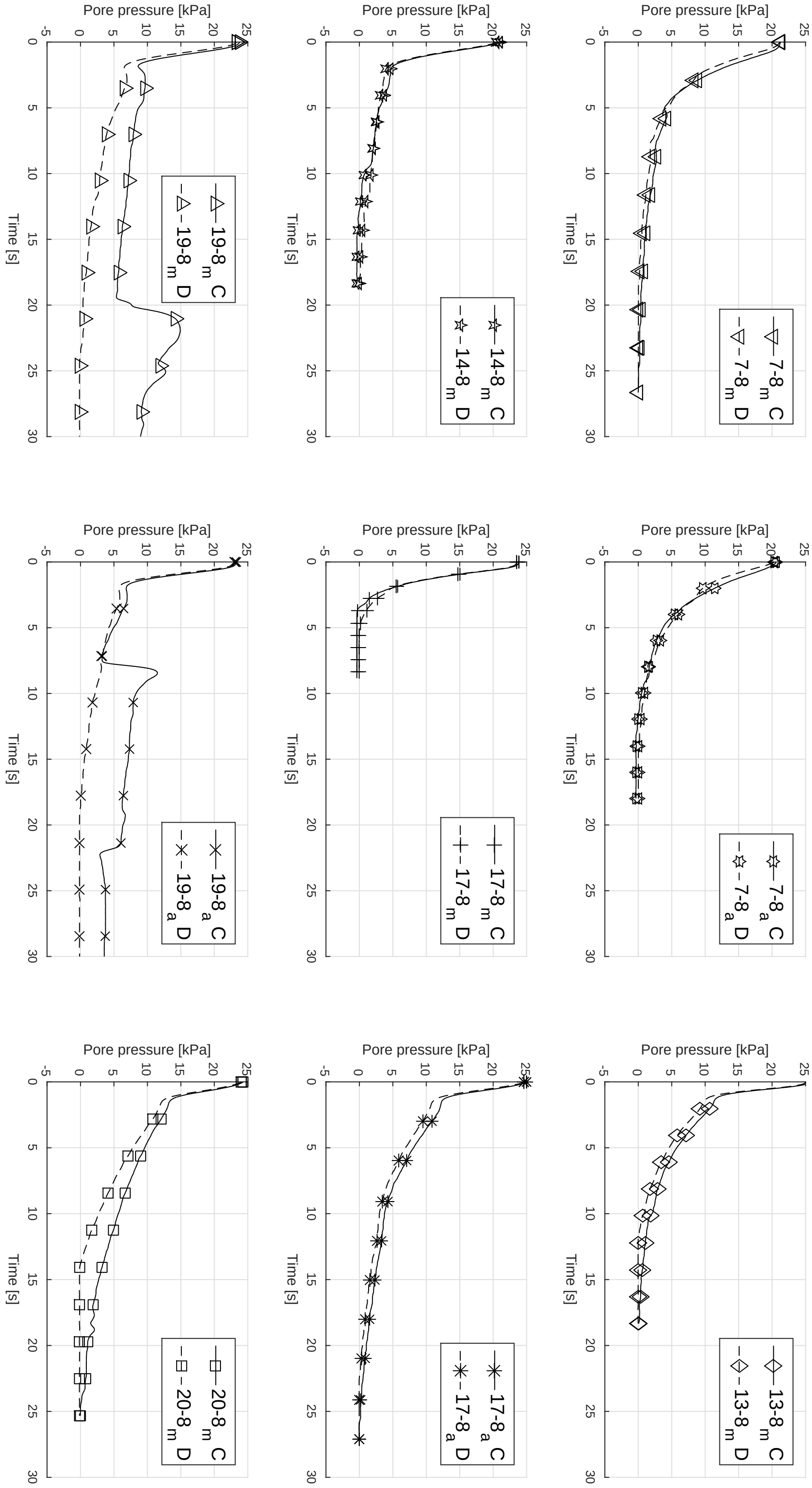

FIGURE 3.8: Pore pressure drop in time for the column infiltration test results.

3.3.3 Short slurry infiltration times

Three tests are done with a short infiltration time. In two tests the infiltration time was six seconds and in one test the infiltration time was twelve seconds. The reason to conduct tests with small infiltration times is to see to what extent the permeability of the mud spurt can be measured. After the slurry infiltration time has passed, the valve is closed and immediately the air pressure is released as well. Then, the top part of the column is dismantled and the slurry is removed. This is a difficult task, since the infiltration front should not be disturbed and all the slurry needs to be removed to be able to conduct a permeability test. In practice, this procedure was difficult. This led to a disturbed infiltration front and not all the slurry was removed. Both this factors influence the consistency, reliability and the veracity of the results.

TABLE 3.2: Measured and calculated parameters for the column infiltration tests with a short infiltration time.

Test	t [s]	x_{sensor} [cm]	n [-]	k_{start} [m/s]	k_{after} [m/s]	$h_{pen;fluid}$ [cm]	Δh_{sl} [cm]
24-8$_m$	6	1.5	0.30	3.0E-04	2.5E-05	2.6	0.4
24-8$_a$	12	1.5	0.30	2.5E-04	N/A	3.7	0.7
25-8$_a$	6	1.5	0.30	2.8E-04	8.2E-05	1.9	0.3

In table 3.2 it is shown that the permeability of the tests with an infiltration time of six seconds is a factor 10 lower than the permeability of the sample without slurry. It makes sense that the permeability is lower, since slurry has infiltrated the sample and this result is consistent with existing literature [12]. However, the differences in k_{after} between the tests are more than a factor 3, which is a big differences since k_{start} is about the same value. The test of twelve seconds had such a low permeability that only drops of water exiting the valve and therefore no permeability test has been done. In this research only three tests with short infiltration times have been conducted, and therefore it is concluded that it is not possible to provide a solid conclusion regarding the permeability of the mud spurt. For future research it is recommended to conduct similar tests, but deeper though has to be given into the design of the column infiltration apparatus. The most important thing to consider is the removal of the slurry after the infiltration period without damaging the infiltration front. This future research is relevant in the case that mud spurt is present in front of the TBM during boring, as seen by the N/S line project. It is also relevant in future research to create some sort of cut in the sample after infiltration into fresh soil to represent the passage of a cutter tooth. After this cut is made, another infiltration cycle can be done to investigate the behaviour of the mud spurt and external filter cake.

3.4 Limitations and remarks

- The sand used in the experiments is manually composed, which means it is composed of different sands and does not originate from the project site.
- The manually composed sand is consists of five different sands, which are mixed extensively. Still, it is possible that the sands are not mixed perfectly, resulting in small variations in the particle size distribution for each test. This has an effect on the results.
- The finest fraction of the Third Sand Layer is not present in the composed sand. During mixing of the sand, a white powder fluttering from the sand sample was clearly visible in the air. This is an explanation of the absence of the finest fraction. This absence has an influence on the permeability of the sand and the slurry infiltration depth, since the smallest sand particles are of importance in blocking the slurry.
- A *Hobort mixer* is used in mixing the slurry. It is recommended that a high shear mixer is used to separate all the individual clay particles. This leads to a higher yield strength of the slurry due to better water absorption. The yield strength of slurry in the laboratory should be as close as possible to the yield strength in the excavation chamber to reach a representative value of the maximum mud spurt length $x_{ms;max}$.

- The excess pressure used in the experiments is lower than the excess face pressure used during boring of the tunnels. For the West tunnel $\Delta s \approx 140\ kPa$ and for the East tunnel $\Delta s \approx 100\ kPa$. For the experiments $\Delta p_{air} \approx 25\ kPa$ is used, due to limitations of the laboratory equipment.
- Tap water is used to compose the slurry. The mineral composition of water from the Delft region is (slightly) different than the water used in the bentonite separation plant in Amsterdam. The mineral composition of the water influences the swelling capacity of the bentonite.
- The infiltration column is filled with water from the bottom to top to create a fully saturated sand column. Nevertheless, it is possible that there is still some air present in the column. This influences the permeability of the sample and could lead to inaccurate results.
- Different mixing and stiffening times are used in composing the slurry, resulting in different values of the yield point. To get consistent yield strengths of the slurry the procedure should be kept constant.

Some general remarks to achieve more accurate column infiltration results are provided:

- Use sand from the project site, preferable as close to the critical passage as possible. Then it is guaranteed that the soil properties are as closest to reality. The permeability should be determined in the laboratory (e.g. with a constant head test) and should be compared with the measured permeability at the project site (e.g. with a pump tests);
- Use the same bentonite as used in the project. Next to that, use the correct bentonite concentration and use the same mixing/stiffening techniques used in the bentonite separation plant. It is also preferred to use water of the same mineral composition;
- Use several pore pressure sensors at different distances of the infiltration front to accurate measure the pore pressure drop as the slurry infiltrates;
- Determine the dry matter content of the infiltrated bentonite when the infiltration test is finished;
- Conduct the infiltration tests at the project specific excess pressure, $\Delta p \approx \Delta s$. In this way the mud spurt depth can be determined accurately, as well as the ratio between the mud spurt length and the filter cake. If Δs cannot be reached due to limitation of the laboratory equipment, column infiltration tests at several excess pressures should be conducted and the results can be extrapolated. Please beware that working with an infiltration apparatus under high pressures is dangerous;

3.5 Fit of the slurry infiltration formulas on the laboratory results

This section presents a fit of the slurry infiltration formulas presented by Broere [18] and the BTL-report 34 [26] on the relevant laboratory results from figure 3.3. The formulas of Broere are used since these are also used in the sensitivity analysis. The formulas of the BTL-report are used to investigate whether an accurate value of parameter a can be calculated with Eq. (3.5). The average of the relevant laboratory results is used as a starting point for the fit, as shown in figure 3.5.

$$x_{max;Broere} = \frac{\Delta p d_{10}}{\alpha \tau_F} \tag{3.2}$$

$$x_{max;BTL} = \frac{\Delta p + \rho_w g L \sin(\theta)}{\frac{\tau_y}{\alpha_{BTL} D_h} + \rho_w g \left(1 - \frac{\rho_s}{\rho_w}\right) \sin(\theta)} \tag{3.3}$$

$$x(t) = \frac{t}{a+t} x_{max} \tag{3.4}$$

$$a_{BTL} = \frac{x_{max;BTL}}{\frac{k}{n}\left\{\frac{\Delta p}{\rho_w g L} + \left(1 + \frac{L_v}{L_s}\right)\sin(\theta)\right\}} \tag{3.5}$$

In table 3.3 an overview is given of the parameter values used as input for the calculations. In Eq. (3.3) the characteristic hydraulic diameter is assumed to be equal to d_{10}, as is assumed by Krause [30].

TABLE 3.3: Input parameters to fit the slurry infiltration formulas from Broere [18] and BTL-report 32 [26] on the average laboratory results.

Parameter	Broere	BTL-34	Obtained from
Δp [Pa]	25,000	25,000	Laboratory
d_{10} [mm]	0.11	D_h	Laboratory
τ_F [Pa]	8.68	8.68	Laboratory
α [-]	6.2		Fit
a [s] ∣ a_{BTL} [s]	11	4.2	Fit
k [m/s]		2.5E-04	Laboratory
n [-]		0.3	Laboratory
ρ_s [kg/m^3]		1,028	Assumption
θ [°]		90	Laboratory
L [m]		0.345	Laboratory
L_v [m]		0.085	Laboratory
L_s [m]		0.26	Laboratory
α_{BTL} [-]		(8/75)	Literature [26]
D_h [mm]		0.11	Assumption

The maximum infiltration depth from the laboratory tests is approximately 0.051 m for an infiltration time of 30 minutes. The parameters in Eq. (3.2) are chosen such to result in $x_{max;Broere} \approx$ 0.051 m. Effectively only parameter α is varied since the other parameters are known from the laboratory tests. In the formula of BTL-report 34 the maximum slurry infiltration depth is calculated with Eq. (3.3), resulting in $x_{max;BTL} \approx 0.038$ m. The maximum slurry infiltration depth measured in the laboratory is approximately 35% bigger than calculated with Eq. (3.3). The time to reach half $x_{max;BTL}$, parameter a_{BTL}, is calculated with Eq. (3.5).

The slurry infiltration depth in time from the laboratory and the fit from Broere and BTL-report 34 are presented in figure 3.9. The fit with Broere underestimates the slurry infiltration depth slightly in the first 25 seconds. The fit from BTL-report shows the opposite. It is clear that the

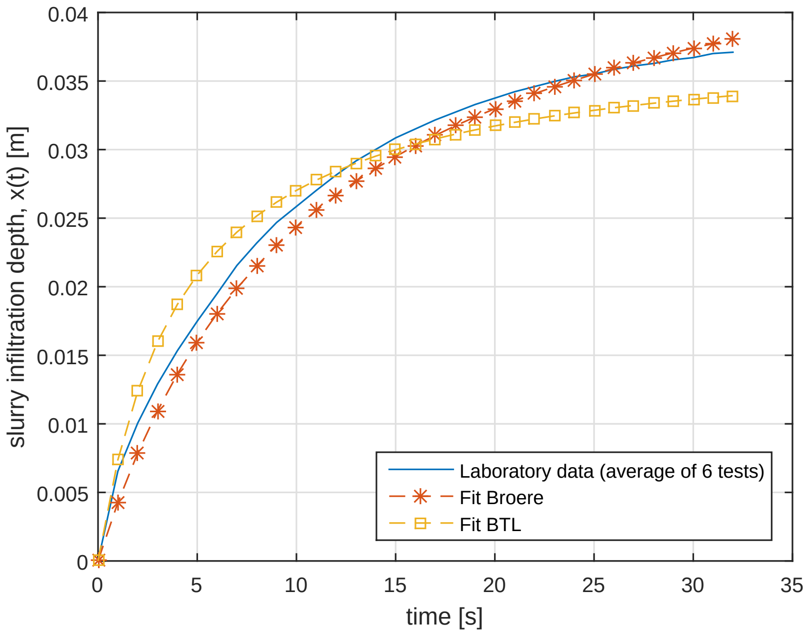

FIGURE 3.9: Fit of the slurry infiltration depth formulas of Broere and BTL-report 32 on the average laboratory results.

formulas of Broere fit better, which makes sense since α and a are tweaked such that the fit is as best as possible. In the fit of the BTL-report both the maximum slurry infiltration depth and the parameter a are calculated and still provides fine results, which is remarkable. Due to the fact that Eqs. (3.2) to (3.5) all consist of a minimum of one parameter that is directly related to column infiltration tests it seems difficult to give a decent estimation of the slurry infiltration depth without conducting column infiltration tests in the laboratory.

The slurry infiltration velocity is calculated by taking the derivative of Eq. (3.4) with respect to time, resulting in

$$v_{slurry} = \frac{dx}{dt} = \frac{a}{(a+t)^2} x_{max}. \tag{3.6}$$

The slurry infiltration velocity in time for the laboratory and the fit are plotted in figure 3.10. Again, the formulas of Broere show a good fit. The fit of the BTL-report shows an overestimation of the laboratory data in the first 5 seconds. After this period an underestimation is seen. The starting value of the slurry infiltration velocity is approximately twice as high for the BTL-report compared to Broere. The slurry infiltration velocity is directly related to the value of a, see Eq. (3.6). Lower values of a indicate faster slurry infiltration, since the same slurry infiltration depth needs to be reached in a shorter period of time. From table 3.3 it is seen that a is smaller for the BTL-report fit and therefore the initial infiltration velocity is higher.

The velocity of the pore water can be compared with the decrease in pore pressure over time in the column infiltration apparatus. The pore water velocity decreases as a result of decreasing excess pore pressures. The excess pore pressure decreases due to the build up of the mud spurt (and in a later stadium the external filter cake). The mud spurt transfers an increasing portion of the excess pore pressure onto the soil skeleton with increasing mud spurt depth and therefore the pore water velocity decreases with increasing mud spurt depth. These effects are seen in both figure 3.8 and 3.10.

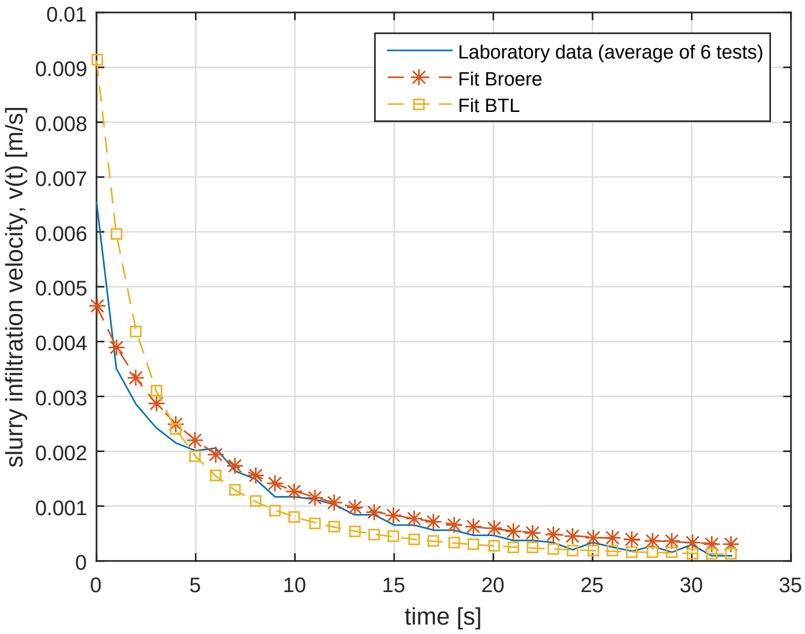

FIGURE 3.10: Fit of the slurry infiltration velocity formulas of Broere and BTL-report 32 on the average laboratory results.

3.6 Usability of laboratory results as input for groundwater flow models in a TBM situation

In this section an investigation is done whether the laboratory results can be used as groundwater flow model input in calculating the rise of excess pore pressure. First the values of x_{max} at pressures normative for the N/S line are determined. After that, field data is used to determine the values of a for the 404 West and East tunnel, respectively. Then, the calculated values of a are compared with the values of a obtained in the laboratory. Next, an investigation is done whether the value of a for a full scale TBM situation can be determined by numerical integration of Eq. (2.16).

Due to laboratory equipment limitations it was not possible to conduct the column infiltration tests at the excess pressures normative for the N/S line. Figure 3.11 shows the maximum infiltration depth for increasing pressure differences and two bentonite concentrations [30]. The sand composition used in this research is similar to the sand of Boden 2 from figure B.7 in Appendix B.2 [30]. The data points of Boden 2 are extrapolated linearly to higher excess pressures to determine the value of the maximum infiltration depth x_{max} at the excess face pressure used during boring of the 404 West tunnel of the N/S line. The linear relationship is in agreement with Eq. (3.2), and with this equation the value of x_{max} is calculated for the 404 East tunnel. The values of x_{max} for the 404 West and 404 East tunnel are shown in table 3.4.

TABLE 3.4: Calculation of x_{max} for the 404 East tunnel and linear extrapolation with Krause [30] for the 404 West tunnel.

Parameter	Value	From
Δs [Pa]	10.3E+04	TBM data
d_{10} [m]	5.0E-05	Sieve curve
α [-]	4	Literature [18]
τ_F [Pa]	8.68	Laboratory
x_{max} [m] 404 East	0.15	Eq. (3.2)
x_{max} [m] 404 West	0.29	Figure 3.11/Eq. (3.2)

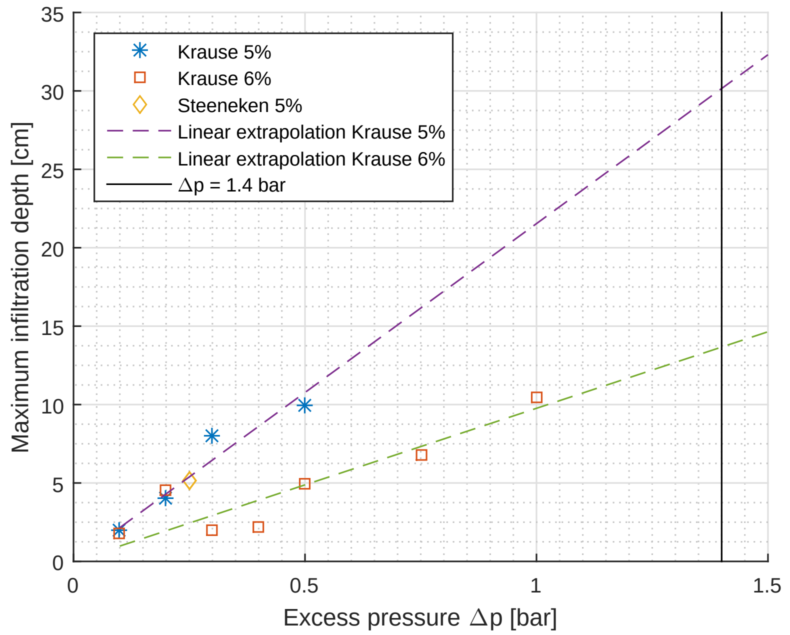

FIGURE 3.11: Linear extrapolation of the maximum infiltration depth with laboratory data from Krause [30].

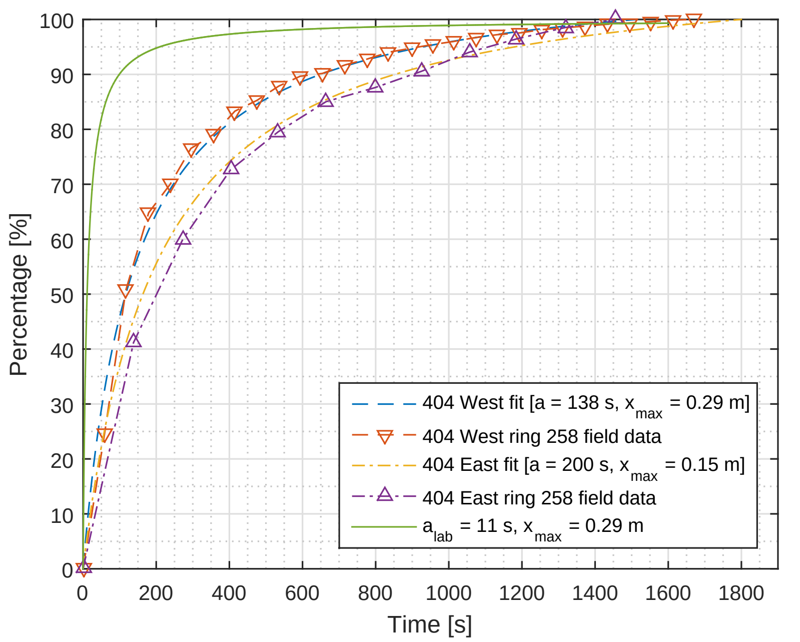

FIGURE 3.12: Fit of parameter a from Eq. (3.4) on the measured piezometric drop at stop boring, shown as a percentage of the total pressure drop.

The value of parameter a is determined by investigating the drop in piezometric head which occurs when boring stops, figures 4.1 and 4.2. For both the 404 West and 404 East tunnel the decrease of piezometric head at stop boring is used to visualize the pressure drop over filter cake in time, see figure 3.12. It is shown as a percentage of the total drop in excess piezometric head, indicating stop boring at 0% and a full pressure drop over the filter cake at 100%. This graph, in combination with the value of x_{max}, is used to fit the value of a with in Eq. (3.4). For the 404 West tunnel a is 138 s and for the 404 East tunnel a is 200 s. The value of a obtained with the fit of Broere [18] from the column infiltration tests is 11 s, see section 3.5. From figure 3.12 it is clear that the value of a determined in the laboratory is significantly smaller than as seen in the field. When the laboratory value of a is used, the drop of piezometric head goes too quick. The difference in magnitude of a can be explained by the fact that the flow around the TBM is different than the flow in the column infiltration apparatus. The parameter a, in case of the TBM, is dependent on the flow and the parameters presented in Eq. (2.16), i.e. the permeability of the soil k_s, the permeability of the consolidated slurry k_{ws}, the radius R of the cutter wheel, the porosity n of the soil, the excess piezometric head φ_0 at the tunnel face and the maximum slurry infiltration depth x_{max}.

The back-calculated values of a are used to calculate the slurry infiltration depth and velocity in time, respectively. The results are presented in figures 3.13 and 3.14. At t = 0 s the slurry infiltrates into fresh soil, which is soil without the presence of slurry. The slurry infiltration depth in time $x(t)$ is greater for the 404 West tunnel compared to the 404 East tunnel, see figure 3.13. This makes sense since the excess face pressure used during boring is greater, the d_{10} of the sand is greater as well and the value of a is smaller. Since the velocity is the derivative of the distance with respect to time, the statements above also holds for the slurry infiltration velocity in figure 3.14.

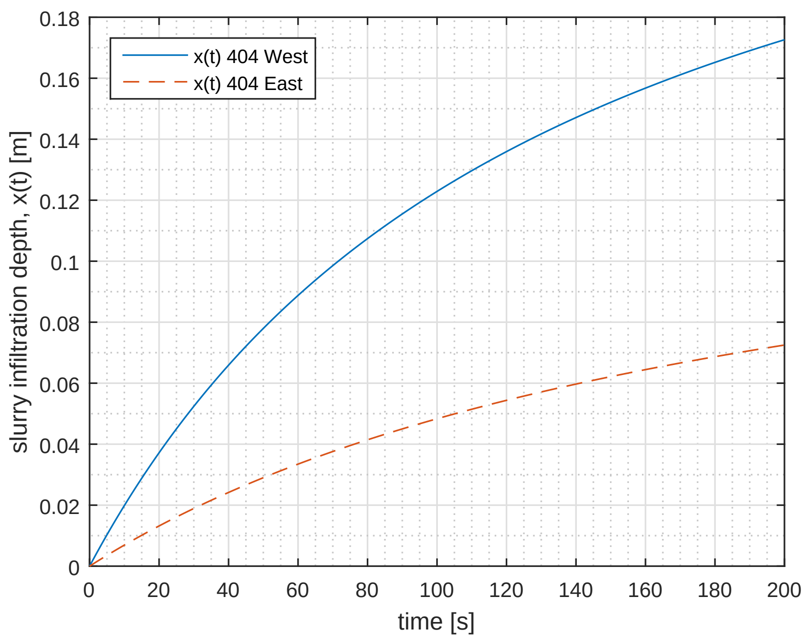

FIGURE 3.13: Calculation of the slurry infiltration depth in time for 404 West and East tunnel, for Δs during boring and a determined with field measurements.

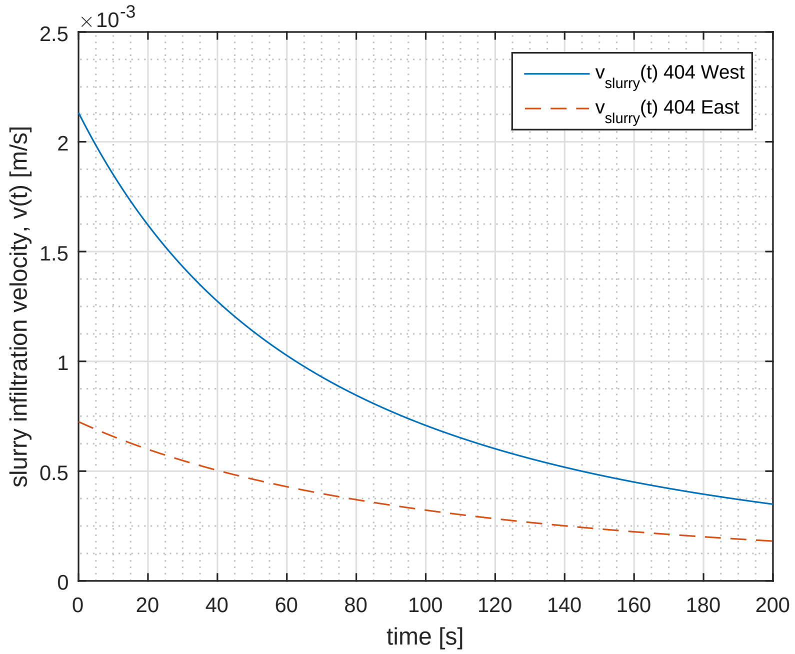

FIGURE 3.14: Calculation of the slurry infiltration velocity in time for 404 West and East tunnel, for Δs during boring and a determined with field measurements.

The back-calculation presented in figure 3.12 is only possible when excess pore pressures are measured during boring. The next step is to investigate whether it is possible to determine a for the TBM case by the use of laboratory results and field parameters without using measured field data. Numerical integration of Eq. (2.16) is done to determine the slurry infiltration depth in time. This relation is used since it combines the TBM specification, laboratory results and field parameters. Is has to be noted that no deviation is made between mud spurt and filter cake formation. First, the numerical integration of Eq. (2.16) is compared with the field measurements in figure 3.15 and after that a comparison is made with the back-calculated values of a in figure 3.16.

For both the 404 West and 404 East tunnel mud spurt is already present in front of the TBM when boring stops, see section 4.1. The magnitude of the mud spurt depth is calculated with Eq. (2.9) and the input values for this calculation are presented in table 3.5. The starting point of the calculation is the excess piezometric head at the far side of the mud spurt, φ_{ms}, which is known from measured field data for both the 404 West and East tunnel, respectively. In combination with the parameter values measured in the field, the mud spurt depth x_{ms} is calculated with Eq. (2.9). For the 404 West tunnel x_{ms} is 14.8 cm (50% of x_{max}) and for the 404 East tunnel x_{ms} is 6.5 cm (40 % of x_{max}) just as boring stops. These mud spurt depths are the starting values of slurry infiltration at t = 0 s.

The result of the numerical integration of Eq. (2.16) is compared with field measurements in figure 3.15. For both the 404 West and East tunnel a decent fit is seen when the input of table 3.5 is considered. For the 404 West tunnel an underestimation of the build up is seen and for the 404 East an overestimation is seen. According to W+B engineers the Third Sand Layer (404 West) has a greater permeability than the Second Sand Layer (404 East), but the value of k is documented equally for both sand layers as 1.0E-04 m/s. The permeability is altered for both tunnels to get a best fit onto the field measurements, resulting in a value of the permeability of 1.8E-04 m/s for the 404 West and 7.5E-05 m/s for the 404 East tunnel. The values are within the possible range of permeabilities, see table 4.4.

It has to be noted that the value of Γ for the 404 East tunnel is back-calculated from φ_{ms} recorded in the field. Due to the fact that only manually composed sand of the Third Sand Layer (404 West) is used in the laboratory experiments this was the only way to determine a value of Γ.

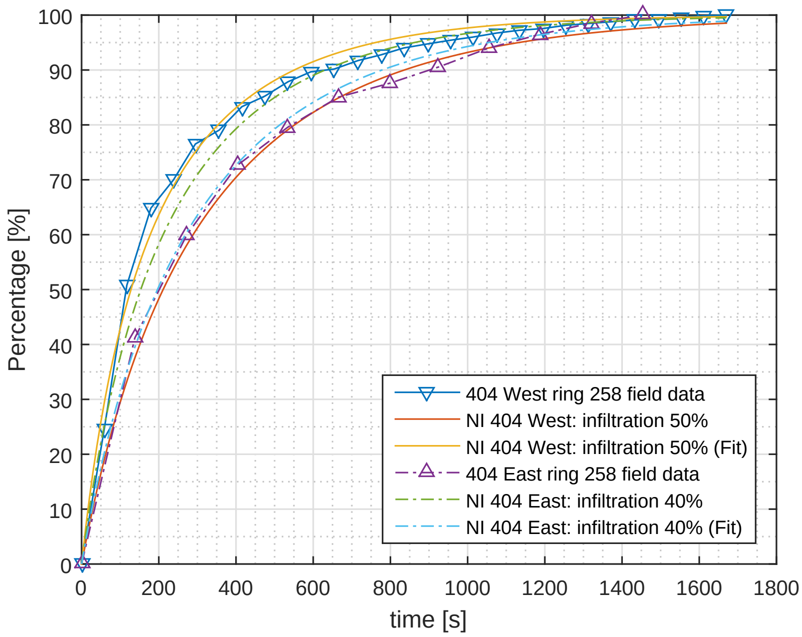

FIGURE 3.15: Numerical integration of Eq. (2.16) fitted on the measured drop of piezometric head at stop boring, taking into account the present mud spurt at stop boring.

TABLE 3.5: Input parameters and calculation results in determining the mud spurt depth x_{ms} with Eq. (2.9).

Parameter	General	404 West	404 East	From
R [m]	3.44			TBM data
k_s [m/s]		1.0E-04	1.0E-04	Field data
$k_{s;fit}$ [m/s]		2.0E-04	7.5E-05	Assumption/Field data
k_{ws} [m/s]	5.0E-06			Assumption/Literature [26]
n [-]		0.35	0.38	Field data
Γ [-]		50	100	Laboratory | Assumption
ψ [s^{-1}]		2.9E-05	2.9E-05	Eq. (2.11)
$\varphi_{ex;face}$ [m]		14.3	10.3	TBM data
φ_{ms} [m]		6.6	3.8	Field data
x_{ms} [m]		0.148	0.065	Eq. (2.9)

Figure 3.16 shows the numerical integration of Eq. (2.16) and a comparison with Eq. (3.4) in which the values of a specific for the 404 West and East tunnel are used. The graphs show good resemblance for both tunnels.

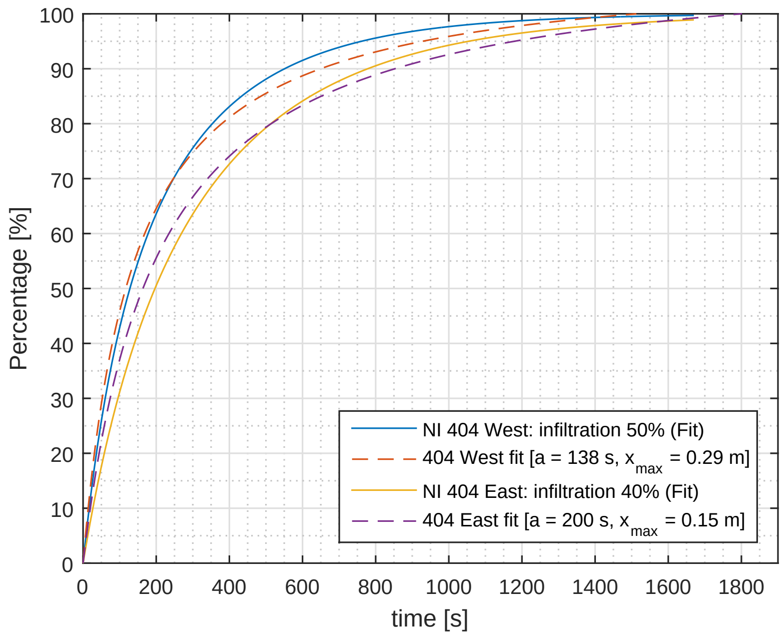

FIGURE 3.16: Numerical integration of Eq. (2.16) and fit of a from Eq. (3.4) on the results.

It can be concluded from figure 3.15 that Eq. (2.16) can be fitted onto the field data accurately via numerical integration. This, in combination with the accurate fit of Eq. (3.4) onto the same numerical integration, resulting in figure 3.16, it is concluded that parameter a specific for the TBM is determined by the parameters in Eq. (2.16). The column infiltration tests are not suitable to find the value of a that can be applied directly in the groundwater flow models, see figure 3.12. But, the column infiltration tests can be used to determine the parameters k_s, k_{ws}, Γ, $x_{ms;max}$ and x_{max}. With this parameters in combination with known TBM specification, numerical integration of Eq. (2.16) can be done and a can be fitted onto this results with Eq. (3.4). In sections 4.2 and 4.4 these values of a are used to determine the excess pore pressures.

For both the 404 West and 404 East tunnel, respectively, the maximum slurry infiltration depth x_{max} in figure 3.12, determined with Eq. (3.4), is not fully reached at 100%. For the both tunnels x_{max} is reached at approximately 110%, indicating that the build up time of the filter cake takes longer than the building time of one ring. This can be explained by the fact that the minimum value of the piezometric head in the aquifer is also not reached at 100%. For the Third Sand Layer the minimum value of the piezometric head in the aquifer is -3.5 m and the recorded value is -3.3 m as boring restarts, see figure 4.1. The last part of infiltration thickens the external filter cake and therefore it can be assumed that the maximum mud spurt length $x_{ms;max}$ is reached at 100%.

The numerical integration of Eq. (2.16) is sensitive to changing parameters and therefore it is important to determine its parameters accurately.

3.7 Conclusions

Laboratory experiments have been conducted with manually composed sand, simulating the Third Sand Layer in the Amsterdam area. The bentonite used in the laboratory experiments is the same as used in the North/South (N/S) line project [39]. A similar infiltration column is used in the laboratory experiment as in existing literature [26, 36].

In total thirteen column infiltration tests have been conducted. The slurry infiltration depth in time shows good resemblance with existing literature. A clear transition between slurry infiltration (mud spurt) and plastering (external filter cake formation) is distinguished, indicating that both processes are present [18, 36]. Visual evidence of both processes is also presented. For the average test with a duration of 30 minutes the mud spurt is approximately 30 mm and the plastering accounts for 20 mm of displaced water height in the infiltration column. The mud spurt is formed in the first 30 seconds of slurry infiltration. Three column infiltration tests with a small infiltration time have been conducted. After six seconds the infiltration process is stopped and the slurry above the infiltration front is removed. Then, a permeability test is conducted to measure the permeability of the mud spurt. The permeability is a factor 10 smaller compared to the permeability of fresh soil, but due to sample disturbances these results are likely to be inaccurate. For future research it is recommended to conduct these tests again, but deeper though has to be given into the design of the test set-up. The most important thing to consider is the removal of the slurry after the infiltration period. This should be done without damaging the infiltration front in order to get accurate results. This future research is relevant in the case that mud spurt is present in front of the TBM during boring, as is seen in the N/S line project.

It is shown that the slurry infiltration formulas of both Broere [18] and BTL-report 34 [26] can be accurately applied to the average laboratory results. The formulas from the BTL-report 34 result in a fine fit, but are less accurate than the formulas of Broere. In the formulas the parameter a (time to reach half x_{max}) is within the range provided in existing literature for the sand (fine to moderately fine) considered in this laboratory experiment [18, 30].

The laboratory experiments could not be conducted at the excess pressure normative for the N/S line due to limitations of the laboratory equipment. Extrapolation with laboratory data from Krause [30] is done to provide a value for the maximum slurry infiltration depth x_{max}. This extrapolation is compared with the calculated values from Broere [18] and the results are the same, approximately. Next, the drop in piezometric head at stop boring is used, in combination with x_{max}, to determine the value of a during boring. For both the 404 West (a = 136 s) and 404 East tunnel (a = 200 s) the calculated value of a is greater than the value determined in laboratory experiments (a = 11 s). Therefore, the value of a determined in the laboratory cannot be used directly in the groundwater flow models. In order to determine a suitable value for a which can be used in the models, numerical integration of Eq. (2.16) is compared with the calculated values of a and a good fit is presented. Since Eq. (2.16) depends on k_s, k_{ws}, n, R, φ_0 and x_{max} it is concluded that the magnitude of a during boring depends on a combination of laboratory parameters, TBM specific parameters and field parameters. It is concluded that laboratory experiments can be used to provide valuable input for Eq. (2.16) and with a known x_{max} a suitable value of a for the TBM can be determined.

Stated above provides accurate results for the 404 West and 404 East tunnel of the N/S line project. It is recommended that this procedure is validated with future projects as well. The numerical integration of Eq. (2.16) is sensitive to changing parameters and therefore it is important to determine its parameters accurately. It is recommended to use sand from the project site and to use the same bentonite in the laboratory experiments as is used in the project. Next to conducting laboratory experiments, it is also recommended to use piezometers to measure the increase and decrease of piezometric head during boring and as boring stops, respectively. With both the laboratory experiments and the field data a decent validation can be done.

Chapter 4

Excess Pore Pressure Prediction

In this section the excess pore pressure is predicted. First, the development of hydraulic head due to tunnel boring is discussed. After that, the excess pore pressure at the far side of the mud spurt is calculated. Next, a new relation to calculate the excess pore pressure at the tunnel face is derived and a comparison is made with measured field data. Also a prediction is done with the transient groundwater flow model comparing the cutter wheel configuration with the average infiltration time. Models limitations are discussed and a sensitivity analysis is conducted. This chapter has a conclusion at the end.

4.1 Development of pore pressures due to tunnel boring

The excess pore pressure build up due to tunnel boring is visualized by many authors [9, 18, 28]. Figures 4.1 and 4.2 show the build up of excess pore pressures boring ring 258 of the 404 West and 404 East tunnel of the North/South line, respectively. Figure 4.3 shows the the build up of excess pore pressures of boring ring 2117 of the Green Heart Tunnel (GHT).

With the development of the hydraulic head during boring an investigation is done to determine whether mud spurt is present during boring. The following is assumed:

- If mud spurt is still present after a cutter tooth has passed $\varphi_0 < \varphi_{ex;face}$, since a part of the excess piezometric head is transferred to the soil skeleton via the mud spurt;
- If all the mud spurt is cut away after a cutter tooth has passed $\varphi_0 = \varphi_{ex;face}$, since only fresh soil is present behind the cutter tooth and the excess face pressure cannot be transferred to the soil skeleton without the presence of mud spurt.

For both the N/S line and the GHT the pore pressure sensors are situated at a small distance (in the order meters) from the tunnel face and therefore the excess pore pressure at the tunnel face is back calculated with

$$\varphi_0 = \frac{\varphi}{\left(\sqrt{1+\left(\frac{x}{R}\right)^2}-\frac{x}{R}\right)}, \tag{4.1}$$

in which φ_0 is the excess pore pressure at the tunnel face in m and φ the measured excess pore pressure head at the equivalent distance x from the TBM, both in m. It is assumed that this model can be used in a semi-confined aquifer for small distances from the tunnel face [10]. Table 4.1 shows the input values for Eq. (4.1) and the calculation results.

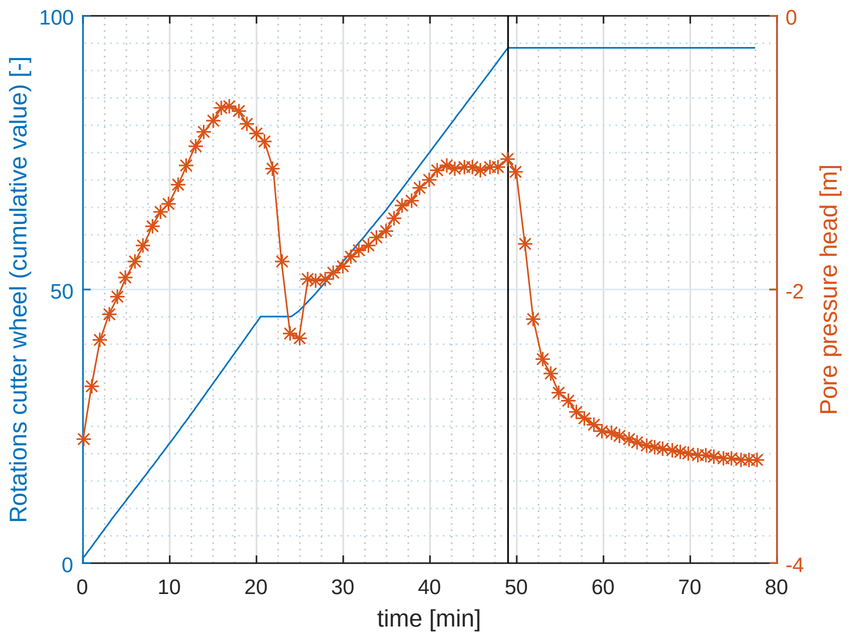

FIGURE 4.1: Pore pressure head (piezometer TB7) and cutter wheel rotations in time during the construction of ring 258 of the 404 West tunnel.

For both the N/S line tunnels it is concluded that $\varphi_0 < \varphi_{ex;face}$ and therefore mud spurt is present during boring, causing the pressure to drop from $\varphi_{ex;face}$ to φ_0. For the GHT the difference is very small. This could indicate a tiny mud spurt, but is it more likely that the back-calculation of φ_0 is slightly inaccurate, due to the greater distance of the piezometer to the tunnel face. In order to check if mud spurt is present during boring of the GHT, the slurry

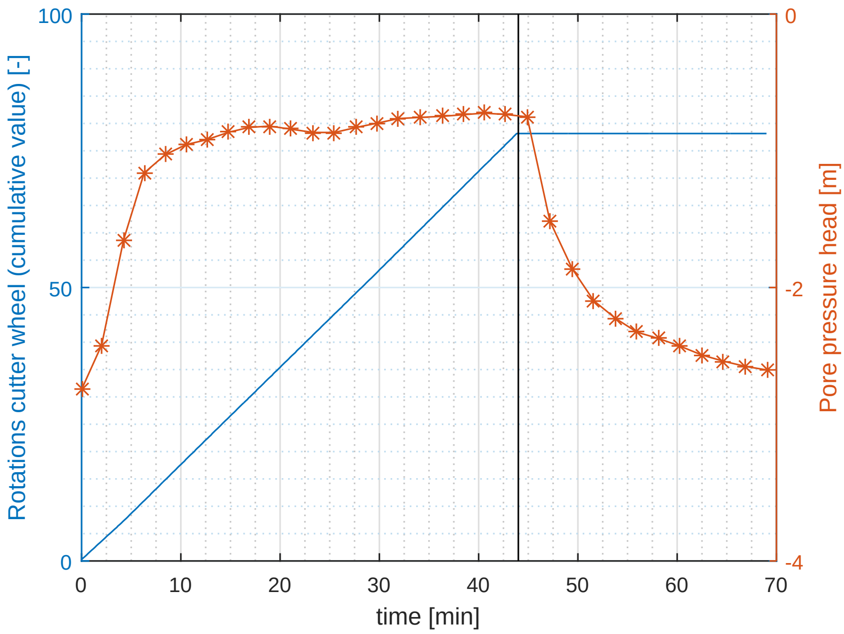

FIGURE 4.2: Pore pressure head (piezometer TB4) and cutter wheel rotations in time during the construction of ring 258 of the 404 East tunnel.

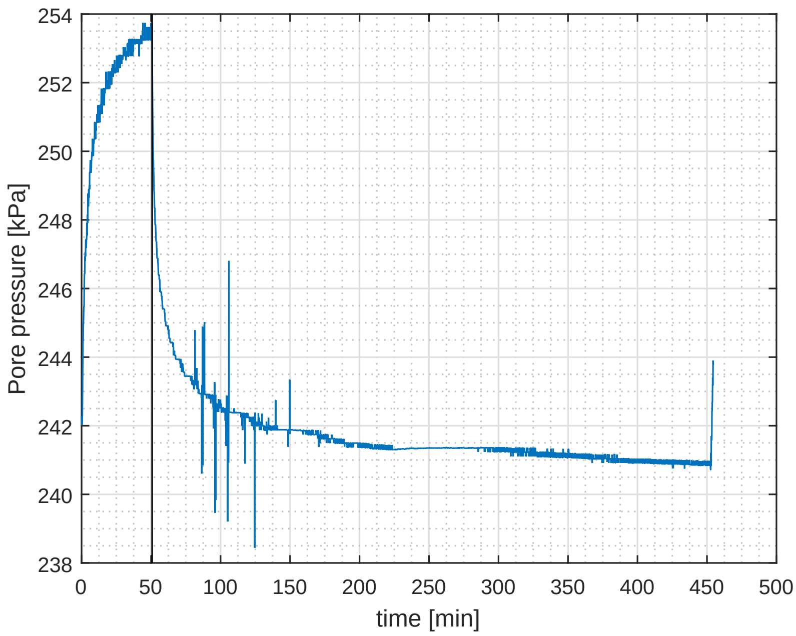

FIGURE 4.3: Pore pressure head (piezometer WD1) in time during the construction of ring 2117 of the GHT.

infiltration velocity calculated with Darcy's law is compared to the velocity of the TBM. If $v_{p;Darcy} < v_{TBM}$ slurry will still infiltrate the soil, but the mud spurt is cut away every time a cutter tooth passes [9].

TABLE 4.1: Parameter input and calculation results for back-calculating the measured pore pressures to the tunnel face.

Project	N/S West	N/S East	GHT
Ring	258	258	2117
Sensor depth [m NAP]	-17.5	-26	-27.2
x_{sensor} [m]	3.3	1.5	9.7
φ_{sensor} [m]	2.8	2.5	1.3
φ_0 (φ_{ms} for ^{1}) [m]	6.6^1	3.8^1	3.8
$\varphi_{ex;face}$ [m]	14.5	10.3	4.1
difference [m]	7.9	6.5	0.3

The velocity of the TBM is calculated as,

$$v_{TBM} = \frac{w_{ring}}{t_{boring}}, \tag{4.2}$$

in which w_{ring} is the width of a tunnel ring in m and t_{boring} the time of boring in s. For the GHT w_{ring} is 2 m and t_{boring} is approximately 3050 s. Using these values in Eq. (4.2) leads to a TBM velocity of 0.66 mm/s. The slurry infiltration velocity in a quasi-static condition is calculated as

$$v_{p;Darcy} = \frac{ki}{n} \text{ with } i = \frac{\varphi_{ex;face}}{R}, \tag{4.3}$$

in which the permeability of the soil k is 2.0E-04 m/s [1], the porosity n is 0.40, the excess face pressure $\varphi_{ex;face}$ is 4.1 m and the radius of the cutter wheel R is 7.44 m. This results in a maximum slurry infiltration velocity of 0.56 mm/s. It is concluded that $v_{p;Darcy} < v_{TBM}$, so slurry infiltrates the soil but the whole mud spurt is cut away with every rotation of the cutter wheel [9].

From back-analysis of the pore pressure data it is concluded that there is no mud spurt present during the boring of GHT. For the N/S line, mud spurt is present during boring close to Bridge 404, resulting in an excess piezometric head at the face which is lower than the excess face pressure of the TBM. Therefore, the φ_0 in table 4.1 is actually the excess piezometric head at the far side of the mud spurt, which makes φ_{ms} a more adequate symbol to represent the value. In figure 4.1 it is seen that a short stop in boring results in a significant decrease of excess pore pressure. Stop and start could be an interesting mitigating measure when boring a critical passage.

4.2 Calculation of excess pore pressures at the far side of the mud spurt

In section 4.1 it is concluded that for the 404 West and 404 East tunnel mud spurt is present in front of the tunnel after a cutter tooth has passed. From TBM data the number of rotations per ring bored are known and combining this with the distance bored, the average cutting depth l_{cut} of one tooth per rotation of the cutter wheel is determined. In order to have mud spurt after a cutter tooth has passed the mud spurt depth x_{ms} should be greater than l_{cut}. For both tunnels the magnitude of x_{ms} is determined in section 3.6. These values are back-calculated from the measured φ_{ms} in the field. Ideally, these values follow from column infiltration tests in the laboratory, but due to equipment limitations this could not be done. With the determined values of a for the 404 West and 404 East tunnel in section 3.6, the excess piezometric head at the far side of the mud spurt, φ_{ms}, are calculated for two situations. First, the cutter wheel configuration is taken into account and second, the mean infiltration time, t_F, is considered. Both the results are compared with the measured piezometric head φ_{ms} in the field.

The quasi-static 1-dimensional flow model of Bezuijen is used to calculate φ_{ms}, outlined in section 2.3.2. Please note that this model is used in a semi-confined aquifer, but since the area of interest is close to the tunnel face (in the order of meters) this is allowed [10]. Therefore, the following formula can be used to calculate the excess piezometric head at the far side of the mud spurt,

$$\varphi_{ms} = \frac{q}{\psi}, \tag{4.4}$$

in which q is the average specific discharge over the tunnel face in m/s and ψ is the 1-dimensional flow resistance of pore water calculated as $\psi = k/R$ in s^{-1}. The value of ψ is assumed constant in the calculations, but can vary in reality due to differences in permeabilities within the aquifer. Following Darcy's law, the specific discharge is calculated as $q = vn$ in which v is the infiltration velocity in m/s and n the porosity of the soil in front of the tunnel. The infiltration velocity decreases with increasing slurry infiltration depth and is described by the hyperbolic function

$$v = \frac{dx}{dt} = \frac{a}{(a+t)^2} x_{max}, \tag{4.5}$$

in which a is the time to reach half x_{max} and is determined for the 404 West (a = 138 s) and 404 East tunnel (a = 200 s) in section 3.6. The specific discharge also decreases with increasing infiltration depth resulting in a decrease of φ_{ms} as the slurry infiltration depth increases as well. This makes sense, because at zero mud spurt depth $\varphi_0 = \varphi_{ms}$ and therefore no excess pressure can be transfered to the soil skeleton. At the maximum slurry infiltration depth x_{max}, φ_{ms} equals zero since all the excess pressure is transferred to the soil skeleton.

In section 3.6 it is seen that x_{max} is not reached in the period of ring building (approximately 90% is achieved). The maximum mud spurt length $x_{ms;max}$ is reached,however, since the mud spurt process occurs prior to the external filter cake formation and consists of 50% and 40% of x_{max} for the 404 West and 404 East tunnel, respectively. In this analysis, it is assumed that the external filter cake is infinitely thin. In figure 4.4 infiltration starts in fresh soil, meaning no mud spurt is present in the soil in front of the tunnel. For the N/S line project this is not the case. Therefore, the slurry infiltration does not start at t = 0 s but at different positions on the graphs, depending on how much mud spurt is cut away by a passing cutting tooth. The amount of mud spurt that is cut away per rotation of the cutter wheel depends on the amount of cutter teeth present in that specific section of the cutter wheel. For the sections with one cutter tooth per rotation the slurry infiltration time t_i is the longest. The sections where four cutter teeth are passing per rotation the infiltration time is smallest and also the cutting depth per cutter tooth per rotation is lower. It makes sense that with decreasing infiltration time t_i the slurry infiltration velocity is smaller, since the amount of mud spurt present in front of the TBM is greater, resulting in a lower excess piezometric head. This leads to a lower pore water velocity. The amount of mud spurt that is cut away at a specific section determines the starting point of slurry infiltration on the graph in figure 4.4, because the mud spurt depth is coupled to a certain time needed to reach this mud spurt depth when fresh soil is considered. The average specific discharge over the entire tunnel face is calculated using the infiltration times combined with the time dependent discharges and the surface areas at which these discharges occur. The average specific discharge is used in Eq. (4.4) to calculate φ_{ms}. For the mean infiltration time t_F the average cutting depth is calculated and this is subtracted from $x_{ms;max}$. This is the starting point of the slurry infiltration. A summary of is presented in table 4.2.

TABLE 4.2: Parameter input and calculation results in determining the excess pore pressure at the far side of the mud spurt for the 404 West and 404 East tunnel.

Parameter	404 West	404 East	From
a [s]	138	200	NI Eq. (2.16)
x_{max} [cm]	29.0	15.0	Figure 3.11/Eq. (2.3)
$x_{ms;max}$ [cm]	14.8	6.5	Eq. (2.9)
$\varphi_{ex;face}$ [m]	14.3	10.3	TBM data
k [m/s]	1.0E-04	1.0E-04	Field data
n [-]	0.35	0.38	Field data
ψ [s^{-1}]	2.9E-05	2.9E-05	Eq. (2.11)
l_{cut} [cm]	1.49	1.74	TBM data
t_F [s]	17	15	Eq. (2.5)
t_{rot} [s]	32	35	TBM data
$v_{p;Darcy}$	5.48E-04	2.91E-04	Eq. (4.3)
$\varphi_{ms;data}$ [m]	6.6	3.8	Field data
Result calculations			
$v_{av;cw}$ [m/s]	5.33E-04	2.89E-04	$q_{av;cw}/n$
$q_{av;cw}$ [m/s]	1.86E-04	1.14E-04	Figure 4.4
$\varphi_{ms;calc;cw}$ [m]	6.4	3.8	Table 4.3
$v_{av;F}$ [m/s]	5.27E-04	2.87E-04	$q_{av;F}/n$
$q_{av;F}$ [m/s]	1.84E-04	1.13E-04	Figure 4.4
$\varphi_{ms;calc;F}$ [m]	6.3	3.9	Table 4.3

TABLE 4.3: Calculation of φ_{ms} for the 404 West and 404 East tunnel, comparing the cutter wheel configuration with the mean infiltration time.

404 West						t_F
t_i [s]	6	9	21	22	29	15
A_i [m^2]	5.3	2.9	2.9	3.2	23.0	37.2
$x_{ms;start}$ [cm]	14.5	14.4	13.8	13.8	13.4	14.1
$l_{i;cut}$ [cm]	0.28	0.42	0.98	1.02	1.35	0.72
$t_{i;period}$ [s] (in Fig. 4.4)	139-146	136-146	126-147	125-147	120-149	130-145
$\varphi_{ms;calc}$ [m] for $t_{i;period}$	6.1	6.2	6.4	6.4	6.5	6.3
404 East						t_F
t_i [s]	6	10	23	24	32	17
A_i [m^2]	5.3	2.9	2.9	3.2	23.0	37.2
$x_{ms;start}$ [cm]	6.2	6.0	5.4	5.3	4.9	5.3
$l_{i;cut}$ [cm]	0.30	0.50	1.14	1.19	1.59	1.18
$t_{i;period}$ [s] (in Fig. 4.4)	141-147	133-143	111-134	109-133	97-129	110-127
$\varphi_{ms;calc}$ [m] for $t_{i;period}$	3.3	3.4	3.8	3.8	4.0	3.9

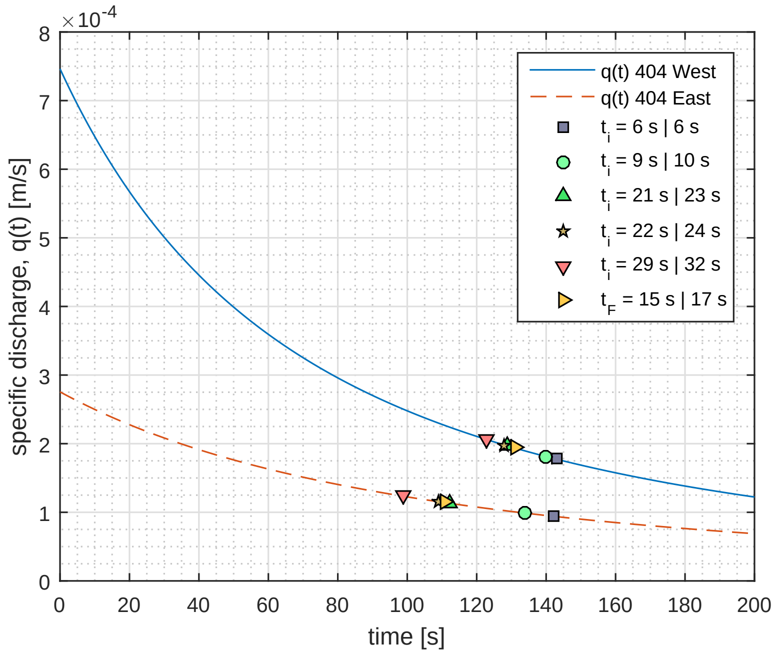

FIGURE 4.4: Calculated specific discharge in time for 404 West and East tunnel, considering both the cutter wheel configuration and the mean infiltration time.

The mean infiltration velocity over the entire tunnel face cannot be greater than the pore water velocity over the entire face, calculated with Darcy's law under quasi static conditions. Just after a cutter tooth has passed the slurry infiltration velocity can be greater than the average pore water velocity as long as the average infiltration velocity over the entire face is equal or smaller than the pore water velocity calculated with Darcy's law with an excess piezometric head of φ_{ms}. For both the 404 West and 404 East tunnel this is the case, see table 4.3.

Comparing the calculated values to the measured values it is concluded that the measured excess piezometric head at the far side of the mud spurt, $\varphi_{ms;data}$ can be estimated well when the determined values of a specific for the TBM are considered. The difference between considering the cutter wheel configuration and the mean infiltration time is small.

4.3 Quasi-static groundwater flow model

In this section a prediction of the excess pore pressure is done with the quasi-static model presented in section 2.5.1. First, a derivation of the α^*-factor is given with which the excess pore pressure at the tunnel face can be calculated. This is followed by a validation with field data from the N/S line and the GHT.

4.3.1 Derivation of the excess pore pressure relation

The excess pore pressure in a unconfined aquifer with homogeneous soil conditions at distance x from the tunnel face can be described by the quasi-static flow model of Bezuijen [9], Eq. (4.6).

$$\varphi = \varphi_0 \left(\sqrt{1 + \left(\frac{x}{R}\right)^2} - x/R \right) \tag{4.6}$$

The most important parameter in this equation is φ_0, since this parameter describes the excess pore pressure at the tunnel face during boring. The excess pore pressure is highest at the tunnel face and it is interesting to investigate a possible relation between the TBM specifications and the relevant parameters of the soil in front of the TBM.

From the measured pore pressures back calculated to the tunnel face it is concluded that there is still mud spurt present after a cutter tooth has passed. The mud spurt increases due to infiltration, but cannot effectively infiltrate faster than the velocity of the TBM. Therefore, it is assumed that the infiltration velocity of the slurry equals the speed of the TBM,

$$v_{slurry} = v_{TBM}. \tag{4.7}$$

Following Darcy's law and assuming quasi-static conditions, the slurry infiltration velocity cannot be greater than the velocity with which the pore water can flow out of the soil [9]. This, in combination with Eq. (4.7) leads to

$$v_{p;Darcy} = v_{TBM}. \tag{4.8}$$

The pore water velocity is calculated following Darcy's law,

$$v_{p;Darcy} = \frac{ki}{n}, \text{ with } i = \frac{\varphi_0}{R}. \tag{4.9}$$

To calculate φ_0 the excess face pressure $\varphi_{ex;face}$ is multiplied by a factor α^*,

$$\varphi_0 = \alpha^* \cdot \varphi_{ex;face}. \tag{4.10}$$

This α^*-factor describes the part of the excess face pressure that is transferred to excess pore pressure [28, 35]. Now, substituting Eq. (4.10) in Eq. (4.9) leads to

$$v_{p;Dacry} = \frac{k\left(\frac{\alpha^* \cdot \varphi_{ex;face}}{R}\right)}{n}. \tag{4.11}$$

Combining Eqs. (4.8) and (4.11) results in a relation for the α^*-factor,

$$\alpha^* = \frac{n}{k} \frac{R}{\varphi_{ex;face}} v_{TBM}, \tag{4.12}$$

and the excess pore pressure at the tunnel face is calculated with

$$\varphi_0 = \left[\frac{n}{k} \frac{R}{\varphi_{ex;face}} v_{TBM} \right] \cdot \varphi_{ex;face} = \frac{n \cdot R}{k} v_{TBM}. \tag{4.13}$$

In Eq. (4.13) n is the porosity of the sand in front of the TBM, k the permeability of the sand in m/s, R the radius of the cutter wheel in m, $\varphi_{ex;face}$ the excess face pressure in m and v_{TBM} the velocity of the TBM in m/s. It has been stated in literature [35] that the α^*-factor is dependent on the configuration and velocity of the TBM, porosity and permeability, which is in accordance with Eq. (4.13).

It is possible however, that the slurry infiltration velocity is smaller or greater than the velocity of the TBM. In the case that $v_{slurry} < v_{TBM}$ the derivation above changes to Eq. (4.14) and when $v_{slurry} > v_{TBM}$ the derivation changes to Eq. (4.15).

$$v_{p;Darcy} < v_{TBM} \;\rightarrow\; \alpha^* < \frac{n}{k}\frac{R}{\varphi_{ex;face}} v_{TBM} \text{ with } \alpha^*_{min} = 1 \tag{4.14}$$

$$v_{p;Darcy} > v_{TBM} \;\rightarrow\; \alpha^* > \frac{n}{k}\frac{R}{\varphi_{ex;face}} v_{TBM} \text{ with } \alpha^*_{min} = 0 \tag{4.15}$$

If the slurry infiltration velocity is smaller than the velocity of the TBM, α^* is 1 since all the build up mud spurt is cut away with each rotation of the cutter wheel resulting in $\varphi_0 = \varphi_{ex;face}$ at the start of slurry infiltration. The right-hand side of Eq. (4.14) is greater than 1 when $v_{slurry} < v_{TBM}$, but the value of α^* can psychically not be greater than 1, see Eq. (4.10). In Eq. (4.15) α^* varies between 0 and 1. The greater the slurry infiltration velocity is compared to the velocity of the TBM the lower the value of α^* is.

4.3.2 Model validation

North/South line validation

An overview of the characteristic values of the permeability and porosity for specific soil layers of the N/S line are given in table 4.4. Only the layers which intersect the cross-sections of the tunnels at the position of the piezometers are provided. The range of values for the permeability are large, between the bottom and the upper value a difference of a factor 10 is seen. The permeability is a difficult parameter to measure accurately, and therefore the range is wide. For the layers in the cross-sections, the horizontal permeability is equal to the vertical permeability, documented in internal documents [39].

TABLE 4.4: Overview of the characteristic values of the permeability and the porosity for specific soil layers of the N/S line [39].

Soil Layer	$k_{lim;bot}$	k_{mean}	$k_{lim;up}$	$n_{lim;bot}$	n_{mean}	$n_{lim:up}$
13	2.7E-04	1.5E-04	2.5E-05	0.33	0.34	0.35
14	5.3E-05	3.0E-05	5.0E-06	0.43	0.44	0.45
17	1.8E-04	1.0E-04	1.7E-05	0.39	0.39	0.39
19	1.8E-06	1.0E-06	1.7E-07	0.50	0.50	0.50
21	1.8E-05	1.0E-05	1.7E-06	0.38	0.39	0.40
24	1.8E-04	1.0E-04	1.7E-05	0.34	0.35	0.36

The TBM bored through multiple soil layers at the piezometer locations, which has several implications. First of all, the quasi-static flow model is designed for homogeneous soils and an unconfined aquifer. The permeability and porosity in front of the TBM are calculated with respect to the present surface area of the layer compared to the total surface area of the cross-section. Please note that this is a rough estimation. The percentages of the different layers for the cross-sections is described in table 4.5.

The results of the excess pore pressures calculations with Eq. (4.13) are presented in table 4.6. The calculated values of $\varphi_{0;calc}$ are compared to the data of the pore pressure sensors $\varphi_{0;data}$ at the tunnel face. Please note that $\varphi_{0;data}$ is back calculated from the piezometer at a certain distance from the tunnel face. The characteristic bottom, mean and upper values from table 4.4 are used in the calculation. Also, the permeability and the porosity are varied such that the best fit is achieved.

TABLE 4.5: Overview of the assumed percentages of soil layers present in the cross-sections from figures A.7a and A.7b.

Soil Layer	% of cross-section			
	404 West	404 East	SS West	SS East
13		0.30	0.10	0.10
14		0.15	0.15	0.15
17		0.55	0.40	0.40
19			0.10	0.10
21	0.10		0.25	0.25
24	0.90			

The results of the different tunnel cross-sections are discussed briefly, starting with the 404 West tunnel. The highest values for the permeability and porosity result in a high value of the pore water velocity. Therefore, the value of α^* is small. Comparing the $\varphi_{0;calc}$ with $\varphi_{0;data}$ it can be stated that the excess pore pressure is underestimated. The mean values of k and n are in better agreement with the measurements. For the upper characteristic values, the pore water velocity is smaller than the velocity of the TBM, resulting in an α^* of 1 and a great overestimation of the excess pore pressure is seen. The closest fit on the measured value equals the mean values of the permeability and the porosity.

For the 404 East tunnel, the best fit is found for the bottom values of the permeability and porosity. The mean values overestimate the excess pore pressures with approximately a factor two and the upper values result in an overestimation of a factor three. Varying k and n close to the bottom values results in the best fit and the excess pore pressures are slightly overestimated. It has to be noted however, that the back-calculation could be inaccurate due to the several soil layers that are bored, since the homogeneous soil criterion is less valid.

The same holds for the tunnels passing the piezometers at the Scheldestraat, SS West and SS East, respectively. Figure A.7a shows a great variation in soil layers and indicate that both tunnels bore through the same layer configuration. For the SS West tunnel the calculated excess pore pressures are overestimated in every scenario and the best fit is found for the bottom values. Considering the SS East tunnel, the excess pore pressures are underestimated in every scenario. It is likely that the back-calculation of the excess pore pressure at the tunnel face from the pore pressure sensors is inaccurate, since it is physically impossible that the excess pore pressure at the face is greater than the excess face pressure at the tunnel face. In Eq. (4.6), φ is measured, R is fixed for the tunnel, leaving the distance x of the sensor to the tunnel face the parameter to investigate for errors. The available data states that the X and Y coordinate for the pore pressure sensors are the same for every sensor. Deviations in placing pore pressure sensors is not uncommon, and therefore the provided X and Y coordinates could be inaccurate. For example, if it is assumed that the pore pressure sensors are off by 1 meters in the direction of the East tunnel, more satisfying results are achieved for both the West and East tunnel, summarized in table 4.7. Another possibility is of course, that the distances of the pore pressure sensors are correct and that the quasi-static model of Bezuijen [10] cannot be used in this situation due to the fact that the cross-section of the tunnels consists of several different soil layers. This option is likely to be correct.

TABLE 4.6: Calculation results of Eq. (4.13) for different input values, compared with measured field data for the N/S line.

	404 West	404 East	SS West	SS East
General				
Ring	258	257	64	65
t_{boring} [min]	49	49	50	49
v_{TBM} [mm/s]	0.51	0.51	0.50	0.51
$\varphi_{ex;face}$ [m]	14.48	10.31	6.81	6.94
i [-]	4.21	3.00	1.98	1.96
$\varphi_{ex;sensor}$ [m]	-0.71	-0.60	-0.92	0.37
$x_{eq;sensor}$ [m]	3.33	1.47	2.30	2.77
bottom values				
k [m/s]	1.6E-04	1.9E-04	1.1E-04	1.1E-04
n [-]	0.35	0.38	0.40	0.40
$v_{p;Darcy}$ [mm/s]	1.95	1.49	0.55	0.56
α^* [-]	0.26	0.34	0.90	0.90
$\varphi_{0;calc}$ [m]	3.79	3.53	6.14	6.25
$\varphi_{0;data}$ [m]	6.58	3.79	4.45	7.66
difference [%]	1.74	1.07	0.73	1.23
mean values				
k [m/s]	9.1E-05	1.1E-04	6.2E-05	6.2E-05
n [-]	0.35	0.38	0.40	0.40
$v_{p;Darcy}$ [mm/s]	1.08	0.82	0.30	0.31
α^* [-]	0.47	0.62	1	1
$\varphi_{0;calc}$ [m]	6.83	6.42	6.81	6.94
$\varphi_{0;data}$ [m]	6.58	3.79	4.45	7.66
difference [%]	0.96	0.59	0.65	1.10
upper values				
k [m/s]	1.56E-05	1.8E-05	1.1E-05	1.1E-05
n [-]	0.35	0.39	0.41	0.41
$v_{p;Darcy}$ [mm/s]	0.18	0.14	0.05	0.05
α^* [-]	1	1	1	1
$\varphi_{0;calc}$ [m]	14.48	10.31	6.81	6.84
$\varphi_{0;data}$ [m]	6.58	3.79	4.45	7.66
difference [%]	0.45	0.37	0.65	1.12
fit k & n within range				
k [m/s]	9.1E-05	1.8E-04	1.1E-04	1.1E-04
n [-]	0.35	0.38	0.40	0.40
$v_{p;Darcy}$ [mm/s]	1.08	1.37	0.55	0.56
α^* [-]	0.47	0.37	0.91	0.91
$\varphi_{0;calc}$ [m]	6.83	3.85	6.23	6.34
$\varphi_{0;data}$ [m]	6.58	3.79	4.45	7.66
difference [%]	0.96	0.99	0.71	1.21

TABLE 4.7: Calculation results of Eq. (4.13) with adjusted sensor distance to the TBM for the SS West and SS East tunnel of the N/S line.

	SS West	SS East
$x_{eq;sensor}$ [m]	3.33	1.77
$\varphi_{0;data}$ [m]	5.58	6.01
bottom values		
$\varphi_{0;calc}$ [m]	6.14	6.25
difference [%]	0.91	0.96
mean values		
$\varphi_{0;calc}$ [m]	6.81	6.94
difference [%]	0.82	0.87
upper values		
$\varphi_{0;calc}$ [m]	6.81	6.84
difference [%]	0.82	0.88
fit k & n within range		
$\varphi_{0;calc}$ [m]	6.23	6.34
difference [%]	0.90	0.95

Green Heart Tunnel validation

Due to the greater dimensions of the GHT it is interesting to check whether this approach is also valid when greater dimensions are considered. The piezometer WD1, shown in figure A.8, is used to back-calculate the excess pore pressures from the sensor to the face. Piezometer WD1 is chosen since the depth of the sensor (-27.2 m NAP) is in agreement with the depth of the TBM axis (-27 m NAP). Unfortunately, only TBM data is available from a distance of 9 meters passed the pore pressure sensor. The input parameters and the results are presented in table 4.8.

TABLE 4.8: Calculation results of Eq. (4.13) compared with measured field data for the GHT.

Ring	2117	2118	2119
t_{boring} [min]	51	52	51
v_{TBM} [mm/s]	0.66	0.65	0.66
$\varphi_{ex;sensor}$ [m]	1.3	1.2	1.1
$x_{eq;sensor}$	9.7	11.7	13.6
p_0 [kPa]	270	270	270
s [kPa]	311	311	311
Δs [kPa]	41	41	41
$\varphi_{ex;face}$ [m]	4.2	4.2	4.2
i [-]	0.56	0.56	0.56
k [m/s] [1]	4.0E-04	4.0E-04	4.0E-04
n [-]	0.35	0.35	0.35
$v_{p;}$ [mm/s]	0.56	0.56	0.56
α^*	1	1	1
$\varphi_{0;calc}$ [m]	4.2	4.2	4.2
$\varphi_{0;data}$ [m]	3.8	4.0	4.4
difference [%]	0.92	0.97	1.06

For the three rings considered, the velocity of the TBM is slightly bigger than the average pore water velocity. Therefore, α^* is 1. In the determination of the velocity of the pore water a permeability of 4.0E-4 m/s [1] and a porosity of 0.40 is considered. The values seem to be in agreement with the calculated values $\varphi_{0;calc}$, although an increasing difference is seen with increasing sensor distance from the tunnel face.

Limitations

In this section the limitations of this approach are discussed. For each cross-section the usability of the quasi-static model is elaborated to check whether the model can theoretically be applied and this is coupled to the results of each cross-section in the conclusion. This is done for both the N/S line and the GHT.

As mentioned in section 2.5.1, the quasi-static model can be used when:

1. The cross-section consists of homogeneous soil;
2. The tunnel is bored in an unconfined aquifer;
3. No plastering takes place during boring;
4. No influence from the surface on the behavior of the groundwater flow;
5. Flow from the mixing chamber is distributed evenly over the tunnel face;
6. Excess pore pressure calculated in front of the tunnel.

TABLE 4.9: Scores overview of the cross-sections with respect to the usability of the quasi-static groundwater flow model.

Cross-section	1	2	3	4	5	6
404 West	+	+	+/-	++	++	+/-
404 East	+/-	- -	+/-	++	+/-	+/-
SS West	- -	- -	+/-	++	-	+/-
SS East	- -	- -	+/-	++	-	+/-
GHT	+/-	++	+/-	++	+	+/-

Table 4.9 gives an overview of the scores of the different cross-section considering the statements regarding the quasi-static model. The cross-sections from figures A.7 and A.8 are used in determining the scores. Cross-section 404 West scores fine on the condition of homogeneous soil and unconfined aquifer, since the cross-section mainly consists of the Third Sand Layer and this layer extents to a great depth. Also, the flow is distributed good onto the entire face due to this homogeneity and due to the fact that the $q_{av;cw} \approx q_{av;F}$, see section 4.2. The 404 East cross-section scores average on the homogeneity, since several different layers are bored, but all the layers consist of sandy material. A clear semi-confined aquifer is present and therefore the score is poor for this statement. Due to the several layers, the flow is not evenly distributed over the face, resulting in an average score. The SS West and East tunnel, respectively, have the same scores since the cross-section is the same. Due to the fact that the Eemclay layer is present in combination with the presence of multiple other layers, the score is poor for homogeneous soil. In this case, a semi-confined situation is present, leading to a poor score as well. Due to the multiple layers, the flow is not evenly distributed over the tunnel face, leading to a low score for this statement.

The GHT scores average on the homogeneity of the soil in front of the TBM, because multiple layers are present, but are all sandy soils. The GHT is bored in an unconfined aquifer, resulting in a good score. Due to the multiple sand layers, the flow is distributed fine instead of good over the face. Point 2, 3 and 6 have the same score for each cross-section, since no plastering is assumed, no influence of the surface on the behavior of the flow is expected and the piezometers are located at the side of the TBM instead of in front of the TBM.

Sensitivity analysis

The parameters in Eqs. (4.9) and (4.13) are varied within specific ranges to visualize how the formulas behave. It is assumed that the α^* is 1 when the average pore water velocity is smaller than the velocity of the TBM, because no mud spurt is present after a cutter tooth has passed. An overview of the parameter values used in this analysis is presented in table 4.10.

TABLE 4.10: Parameter input values for the sensitivity analysis of the α^*-factor.

Parameter	Min.	Ref.	Max .
k [m/s]	1.0E-05	1.0E-04	1.0E-03
n [-]	0.25	0.35	0.5
R [m]	2.5	5	10
$\varphi_{ex;face}$ [m]	2.5	15	25
v_{TBM} [mm/s]	0.5	1.0	2.0

Eqs. (4.9) and (4.13) consist of linear relationships and therefore the permeability has the greatest effect on the result, since the difference between the minimal and maximum value is a factor 100. The minimum, mean and maximum pore water velocities are calculated with increasing permeability and compared with the velocity of the TBM. For example, the minimum pore water velocity is calculated with parameters from table 4.10 such that the minimum pore water velocity is achieved. The TBM velocity is increased to visualize the effect of increasing the boring velocity with respect to the excess pore pressure creation at the tunnel face. The result of the sensitivity analysis is shown in figure 4.5.

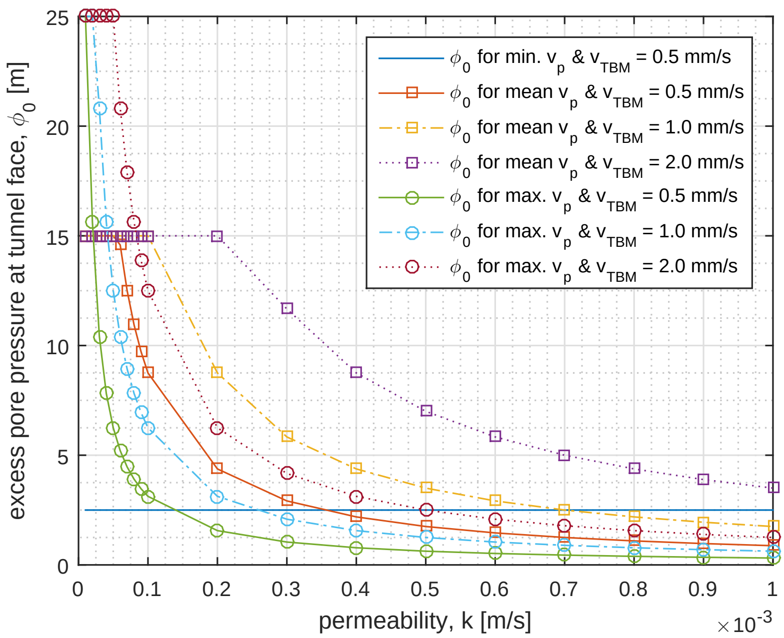

FIGURE 4.5: Sensitivity analysis for the α^*-factor for increasing permeability and TBM velocity.

For the minimum pore water velocity $v_p < v_{TBM}$ for every permeability considered, resulting in an α^* of 1 and a constant φ_0 of 2.5 m with increasing permeability. Only the lowest TBM velocity is considered, since at this lowest velocity α^* is already 1. For the mean v_p it is seen that $v_p > v_{TBM}$ is reached at a permeability of 6.0E-05 m/s for v_{TBM} is 0.5 mm/s. With increasing v_{TBM} the excess pore pressure increases, considering the same permeability. Also, the gradient of decreasing excess pore pressure gets smaller as v_{TBM} increases, especially in the lower permeability range. Both these effects, to a larger extend, are also seen when the maximum v_p

is considered. Higher permeability results in a greater mud spurt and leads to a smaller excess pore pressures in front of the face, which is consistent with the results. It is recommended that $v_p > v_{TBM}$ during boring, since this results in a mud spurt and a lower excess pore pressures at the tunnel face.

From figure 4.5 it can be concluded that the excess pore pressure at the tunnel face is smaller when the velocity of the TBM is decreased. It is possible to bore with very low TBM velocities to minimize the excess pore pressure at the tunnel face, but at a certain point this method is simply too expensive. Stated above is elaborated with an example.

The daily user costs of a slurry TBM are approximately €70k. The number of rings bored in this example is 35, which equals a total distance of 52.5 m ($w_{ring} = 1.5\ m$). It is assumed that the building time is independent from the boring time and therefore the building time is assumed constant. The costs and the excess pore pressures at the tunnel face are calculated considering the velocity of the TBM equal to the 404 West tunnel. The TBM velocity is decreased by with a factor 5, and the increase in costs and decrease in excess pore pressures are calculated. The results are presented in table 4.11.

TABLE 4.11: Numerical example of increasing boring costs when decreasing TBM velocity.

v_{TBM} [mm/s]	0.51	0.1
t [days]	2.5	7.3
Costs	€175k	€510k
α^* [-]	0.47	0.09
φ_0 [m]	6.8	1.3

A decrease of TBM velocity leads to a proportional decrease of excess pore pressure at the tunnel face. The costs increase with a factor 3, approximately. Decreasing the TBM velocity might be more expensive than other mitigating measures. Whether this is the case is project dependent.

4.3.3 Conclusions quasi-static groundwater flow model

A derivation of the α^*-factor is provided and the calculated values are compared to the measured values in the field. Coupling the scores from table 4.9 to the comparison of the calculated and measured values it is concluded that the 404 West tunnel provides the best results. Due to the high scores it is also more likely that the back-calculated excess pore pressures at the tunnel face from the piezometers are accurate. The 404 East tunnel provides fine results when the parameters k and n are fitted on the back-calculated excess pore pressure at the face. For SS West and East, respectively, it seem unlikely that the excess pore pressures at the face are calculated accurately. For the GHT the scores indicate that an estimation can be done, but too little information regarding the distribution of the parameters k and n are available to validate this statement.

In order to achieve excess pore pressures which are lower than the excess face pressure used during boring, the average pore water velocity should be greater than the velocity of the TBM. The greater the difference, the greater the mud spurt depth and therefore the greater the difference between the excess face pressure and the excess pore pressure at the tunnel face. For additional validation it is recommended that piezometers are installed in future projects. In this way excess pore pressure predictions with Eq. (4.13) can be validated with measured field data.

4.4 Transient groundwater flow model

In this section a prediction of the excess pore pressures with a transient flow model for a semi-confined aquifer is conducted. First, the formula from the literature review is provided. Then, the values of the input parameters are elaborated. Special attention is given to the calculation of the discharge and a comparison is made between considering the cutter wheel configuration and the average infiltration time t_F. A validation is done combining the calculation results with the measured field data for the N/S line 404 West and East tunnel, respectively. The SS West and East tunnel are not considered, because an aquitard crosses the tunnel cross-section and therefore the model is not valid. The GHT is not considered, because the cutter wheel configuration could not be retrieved and not enough information is available with respect to the input parameters.

The excess pore pressure in a semi-confined aquifer at distance x from the tunnel face is described by the transient flow model of Broere [18],

$$\varphi = \varphi_\infty + \frac{Q\lambda}{4kH}\left[\operatorname{erfc}\left(\frac{xu}{2\sqrt{t}} + \frac{\sqrt{t}}{u\lambda}\right)\exp\Big(\frac{x}{\lambda}\Big) - \operatorname{erfc}\left(\frac{xu}{2\sqrt{t}} - \frac{\sqrt{t}}{u\lambda}\right)\exp\Big(-\frac{x}{\lambda}\Big)\right], \tag{4.16}$$

in which $u = \sqrt{S_s/k}$ and $\lambda = \sqrt{kH\tilde{c}}$. In this formula the discharge is related to the slurry infiltration processes.

4.4.1 Model input parameters

The cutter wheel specific discharge is determined following to the same principles as in section 4.2. After a cutter tooth has passed, mud spurt is still present and this mud spurt depth $x_{ms;start}$ is the starting point of slurry infiltration. This $x_{ms;start}$ is coupled to a certain time required to achieve this mud spurt when fresh soil is considered. Therefore, the starting point of infiltration during boring is not at t = 0 s, but at several points on the graph, depending on the amount of cutting teeth present in that specific section. The slurry infiltration velocity and the specific discharge decrease with increasing slurry infiltration depth. The starting points of the specific discharges are plotted in figure 4.4 for the 404 West and 404 East tunnel.

The discharge Q_{cw} in m^3/s is calculated for each partial surface of the cutter wheel as $Q_{cw} = q_{cw} \cdot A_i$. Note that A_i is divided into pieces equal to the length of vector t_i, e.g. for $t_i = 6\ s$, A_i is divided into seven equal parts. Each part is multiplied by the specific discharge belonging to a specific time. Dividing the cutter wheel into smaller parts would lead to more accurate results. It is assumed that no over cutting of the cutter teeth into other sections occur. Above is summarized in Eqs. (4.17) to (4.19) and the values regarding the infiltration times and cutter wheel partial surfaces are summarized in table 4.3.

$$A_i(t_i) = \frac{A_i}{(t_i+1)} \tag{4.17}$$

$$Q_{cw}(i,t_i) = q_{cw}(1+i)\cdot A_i(t_i) \text{ for } i = [0:t_i] \tag{4.18}$$

$$\begin{aligned} Q_{cw} = \sum_{i=0}^{t_{i;1}} Q_{cw}(1+i, t_{i;1}+1) + \sum_{i=0}^{t_{i;2}} Q_{cw}(1+i, t_{i;1}+1) + \sum_{i=0}^{t_{i;3}} Q_{cw}(1+i, t_{i;3}+1) \\ + \sum_{i=0}^{t_{i;4}} Q_{cw}(1+i, t_{i;4}+1) + \sum_{i=0}^{t_{i;5}} Q_{cw}(1+i, t_{i;5}+1) \end{aligned} \tag{4.19}$$

The mean infiltration time is calculated with Eq. (2.5). With the mean infiltration time t_F, the rotation time t_r and the cutting depth per rotation l_{cut}, the mean cutting depth per t_F is calculated. The mean cutting depth is subtracted from the maximum mud spurt length $x_{ms;max}$ and this is the starting point of the slurry infiltration. The mean specific discharge is determined for the mean infiltration period and the discharge over the entire cutter wheel in m^3/s is calculated in Eq. (4.20). For additional information please see table 4.3 in section 4.2.

$$Q_F = q_{av;F} \cdot A_{cw} \tag{4.20}$$

The values of the input parameters in Eq. (4.16) are divided into two groups. The first group is independent of the behavior of the TBM, e.g. the height of the aquifer. The second group is dependent on the behavior of the TBM, e.g. t_{boring}. The values of the input parameters are summarized in table 4.12. It is concluded that for both tunnels considered, the cutter wheel specific discharge calculation is similar to the mean infiltration time discharge calculation. Please note that the Q in Eq. (4.16) is per unit width of the aquifer (m^2/s), and both Q_{cw} and Q_F are calculated as the discharge of the entire face (m^3/s). Therefore, these values need to be divided by the average width of the face, which is $\sqrt{A_{cw}} \approx 6.1m$, before being used in Eq. (4.16). Also, a minus sign should be assigned to the discharge because water is added in stead of withdrawn from the system [19].

TABLE 4.12: Overview of the model input parameters for the transient groundwater flow model.

Parameter Eq. (4.16)	404 West	404 East	From
Independent			
k [m/s]	1.0E-04	5.0E-05	Field data
S_s [m^{-1}]	3.5E-04	8.0E-04	Assumption/Literature [6]
H [m]	85	12	Field data
$\tilde{c}$ [s]	5.0E+08	1.0E+08	Field data
φ_∞ [m]	-3.5	-3.1	Field data
x [m]	6.3 - 90	4.5 - 55	
Dependent			
t_{boring} [min]	49	49	Eq. (4.2)
Q_{cw} [m^3/s]	6.9E-03	4.2E-03	Eq. (4.19)
$Q_{cw;input}$ [m^2/s]	-1.1E-03	-6.8E-04	$-Q_{cw}/\sqrt{A_{cw}}$
V_{cw} [m^3]	20.4	12.2	$Q_{cw} \cdot A_{cw} \cdot t_{boring}$
Q_F [m^3/s]	6.9E-03	4.2E-03	Eq. (4.20)
$Q_{F;input}$ [m^2/s]	-1.1E-03	-6.9E-04	$-Q_F/\sqrt{A_{cw}}$
V_F [m^3]	20.2	12.3	$Q_F \cdot A_{cw} \cdot t_{boring}$
V_{pores} [m^3]	19.5	21.1	$A_{cw} \cdot w_{ring} \cdot n$

The values presented in table 4.12 are used to calculate the excess pore pressures at a distance x from the tunnel face. The calculation results combined with the measurements are presented in the next section.

4.4.2 Model validation

In this section a validation is done for the transient groundwater flow model for the N/S line project. First, the calculation results are compared with the measured field data for the 404 West and East tunnel, respectively. After that, the limitations are discussed. Then, a sensitivity analysis is conducted for the 404 West tunnel considering the cutter wheel specific discharge.

In figures 4.6 and 4.7 the piezometers are situated at approximately 6.3 and 4.5 meter from the tunnel axis, respectively. Therefore, the graphs do not start at $x = 0\ m$. The TBM direction with respect to the x-axis is from *right to left*, indicating that the TBM is boring towards the piezometers.

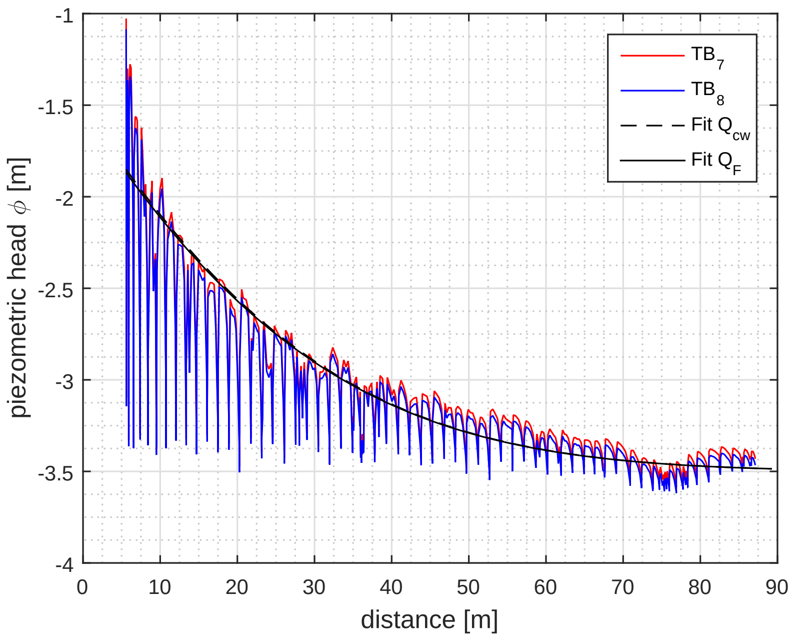

FIGURE 4.6: Excess pore pressure prediction with the transient flow model for the 404 West tunnel (ring 202 - 258) compared with field measurements.

For the 404 West tunnel it is seen that the excess pore pressure is predicted good from approximately 10 meters until 35 meters from the sensor, see figure 4.6. At a greater distance, a slight underestimation is seen. Closer to the sensor the excess pore pressures are underestimated to a greater extend. When the graph is extended to the tunnel face (x = 0 m), the model provides an excess pore pressure in the range of 22 kPa. The back-calculation from the field measurements in section 4.1 resulted in an excess pore pressure of approximately 65 kPa at the tunnel face. The conclusion is that the excess pore pressure is underestimated by approximately a factor of two-and-a-half. The results of the cutter wheel specific discharge and the mean infiltration time shown similar results, which corresponds with section 4.2.

For the 404 East tunnel it is seen, in figure 4.7, that the excess pore pressure is predicted good from approximately 5 meters to 20 meters considering both the cutter wheel configuration and the mean infiltration time. An underestimation is seen close to the sensor. Extending the graph to the tunnel face leads to an excess pore pressure in the range of 25 - 30 kPa. The back-calculation resulted in a value of approximately 38 kPa. The excess pore pressures are also underestimated, but to a smaller extend than seen at the 404 West tunnel.

The discharge is calculated with the assumption that mud spurt is still present after a cutter tooth has passed. This assumption is valid, see section 4.1. To fit the 404 East tunnel the permeability is equal to $k_{s;fit}$ in table 3.5 in the numerical integration of Eq. (2.16). The value for the specific storage S_s indicates a fine sand [6].

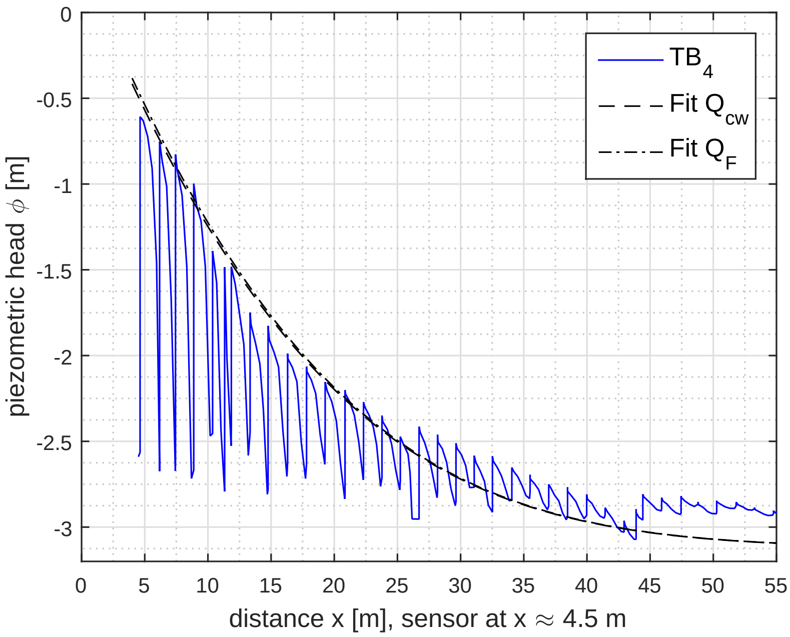

FIGURE 4.7: Excess pore pressure prediction with the transient flow model for the 404 East tunnel (ring 224 - 258) compared with field measurements.

Limitations

The model is designed to model drainage of water through a well, but in stead the model is used to determine the rise of excess pore pressures when water is added to the system. It is likely that the soil behaves different when subjected to addition in stead of drainage. This is not further investigated in this research.

The transient flow model of Broere [18] is used to fit the maximum recorded pore pressures in the aquifer. It is also possible to calculate the rise of excess pore pressure in time for a fixed distance from the tunnel face. Conducting this calculation and comparing the results with the measured pore pressures in the field is recommended for future research. This way it can be determined whether the rise of excess pore pressure in time can be predicted accurately when considering the calculated values of a.

Sensitivity analysis

A sensitivity analysis is conducted to visualize the impact of changing parameter values on the results. In this analysis the 404 West tunnel is considered with the cutter wheel specific discharge. The range of values used are presented in table 4.13. One parameter is varied while keeping the other parameters at the reference value. The permeability varies within the range which is provided in internal documents of the N/S line [39]. The specific storage is chosen such that the range varies between moderately fine sand to silty sand.

TABLE 4.13: Parameter values for sensitivity analysis of the transient groundwater flow model.

Parameter	Min.	Ref.	Max.
k [m/s]	1.7E-05	1.0E-04	1.8E-04
S_s [m^{-1}] [6]	1.0E-04	3.5E-04	1.0E-03
H [m]	45	85	125
$\tilde{c}$ [s]	5.0E+04	5.0E+08	5.0E+11

The results of the sensitivity analysis are presented in figures 4.8 and 4.9. The permeability and the specific storage are especially sensitive to change and in combination with the difficulty to determine this parameters from a desk study it is likely that errors would occur due to this parameters. The height of the aquifer is quite easy to determine accurately (through cone penetration tests) and therefore it is less likely errors will be encountered. The hydraulic resistance has a asymptotic value. The lower the value, the higher the permeability of the aquitard on top of the aquifer, resulting in lower excess pore pressures. It is a difficult parameter to determine accurately from a desk study since the permeability of the aquitard is needed in combination with the thickness of the aquitard The permeability, specific storage and the hydraulic resistance can be determined with pump-tests and laboratory tests (e.g. constant head test). It is recommended to conduct such tests when there is a critical passage in the trajectory. In an early stage of the project it is difficult to use this model due to the great number of parameters. However, if pump-tests and laboratory tests are conducted to accurately determine the values the model is likely to provide good results [18].

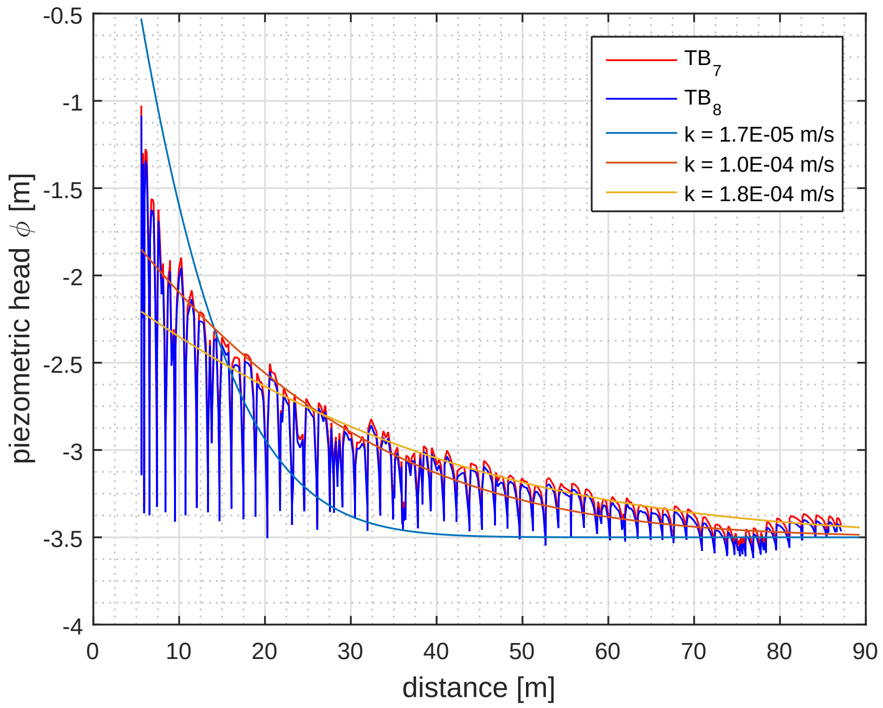

(A)

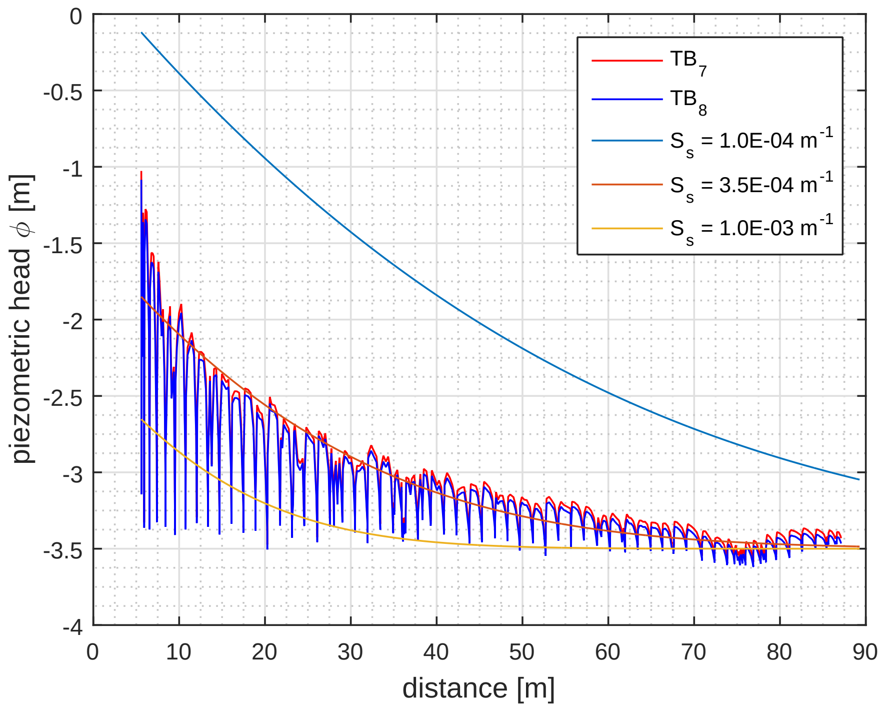

(B)

FIGURE 4.8: Sensitivity analysis of the transient groundwater flow model, part 1: permeability (A) and specific storage (B).

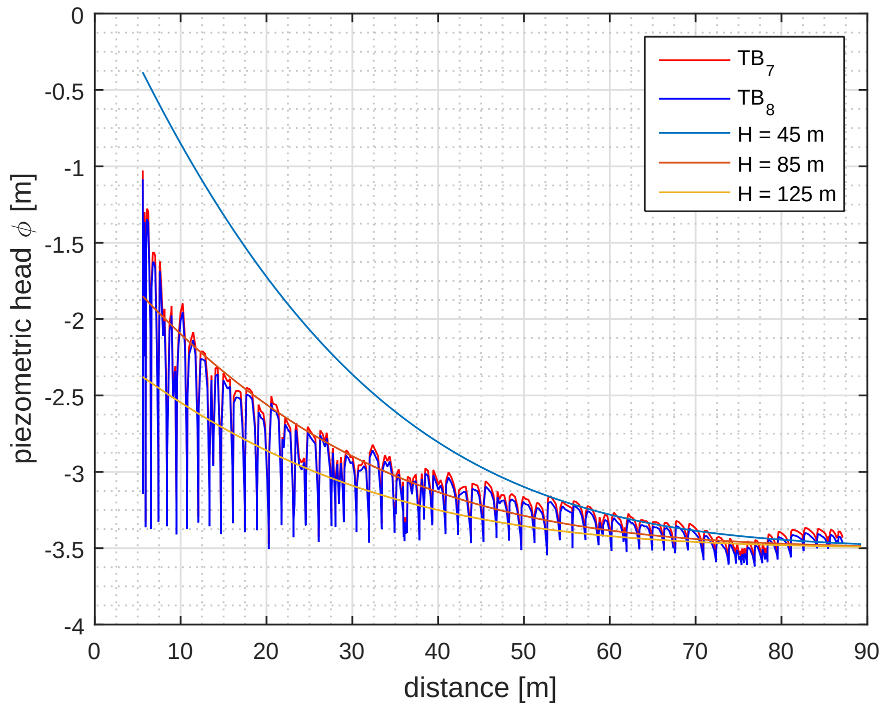

(A)

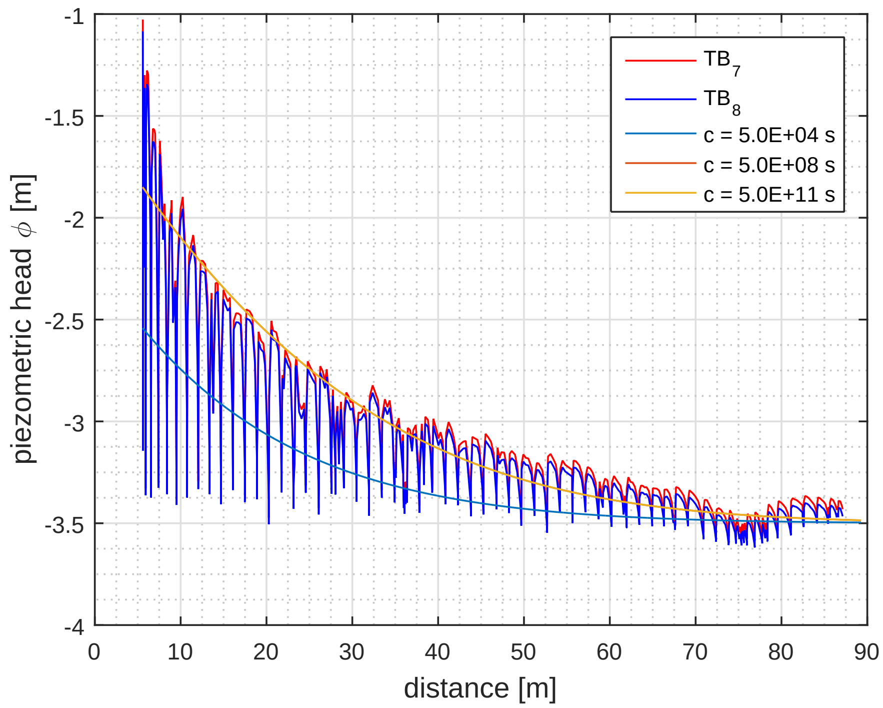

(B)

FIGURE 4.9: Sensitivity analysis of the transient groundwater flow model, part 2: height aquifer (A) and hydraulic resistance (B).

4.4.3 Conclusions transient groundwater flow model

The transient groundwater flow model can be used to predict excess pore pressures in front of a TBM [18]. In this section a prediction for the 404 West and 404 East tunnel for the N/S line are presented. A good fit is shown from a distance of 10-35 meters for the 404 West tunnel and 5-20 meters for the East tunnel. For the 404 West tunnel the difference between the measured excess pore pressure and the prediction with this model is approximately a factor two-and-a-half. For the 404 East tunnel the difference is approximately a factor 0.3.

The specific discharge is calculated by multiplying the slurry infiltration velocity by the porosity of the soil in front of the tunnel. The decrease of the specific discharge in time depends on the value of a. In this analysis the determined values of a from field data are used and show good results for both the 404 West and 404 East tunnel. The discharge taking into account the cutter wheel configuration is compared to the discharge calculated with the mean infiltration time t_F and shows similar results. This could indicate that the mean infiltration time can be used whenever mud spurt is present during boring, but this statement should be validated with other projects.

The transient groundwater flow model is sensitive to especially the permeability and the specific storage. Accurate determination of the permeability of an aquifer is difficult from desk study [38], but can be determined accurately with a pump-test and/or laboratory tests. The same statement holds for the determination of the specific storage and the hydraulic resistance of the overlying aquitard. Due to the number and sensitivity of the parameters present in the model it is not likely that an accurate prediction of the excess pore pressures at the tunnel face can be given at an early stage of a project. Extensive soil investigation is required to accurately determine the parameter values. Due to the variability of soil it is also recommended to conduct the soil investigation at the location of the critical passage.

4.5 Conclusions

From field measurements the excess pore pressure is back-calculated to the tunnel face and compared to the excess face pressure used during boring. For the North/South (N/S) line the back-calculated pressure is smaller than the excess face pressure. It is therefore concluded that mud spurt is present during boring. For the Green Heart Tunnel (GHT) it is concluded that no mud spurt is present during boring, since the excess pore pressure is equal to the excess face pressure. The pore pressure build up is similar to reference projects from existing literature [9, 10, 18, 28] and for both the N/S line and the GHT a decrease in excess pore pressure is seen after boring has stopped. This decrease is the result of the mud spurt (slurry infiltration) and plastering (external filter cake formation) processes. The decrease in pore pressure is slower than is seen in the laboratory experiments, which indicates that the column infiltration test results cannot be used directly in the groundwater flow models.

With the determined values of a and x_{max} in Chapter 3 an investigation is done whether the excess piezometric head at the far side of the mud spurt, φ_{ms}, can be calculated. For this analysis the 1-dimensional groundwater flow model of Bezuijen is used, which is valid since small distances from the tunnel face (in the order of meters) are considered [13]. Considering both the cutter wheel configuration and the mean infiltration time, the specific discharge is calculated. With this discharge φ_{ms} is determined. The cutter wheel configuration and mean infiltration time show similar results. In quasi-static conditions, the infiltration velocity of the slurry cannot be greater than the pore water velocity calculated with Darcy's law [10]. It has been shown that both calculation methods result in an average slurry infiltration velocity smaller than calculated with Darcy's law.

Considering quasi-static conditions a relation is derived to determine the excess pore pressure at the tunnel face, see Eqs. (4.21) and (4.22). The TBM specification, as well as the parameters of the soil in front of the TBM, are incorporated in this relation. For both $v_{slurry} < v_{TBM}$ and $v_{slurry} > v_{TBM}$ a relation is derived. The excess pore pressure at the tunnel face is calculated with Eq. (4.23).

$$v_{p;Darcy} < v_{TBM} \;\rightarrow\; \alpha^* < \frac{n}{k}\frac{R}{\varphi_{ex;face}} v_{TBM} \text{ with } \alpha^*_{min} = 1 \tag{4.21}$$

$$v_{p;Darcy} > v_{TBM} \;\rightarrow\; \alpha^* > \frac{n}{k}\frac{R}{\varphi_{ex;face}} v_{TBM} \text{ with } \alpha^*_{min} = 0 \tag{4.22}$$

$$\varphi_0 = \alpha^* \cdot \varphi_{ex;face} \tag{4.23}$$

The calculated values from Eq. (4.23) are compared with the measured field data. The more or less homogeneous cross-section of the N/S line (404 West tunnel) is best in agreement with the measurements. The calculated value is approximately 4% larger than the measured value. For the GHT the slurry infiltration velocity is smaller than the TBM velocity, resulting in α^* is 1. This is in agreement with the measurements. To validate Eq. (4.23) more projects should be considered. Due to the limit availability of data from other projects this is not done within this research. From the sensitivity analysis it is concluded that the permeability has a great influence on the slurry infiltration velocity and therefore on the magnitude of the excess pore pressure at the tunnel face. To ensure an excess pore pressure lower than the excess face pressure during boring, the pore water velocity should be greater than the velocity of the TBM. When this is the case, mud spurt is formed during boring and a pressure drop is initiated after a cutter tooth has passed. Eq. (4.23) can serve as a tool in determining whether or not mud spurt is present in front of the TBM during boring.

The transient flow model can be used to predict excess pore pressures in front of a TBM, which is in accordance with existing literature [18]. From a distance of approximately 5 to 10 meters from the tunnel face a fine prediction is seen. Close to the tunnel face the excess pore pressure is underestimated. The calculated discharge specific for the cutter wheel is compared to the discharge calculated with the mean infiltration time t_F and shows similar results. If the mud spurt is present after a cutter tooth has passed it is possible to use the mean infiltration time t_F in stead of taking the cutter wheel configuration into account. Please note that this similarity is only shown in the case that mud spurt is present after a cutter tooth has passed and only shown for the N/S line project. It is therefore not necessarily applicable in case that all the mud spurt is cut away with every passage of the cutter tooth. In all cases, a suitable value of a needs to be determined in order to calculate the discharges accurately.

The transient flow model is especially sensitive to the permeability and the specific storage of the aquifer. Due to the number and sensitivity of the parameters present in the model, it is not likely that an accurate prediction of the excess pore pressures at the tunnel face can be given with only a desk study. It is therefore concluded that the permeability, specific storage, hydraulic resistance of the aquitard and the height of the aquifer should be determined by field tests (e.g. pump-tests and cone penetration tests) and laboratory test (e.g. constant head test). With accurate parameter values it is possible to calculate the excess pore pressures accurately, especially at a certain distance from the tunnel face.

Chapter 5

Discussion

This chapter provides additional explanation on the choices made in this research. It explains the choices for the slurry infiltration formulas and groundwater flow models. Furthermore, it focuses on the aspects that could influence the laboratory results. Also, the assumptions made in the calculations are elaborated as well as the limitations of this research.

5.1 Slurry infiltration formulas and groundwater flow models

- To model the slurry infiltration an idealized pore channel is considered. It is assumed that the hydraulic diameter of the channel equals the d_{10} value of the sand in which the slurry infiltrates [30]. Other values for the hydraulic diameter are also used in existing literature [26], but the method described above is used in this research due to its simplicity and accuracy in existing literature [16].
- The geology at the North/South (N/S) line consists of a variety of Holocene and Pleistocene layers. Due to the heterogeneity of the subsoil, in combination with the tunnel trajectories, the groundwater flow model by Broere [18] for a semi-confined aquifer seems most suitable [18, 38]. However, this groundwater flow model is designed for drainage [19] and in this analysis it is used to add water to the aquifer. Therefore, a minus sign is assigned to the discharge. The soil reacts slightly different to addition of water compared to abstraction, but this effect is not investigated in this research.
- For small distances to the tunnel face (in the order of meters) the quasi-static groundwater flow model for an unconfined aquifer can be used in a semi-confined aquifer [10]. For the heterogeneous cross-sections the average permeability and porosity are calculated with respect to their surface area in the cross-section. The calculation results for the heterogeneous cross-section are likely to be inaccurate, which is expected since this model is not designed for these soil conditions. For more homogeneous cross-section the results are fine when compared to the measured data.
- The transient flow model of Broere [18] is especially sensitive to the permeability and the specific storage of the aquifer. When this model is used, accurate values of these parameters are necessary. These parameters are difficult to determine from a desk study and therefore field and laboratory tests are required, respectively.

5.2 Aspects influencing laboratory results

- The laboratory tests have been conducted with manually composed sand approximating the Third Sand Layer. This sand is a mixture of five different sands. The sieve curves of the composed sand and the Third Sand Layer are similar, but the finest fraction is missing in the composed sand mixture. During mixing of the sand a powder fluttered through the air. It is assumed that the finest fraction is missing due to the mixing of the sands. Finer sand leads to a smaller slurry infiltration depth [30], and this could implicate that the slurry infiltration depth from the laboratory is an overestimation. The 404 East tunnel bored mainly through the Second Sand Layer, which makes laboratory experiments with sand approximating the Second Sand Layer also valuable. Unfortunately, it was not possible to compose such a mixture due to unavailable materials at the laboratory.

- Mixing of the bentonite slurry is done with a Hobort mixer, which is an ordinary mixer and the only available mixer in the laboratory. However, in mixing bentonite slurries it is more appropriate to use a high shear mixer. This type of mixer ensures that all the clay platelets are separated, resulting in maximal uptake of water and a higher viscosity of the slurry. In order to reach the maximum shear strength, the slurry has to stiffen for a number of hours, which varied from 8 to 24 hours in this research. No data of the shear strength of the slurry used in the Nth/S line project is found [39], and therefore no comparison between the measured shear strength in the laboratory and the project was possible. A shear strength which is too high or too low has a great influence on the slurry infiltration depth.
- Due to limitations of the laboratory equipment the column infiltration tests are conducted at lower excess pressures than used during boring of the tunnels. The 404 West tunnel is bored with an excess face pressure of approximately 140 kPa and the laboratory experiments are conducted with an excess pressure of approximately 25 kPa. At higher excess pressures leakage of the column infiltration apparatus occurred, leading to inaccurate results.
- The value of a determined in the laboratory (a = 11 s) cannot be used directly in the groundwater flow models. From figure 3.12 it is clear that the value of a determined in the laboratory is significantly smaller than the value of a determined with field measurements, e.g. for the 404 West tunnel a = 136 s. When the value of a from the laboratory is used, the drop of piezometric head goes too quick. The difference in magnitude of a can be explained by the fact that the flow around the TBM is different than the flow in the column infiltration apparatus. The value of a for the TBM also depends on the permeability of the slurry and the pressure gradient with respect to the TBM.

5.3 Assumptions in calculations and research limitations

- For the Third Sand Layer (404 West tunnel) the value of x_{max} is determined with an extrapolation of the laboratory data of Krause [30]. The sand used in this research is similar to the sand used by Krause, as well as the bentonite concentration of the slurry. However, the yield stress could be different due a different type of bentonite. The extrapolation is compared to the calculated value of x_{max} with the slurry infiltration formulas of Broere [18] and show similar results. This fact provides confidence that the value of x_{max} is appropriate, but it is more accurate to conduct column infiltration tests at the excess face pressure used during boring. For the Second Sand Layer (404 East tunnel) the value of x_{max} is calculated with Broere [18] as well. Unfortunately, no comparison with existing literature could be done and therefore it is concluded that the determined value of x_{max} can be inaccurate. The parameter x_{max} is used to calculate the discharge from the tunnel face and therefore it is important to determine x_{max} accurately.
- The parameter Γ is determined with column infiltration tests and is defined as the excess piezometric head used in the column infiltration test divided by the measured value of x_{max}. For the 404 West tunnel the value of Γ determined in the laboratory is used in the calculations and is in agreement with the linear extrapolation of x_{max}. For the 404 East tunnel x_{max} is smaller due to a lower value of d_{10} and therefore Γ is greater compared to the 404 West tunnel. This assumption is checked with field measurements (calculation of φ_{ms}) and shows fine results. It is however more accurate to determine the value of Γ in a column infiltration test for this type of sand. The parameter Γ is used to calculate the maximum mud spurt length $x_{ms;max}$. This parameter is then used to determine the discharge from the tunnel face and therefore it is important to determine Γ accurately.
- For both the 404 West and 404 East tunnel, respectively, the maximum slurry infiltration depth x_{max} in figure 3.12 is not fully reached at 100% of the pressure drop. For both the tunnels x_{max} is reached at approximately 110%, indicating that the build up time of the filter cake takes longer than the building time of one ring. This can be explained by the fact that the minimum value of the piezometric head in the aquifer is also not reached at 100%. For the Third Sand Layer the minimum value of the piezometric head in the aquifer is -3.5 m and the recorded value at 100% is -3.3 m, see figure 4.1. The last part of

infiltration only thickens the external filter cake and therefore it can be assumed that the maximum mud spurt length $x_{ms;max}$ is reached at 100%.

- It is assumed that the permeability of the consolidated slurry, k_{ws}, is 5.0E-06 m/s. This value is obtained from existing literature [26]. In this research a value for k_{ws} is determined. Three column infiltration tests with a small infiltration time are conducted. In all cases the sample was disturbed, resulting in inaccurate results. It is therefore decided to use the values of k_{ws} presented in existing literature instead of the measured values from the experiments conducted in this research.
- The cutter wheel is divided into areas with the same amount of cutter teeth passages per rotation. With the rotational speed in combination with the amount of cutter teeth passing per rotation, equal slurry infiltration areas are determined. This is done for an interval of 1 second. To determine the total discharge of the tunnel face, the specific discharge at a certain time is multiplied by this area. The accuracy of the discharge calculation can be increased by decreasing the infiltration interval. The cutter disks present on the cutter wheel are not taken into account. Possible over cutting into other infiltration areas during boring is also neglected.
- The relations presented by Bezuijen in section 2.3.2 do not take slurry infiltration into account during boring. It is seen that slurry infiltration occurs during boring of the North/South line. The calculation results are accurate when compared to field data, but investigation into incorporating slurry infiltration during boring into this relations is recommended.
- The quasi-static flow model is used to back-calculate the excess pore pressures at the tunnel face from the pore pressure sensors within a semi-confined aquifer. At small distances this is valid [10]. It is seen that the results are inaccurate when the cross-section is heterogeneous (SS West and East tunnel). Considering the more or less homogeneous cross-sections (404 West and East tunnel), the back-calculated results are fine.
- For the cross-section of the GHT it is seen that it consists of several (sand) layers, but due to the fact that no additional information is available the permeability and porosity are assumed constant over the entire cross-section of the tunnel. The permeability is 4.0E-04 m/s [1] and the porosity is assumed to be 0.40.
- The different layers within the tunnel cross-section in calculating the excess pore pressure with the transient flow model are not considered. The accuracy of the results could increase by taking this into account. For the consideration of multiple layers within the model, other formula need to be derived, which was not in the scope of this research.

Chapter 6

Conclusions and Recommendations

The goal of this research is to investigate whether it is possible to predict the excess pore pressures in front of a TBM during boring more accurately than is currently being performed. The applicability of laboratory results to model input parameters is investigated and a new derivation to calculate excess pore pressures at the tunnel face is presented. Furthermore, a comparison is made in considering the cutter wheel configuration versus the mean infiltration time in calculating the discharge from the tunnel. Laboratory results, TBM data and field data provided an excellent and indispensable source of information for this research.

6.1 Conclusions

A slurry tunnel boring machine (TBM) is widely used in saturated, non cohesive soils [22]. The supporting face uses a bentonite suspension (slurry) which is subjected to an excess pressure to keep the bore front stable [18]. Pressurized slurry is the driving force in the slurry infiltration process during boring. Tunnel face stability calculations made with a wedge shaped failure mechanism are widely used in engineering practices [4, 13, 25, 39]. Excess pore pressures in front of the tunnel face due to boring have been measured by half a dozen projects in the Netherlands alone [9, 10, 18, 35]. The presence of excess pore pressures results in a less effective face support on the triangle soil column. To keep the tunnel face stable under these conditions the minimal allowable face pressure should be increased significantly [11, 18].

An idealized pore channel is used to model the slurry infiltration depth into the soil [18, 30]. During infiltration the slurry experiences increasing shear resistance τ from the sand grains, resulting in a maximum infiltration distance x_{max} at a given excess pressure Δp. This distance is called the mud spurt $x_{ms;max}$, which can only occur in the soil body in front of the tunnel. The external filter cake is formed due to consolidation (plastering) of the slurry and is formed within the excavation chamber. Several slurry infiltration formulas are found in existing literature and are compared in this research. Each relation relies on at least one parameter that is determined in a column infiltration test. Therefore, laboratory experiments have been conducted to provide a deeper understanding of the slurry infiltration processes with respect to North/South (N/S) line project.

The laboratory results show good resemblance with literature. A clear transition between mud spurt (slurry infiltration) and external filter cake (plastering) is distinguished, indicating that both processes are present [18, 36]. Visual evidence of both processes is presented as well. On average, a mud spurt of approximately 30 mm is seen. The total distance of displaced pore volume in the infiltration column is approximately 50 mm, based upon a test duration of 30 minutes. It is shown that the slurry infiltration formulas of both Broere [18] and Huisman [26] can be accurately applied to the average laboratory results. The laboratory experiments could not be conducted at the excess pressure normative for the N/S line due to limitations of the laboratory equipment. An extrapolation with laboratory data of Krause [30] is done to provide a value of the maximum slurry infiltration depth x_{max}.

The drop in piezometric head at stop boring is used, in combination with x_{max}, to determine the value of a (time to reach half x_{max}) specific for the TBM. For both the 404 West (a = 136 s) and 404 East tunnel (a = 200 s) the value of a is greater than the value determined in the laboratory (a = 11 s). Therefore, the value of a determined in the laboratory cannot be used directly in the groundwater flow models. In order to determine a suitable value for a, without the use of field measurements, numerical integration of Eq. (2.16) is compared with a fit of a and shows good results. It is concluded that the magnitude of a, in the case of the TBM, depends on a combination of laboratory parameters, TBM specific parameters and field parameters. It is concluded that laboratory experiments can be used to provide valuable input for Eq. (2.16) and with a known x_{max} a suitable value of a can be determined.

For the N/S line the back-calculated excess pressures at the tunnel face are smaller than the excess face pressures used during boring. Therefore, it is concluded that mud spurt is present during boring. With the determined values of a, in combination with the calculated values of x_{max}, the excess piezometric head at the far side of the mud spurt, φ_{ms}, can be calculated. Similar results are shown comparing the cutter wheel configuration and the mean infiltration time.

Considering quasi-static conditions, a relation is derived to determine the excess pore pressure at the tunnel face, see Eqs. (6.1) and (6.2). The TBM specification as well as the parameters of the soil in front of the tunnel are incorporated in this relation. The excess pore pressure at the tunnel face is calculated with Eq. (6.3).

$$v_{p;Darcy} < v_{TBM} \;\rightarrow\; \alpha^* < \frac{n}{k}\frac{R}{\varphi_{ex;face}} v_{TBM} \text{ with } \alpha^*_{min} = 1 \tag{6.1}$$

$$v_{p;Darcy} > v_{TBM} \;\rightarrow\; \alpha^* > \frac{n}{k}\frac{R}{\varphi_{ex;face}} v_{TBM} \text{ with } \alpha^*_{min} = 0 \tag{6.2}$$

$$\varphi_0 = \alpha^* \cdot \varphi_{ex;face} \tag{6.3}$$

The calculated values from Eq. (6.3) are compared with the measured field data back-calculated to the tunnel face with the quasi-static groundwater flow model of Bezuijen [9]. The more or less homogeneous cross-section of the N/S line (404 West tunnel) shows the best agreement with the measurements and the calculated value is approximately 4% larger than the measured value. For the Green Heart Tunnel (GHT) the slurry infiltration velocity is smaller than the TBM velocity, resulting in an α^* of 1. From the sensitivity analysis it is concluded that the permeability has a great influence on the slurry infiltration velocity and therefore on the value of the excess pore pressure at the tunnel face.

The transient flow model can be used to predict excess pore pressures in front of a TBM, which is in accordance with existing literature [18]. From a distance of approximately 5 to 10 meters from the tunnel face a fine prediction is seen. The calculated discharge specific for the cutter wheel is compared to the discharge calculated with the mean infiltration time and shows similar results. The transient flow model is especially sensitive to the permeability and the specific storage. Accurate determination of the parameters is needed from field tests (e.g. pump-tests) and laboratory tests (e.g. constant head tests) to determine the excess pore pressures accurately with this model.

6.2 Recommendations for future research

- To validate the relation of α^* in Eq. (6.3) it is recommended to measure the pore pressures at future projects. In this way the excess pore pressures can be predicted prior to construction and compared with the measured data. Measurements should be done in both homogeneous and heterogeneous soils configurations, respectively, so as to see how this relation behaves. Piezometers have been used in half a dozen projects in the past, but this data is very difficult to retrieve, interpret and is often incomplete. Measuring pore pressures is quite cheap compared to the total project costs and provides vital information in understanding and predicting the excess pore pressures in the future.
- The configuration of the cutter wheel should be taken into account in calculating the discharge in front of the TBM for future projects. A comparison should also be made with the discharge calculation considering the mean infiltration time. For the N/S line it is concluded that the results are similar, but this is not a generally valid statement yet. It is therefore recommended to perform this calculations in future projects.
- For future column infiltration tests it is recommended to use an excess pressure normative for the excess face pressure used during boring. It is also recommended to use in-situ sand from the project location in combination with the same bentonite as used in the project. Considering this, an accurate value of x_{max} and Γ can be determined in the laboratory and used in the calculation of the discharge from the tunnel face.
- A relation is provided to calculate the value of a that can be used for a TBM. This relation incorporates the 1-dimensional flow resistance and a contribution of the yield stress. In the case of the N/S line this relation provides accurate results. This relation should however be validated with future projects.
- The permeability of the consolidated slurry is a parameter used in the relation to determine the value of a for the TBM. This value can be determined in the laboratory. This is shown in this research, but due to disturbed samples the results are likely to be inaccurate. It is recommended to determine this value in the laboratory, but greater thought should be given into the testing procedure to prevent inaccurate test results.
- The relations presented by Bezuijen in section 2.3.2 do not take slurry infiltration into account during boring. It is seen that slurry infiltration occurs during boring of the N/S line. The calculation results are accurate when compared to field data, but investigation into incorporating slurry infiltration during boring into this relations is recommended.
- Nowadays the TBM and field data are not easily available for research purposes. The data is stored at several institutions and is therefore difficult to access. From experience in this research it is also not organized in an orderly fashion. It is therefore recommended to store data from future project at an organization which is more easily accessible to researchers, e.g. Centrum voor Ondergronds Bouwen (COB).
- In this research no investigation is done in modelling the excess pore pressures with a finite element model. An interesting topic would be to investigate the accuracy of a numerical groundwater flow model compared to the analytical groundwater flow models.
- The transient flow model of Broere [18] is used to fit the maximum recorded pore pressures in the aquifer. It is also possible to calculate the rise of excess pore pressure in time for a fixed distance from the tunnel face. Conducting this calculation and comparing the results with the measured pore pressures in the field is recommended for future research. This way it can be determined whether the rise of excess pore pressure in time can be predicted accurately when considering the determined value of a for the TBM.

Appendix A

Project information

A.1 North/South line

A.1.1 Project introduction

In April 2003, the construction of the N/S metro line started, the trajectory is visualized in figure 1.1. For this thesis the part constructed with a (slurry) tunnel boring machine (TBM) is of most interest. The total distance of the bored part is 3.8 kilometers and consists of two tunnels, each with an outer diameter of approximately 6.88 meters. The bored tunnels follow the street pattern as much as possible to limit settlements of the historical buildings. The project had to cope with a lot of delays, and was even stopped for nearly a year in 2009. The current completion date is set in 2017, but due to the bankruptcy of installation firm Imtech (Aug, 2015) the project will possibly be delayed yet again.

One of the critical parts of the construction of the bored tunnel was the passage of Bridge 404. The location of the bridge is shown in figure 1.1, and a cross-section of the bridge including the two bored tunnels is shown in figure 1.2. It is seen that the East tunnel is constructed very close to the pile tips of the bridge, at a distance of approximately 1.5 meters. Both tunnels have passed the bridge at a different depth, due to the configuration of metro station Ceintuurbaan, where the tunnels are aligned vertically. Three issues had to be prevented during the passage of the East tunnel [28]:

- Structural bridge damage due to settlements;
- Face instability due to low face pressure;
- Surface blow out caused by a high face pressure.

Regarding the first issue a 3D soil structure interaction model was made, as well as a design of mitigating measures during boring. Those measures and the compensation grouting layer at the pile tips as well as the settlement issues are not elaborated in this thesis [28]. The issues concerning the face stability are elaborated in the next section.

A.1.2 Stability calculation

All face stability calculation of the N/S line are done according to the German standard DIN 4085:1987 [7]. By applying this design approach, the minimum allowed slurry pressure directly below the pile tips was (much) higher than the maximum allowed slurry pressure in the middle of the canal. This made the TBM passage not feasible since it was considered too risky to apply very substantial discrete adjustments in face pressure at the transition from abutment to the canal in order to avoid a blow out or cave in, as adapting this face pressure too late/early is likely to happen. Also, the TBM control system requires a difference of at least 20 kPa between the minimum and maximum face pressure which makes rapid changes in face pressures even more difficult to execute accurately within a short time frame [28]. Figure A.1 shows the transition of the face pressure between the abutments and the canal and the in-feasibility since the TBM face pressure is lower than the calculated minimal face pressure needed to prevent a cave-in.

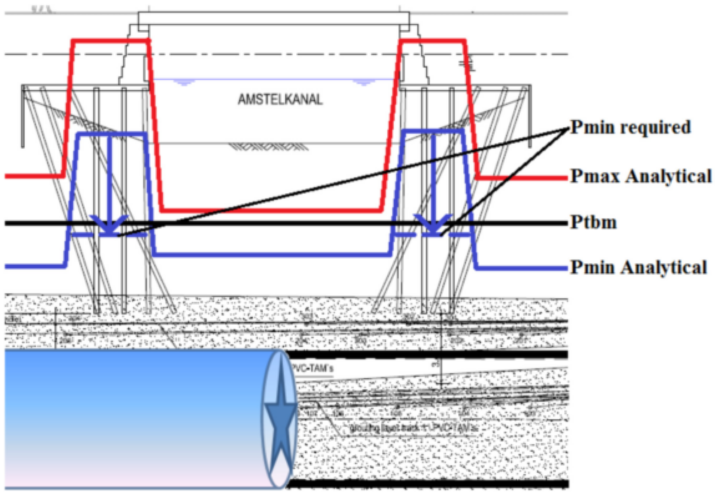

FIGURE A.1: Systematization of analytical calculation results in crossing Bridge 404, from [28].

The design team of W+B came up with two solutions which would make the crossing theoretically feasible [28]:

- Increase the strength and density of the soil by means of ground improvement under the canal as well as under the foundations of the bridge;
- Decrease the minimum required soil pressure by means of application of advanced 3D FEM calculations, indicated with the blue arrows in figure A.1.

Since the minimal required face pressure is calculated with a 3D FEM calculation, the safety philosophy of DIN 4085:1987 is implemented in this model [28]. The maximum allowable face pressure was not calculated by means of 3D FEM since this failure mechanism depends mainly on the heterogeneity of the soil. Blow-out can occur when just a small stream of bentonite reaches the surface (e.g. along the pile shafts). Because this in turn would lead to a very rapid pressure drop inside the excavation chamber, active failure is likely to occur. The maximum allowable face pressure at a blow-out mechanism indicated by 3D FEM will therefore most likely be too optimistic in reality. The maximum allowable face pressure was therefore determined with the analytical method according to the DIN 4085:1987. In this (simple) method the vertical total stress of the soil above the crown of the tunnel has to be greater than the isotropic face pressure.

However, in the analytical calculation according to DIN4085 the excess pore pressures created during boring in sandy soils are not taken into account [7], but it is proven earlier in Dutch soil conditions that these are present [8, 18]. The minimum slurry pressure strongly depends on the pore pressures in the surrounding soil. Also, it is shown that the excess pore pressures have a major influence on the stability of the tunnel face as they reduce the effectiveness of the support force from the slurry and also lower the effective stresses in the soil, reducing the friction capacity [16].

A.1.3 Back-analysis of excess pore pressures

Fortunately, the two tunnels cross the bridge at different depths and piezometers were installed, see figure A.2. The measured excess pore pressures from the not critical (West) tunnel, could be used to back calculate the excess pore pressures at the tunnel face and used for the critical (East) tunnel.

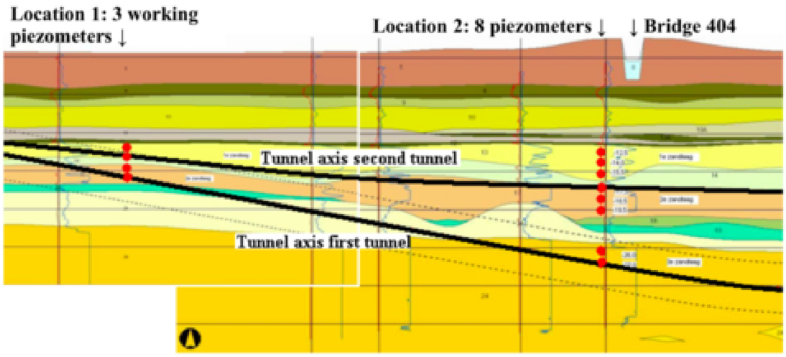

FIGURE A.2: Geological cross-section indicating tunnel depth configuration and piezometer locations, from [28].

The piezometers are located approximately in the middle of the two TBM trajectories and therefore it was possible to monitor both passages and to keep on monitoring after the TBMs had passed. The face pressure and the measured pore water pressures were linked to the position of the TBM. The measured pore pressures and the back-analysis of the excess pore pressures are presented in figure A.3 [35].

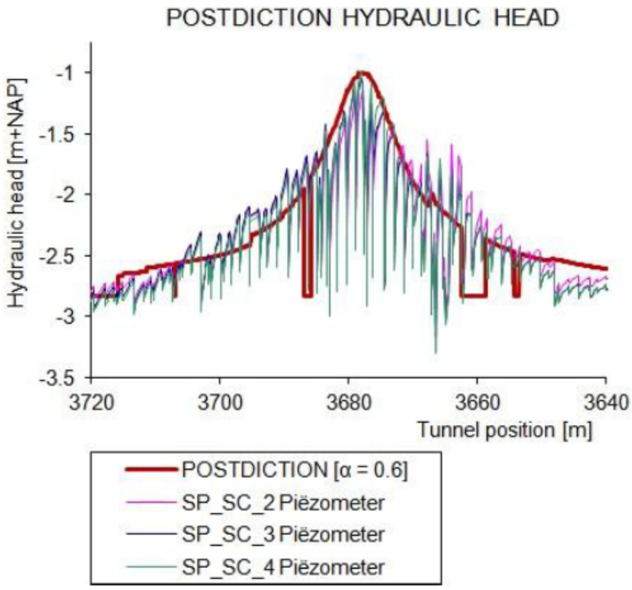

FIGURE A.3: Recorded pore pressures at Scheldestraat and the conducted back-analysis, from [35].

A.1.4 Geological setting

In the Amsterdam area the soil consists of Holocene and Pleistocene layers. The upper part is the Holocene layer, consisting of sand (Ophooglaag), peat (Hollandveen/Basisveen) and clay layers (Oude Zeeklei and Hydrobiaklei) and a permeable sandy-clay layer (Wadzandlaag). The Pleistocene deposits are below the Holocene sequence, consisting of the First Sand Layer, an intermediate mix Allerød Layer, the Second Sand Layer, the Eem Clay Layer and the Third Sand Layer. The groundwater table is located near surface level [28, 35].

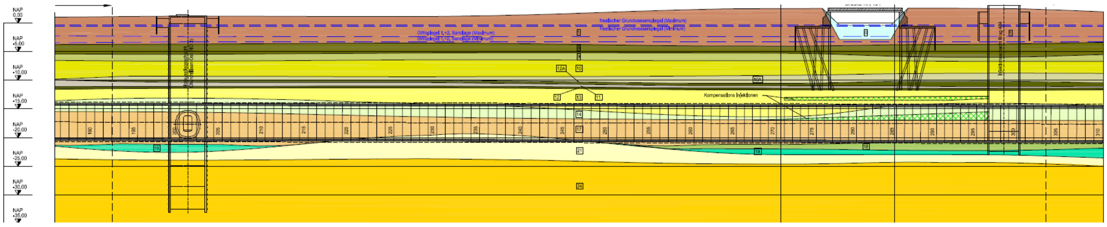

(A) East tunnel

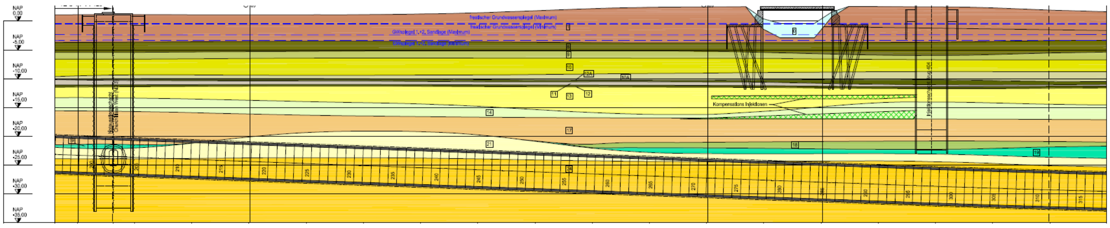

(B) West tunnel

FIGURE A.4: Geological cross-sections at Bridge 404 for the East (A) and West (B) tunnel, respectively [39].

A great variety of layers is present at the project location, see figure A.4. Both tunnels are mainly bored through sand layers. For the East tunnel these layers consists mainly of the Second Sand Layer (#17) and two mixed intermediate layers (#14/21). For the West tunnel the main layer is the Third Sand Layer (#24) and for a smaller part an intermediate layer (#21). In the area of interest, close to Bridge 404, it is seen that no clay or peat layers are bored.

A.1.5 Cutter wheel configuration

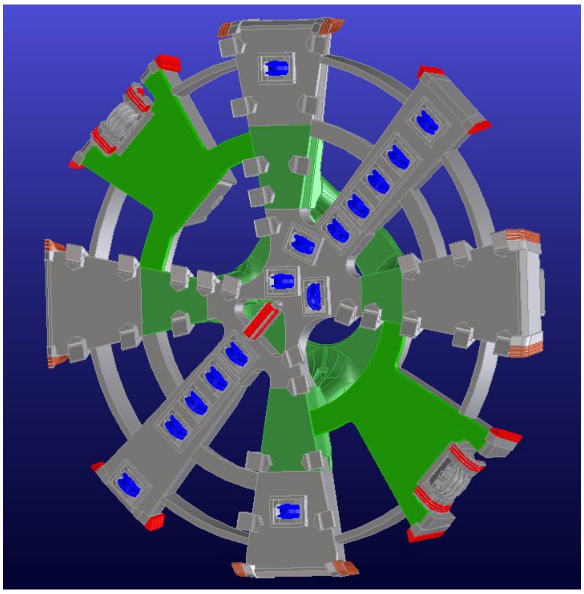

FIGURE A.5: Three dimensional visualization of the N/S line cutter wheel, from [39].

The cutter wheel used for the N/S line is asymmetrical and consists of overlapping cutter teeth. The cutter wheel is divided into parts with the same number of teeth passing each rotation, indicated in table A.1 and shown in figure A.6. For each infiltration time t_i the surface area of the cutter wheel is calculated. These areas are used in the discharge calculation.

Regarding the cutter wheel, the following assumptions and simplifications are made:

- The cutter disks are not taken into account;
- The total surface area per number of teeth is used in the calculation of the discharge, but no infiltration can take place at the cutter teeth;
- The center of the cutter wheel is considered to be as two cutter teeth passing.

It seems that the cutter disks lie deeper than the cutting teeth, see figure A.5, and therefore it can be assumed that the disks do not cut any soil earlier than the teeth.

TABLE A.1: Different sections of the cutter wheel of the N/S line 404 West tunnel.

Number of teeth	Colour	t_i [s]	t_i [s]	A_i [m^2]
1	Blue	29	6	5.3
	Purple	29	9	2.9
	Green	29	21	2.9
	Orange	29	22	3.2
2 (middle)	Red (rsm)	9	29	23.0
	Red (rlm)	21	A_{cw}	37.18
2 (outer)	Red (rso)	6		
	Red (rlo)	22		
4	Brown	6		

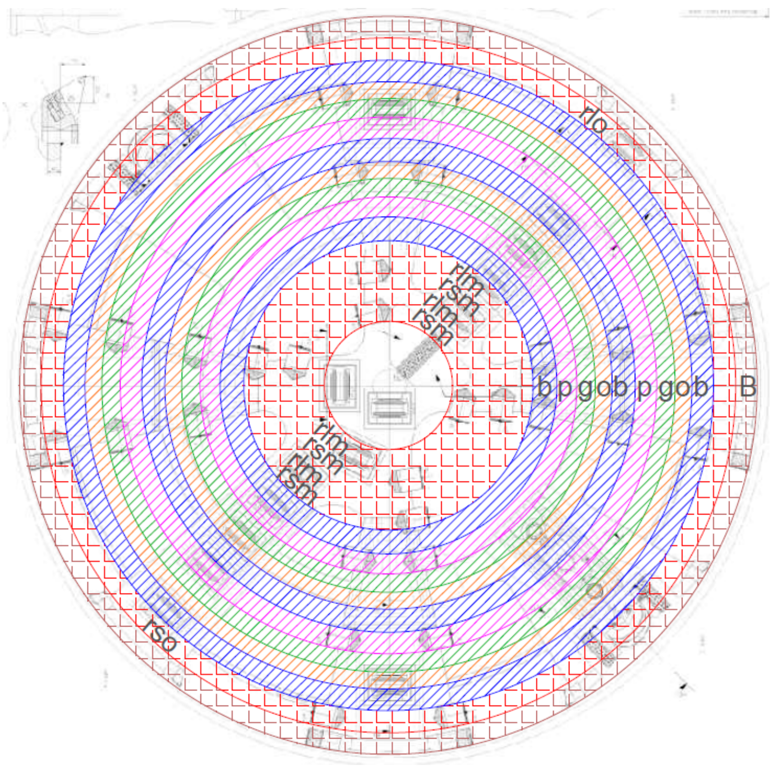

FIGURE A.6: Areas with different cutter teeth configuration for the N/S line cutter wheel, adjusted from [39].

A.1.6 Available data

Extensive TBM data is available, approximately 300 different parameters are recorded during boring. The most relevant parameters are the pressure in the excavation chamber (at four positions in bar), unique ring numbers $(-)$, boring time (h), rotations of the cutter wheel $(-)$, date and time and the effective distance bored (m). Approximately every 10 seconds a measurement is done, which makes the dataset very accurate.

Piezometers are installed at different locations; Scheldestraat, Bridge 404 and station Ceintuurbaan. In total four piezometers are placed at Scheldestraat and eight at Bridge 404. The piezometers measured the absolute pressure and reference pressure approximately every 60 seconds. The sensors are placed in between the East and West tunnel, see figure A.7.

The exact position of the pore pressure sensors with respect to the TBM is important, because in this way the recorded pore pressures can be linked to the construction of a specific tunnel ring. Both the pore pressure sensors and the TBM lining have unique coordinates in the X,Y,Z planes. With this information the distance between the piezometers and the tunnel axis is calculated and at the smallest distance, the piezometers are closest to the TBM lining. At this position the highest recorded pore pressures are expected.

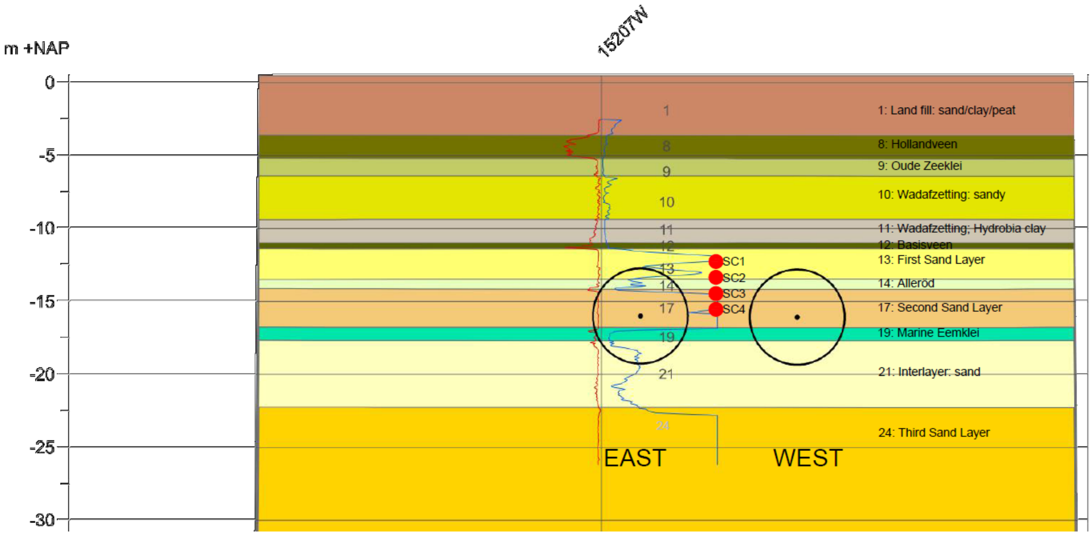

(A) Scheldestraat, sensor at ring number 65 (East) and 65 (West), respectively.

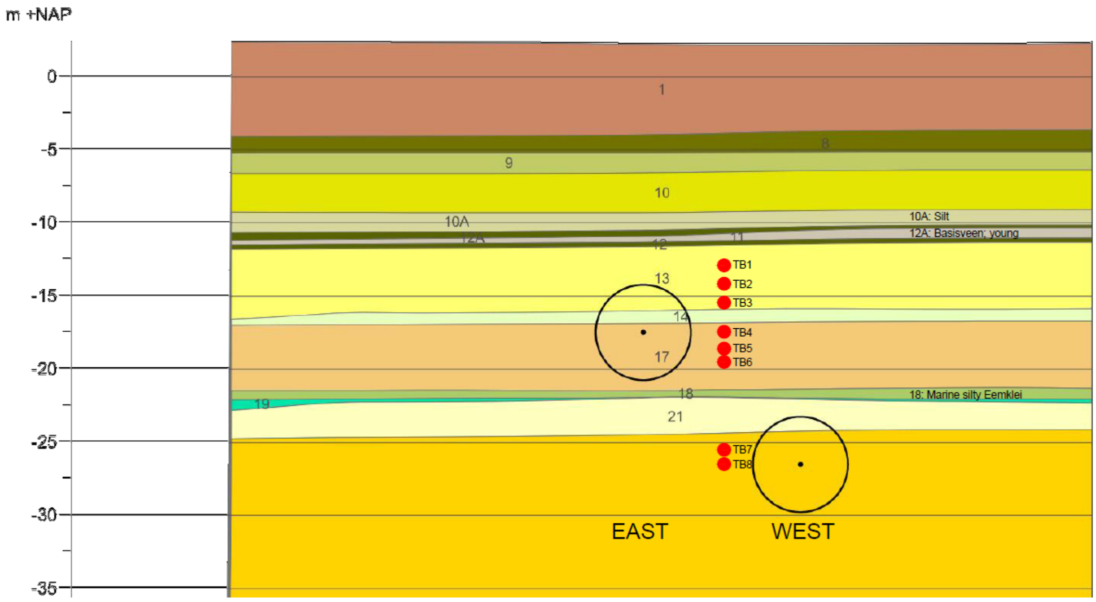

(B) Bridge 404, sensor at ring number 258 (East) and 258 (West), respectively.

FIGURE A.7: Piezometer positions at Scheldestraat (A) and Bridge 404 (B) with respect to the bored tunnels, from [39].

A.2 Green Heart Tunnel

The Green Heart Tunnel (GHT) is constructed between 2000 and 2004. The diameter of the cutter wheel is approximately 14.9 meters and the total length of the tunnel is 8670 meters [1]. During the construction pore pressures have been measured at several positions around the TBM, see figure A.8 for an overview. Also several TBM parameters are recorded. The most relevant parameters are the face pressure, position of the TBM, unique ring numbers and advance rate.

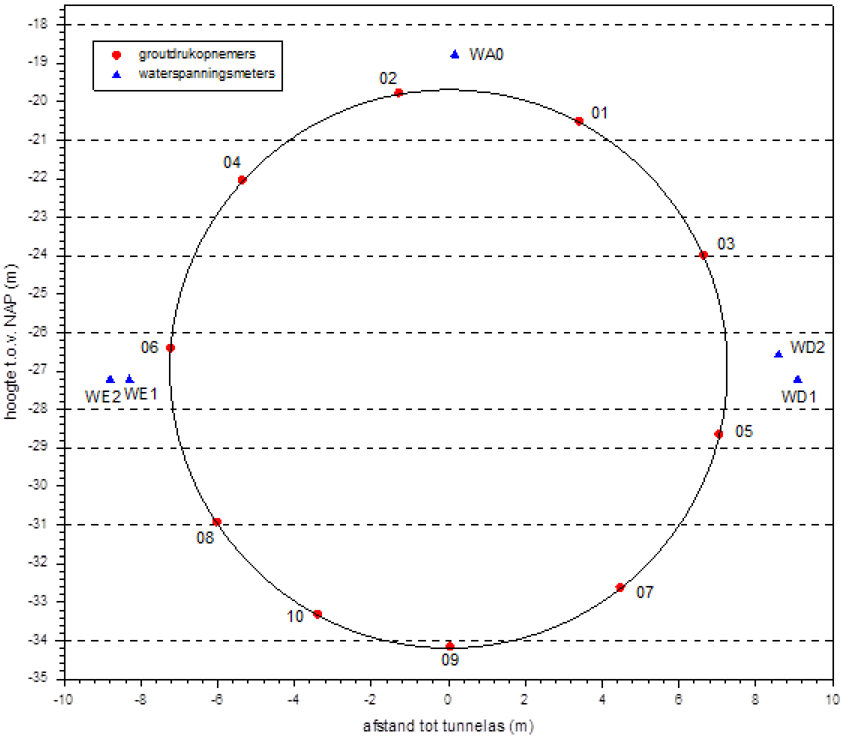

FIGURE A.8: Overview of the piezometer locations at the GHT project.

Appendix B

Laboratory Experiments: Additional Information

B.1 Sensitivity analysis with slurry infiltration formulas for the North/South line

B.1.1 Third Sand Layer

The results of the first part of the sensitivity analysis are presented in figure B.1. The different sub figures are discussed briefly to see whether the results are consistent. When a is increased, it should take longer to reach the maximum infiltration depth. As the excess pressure Δp is increased, the slurry should infiltrate further since the driving force is greater. An increased characteristic hydraulic pore channel diameter d_{10} leads to a higher infiltration depth. The factor α is used to fit the formulas presented by Broere [18] onto the laboratory results. As the yield stress τ_F increases the slurry experiences more resistance from the sand grains, resulting in a lower infiltration depth. It is concluded that the physical behavior is consistent.

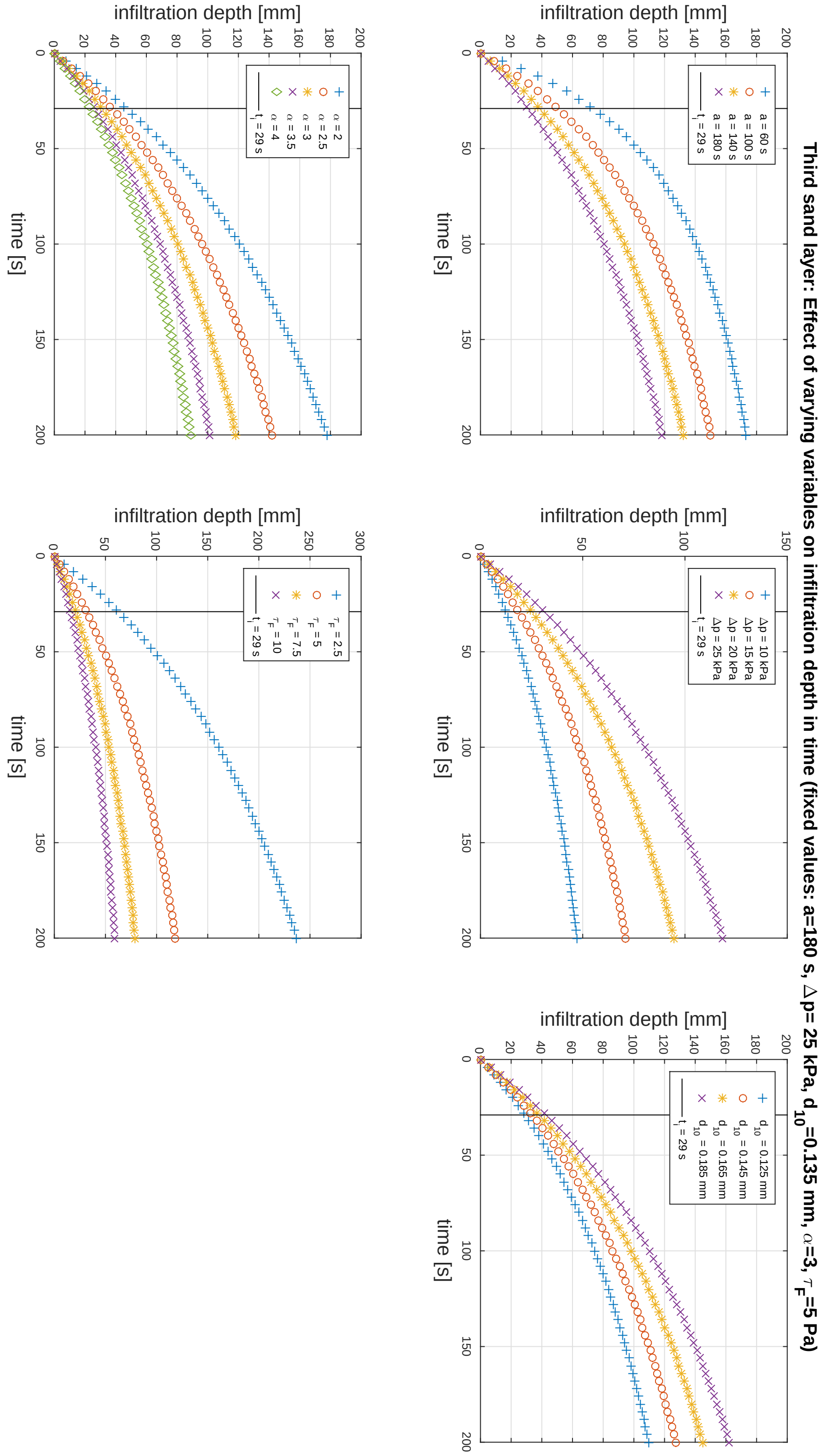

FIGURE B.1: Sensitivity analysis of parameters on the slurry infiltration depth in time for the Third Sand Layer.

B.1.2 Second Sand Layer

For the second sand layer a sensitivity analysis is done to determine the infiltration depth of the slurry in a column infiltration test. Unfortunately, it was not possible to use this material in the laboratory experiments, because the sand was too fine for the filter, too fine to compile with available sieving devices and the material was not available in the laboratory. Slurry infiltration formulas of Broere are used to calculate the slurry infiltration depths in time. An estimation of the minimum and maximum infiltration depth in time is presented in figure B.2 and the parameter sensitivity study is presented in figure B.3. The values of the parameters used in the formulas are presented in table B.1.

TABLE B.1: Overview of parameters used in the sensitivity analysis of the Second Sand Layer.

Parameter	Value(s)	
	Fixed	*Range*
a [s]	20	[5, 10, 15, 20]
Δp [Pa]	25E+03	[10E+03, 15E+03, 20E+03, 25E+03]
d_{10} [mm]	0.05	[0.045, 0.05, 0.055, 0.060]
α [-]	3	[2, 2.5, 3, 3.5, 4]
τ_F [Pa]	5	[2.5, 5, 7.5, 10]

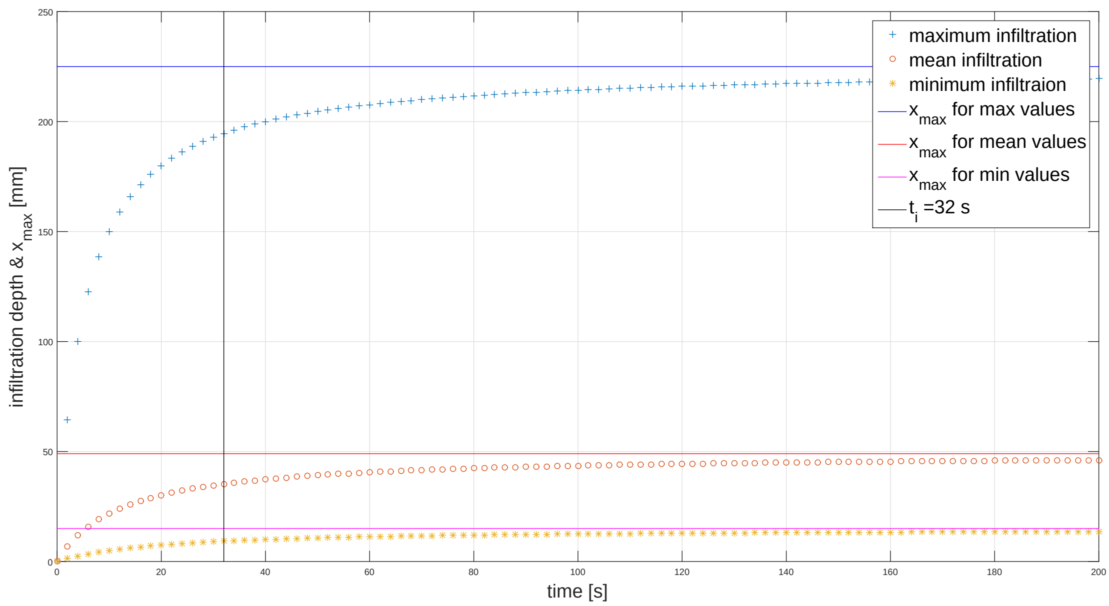

FIGURE B.2: Sensitivity analysis of parameters on the maximum and minimum slurry infiltration depth for the Second Sand Layer.

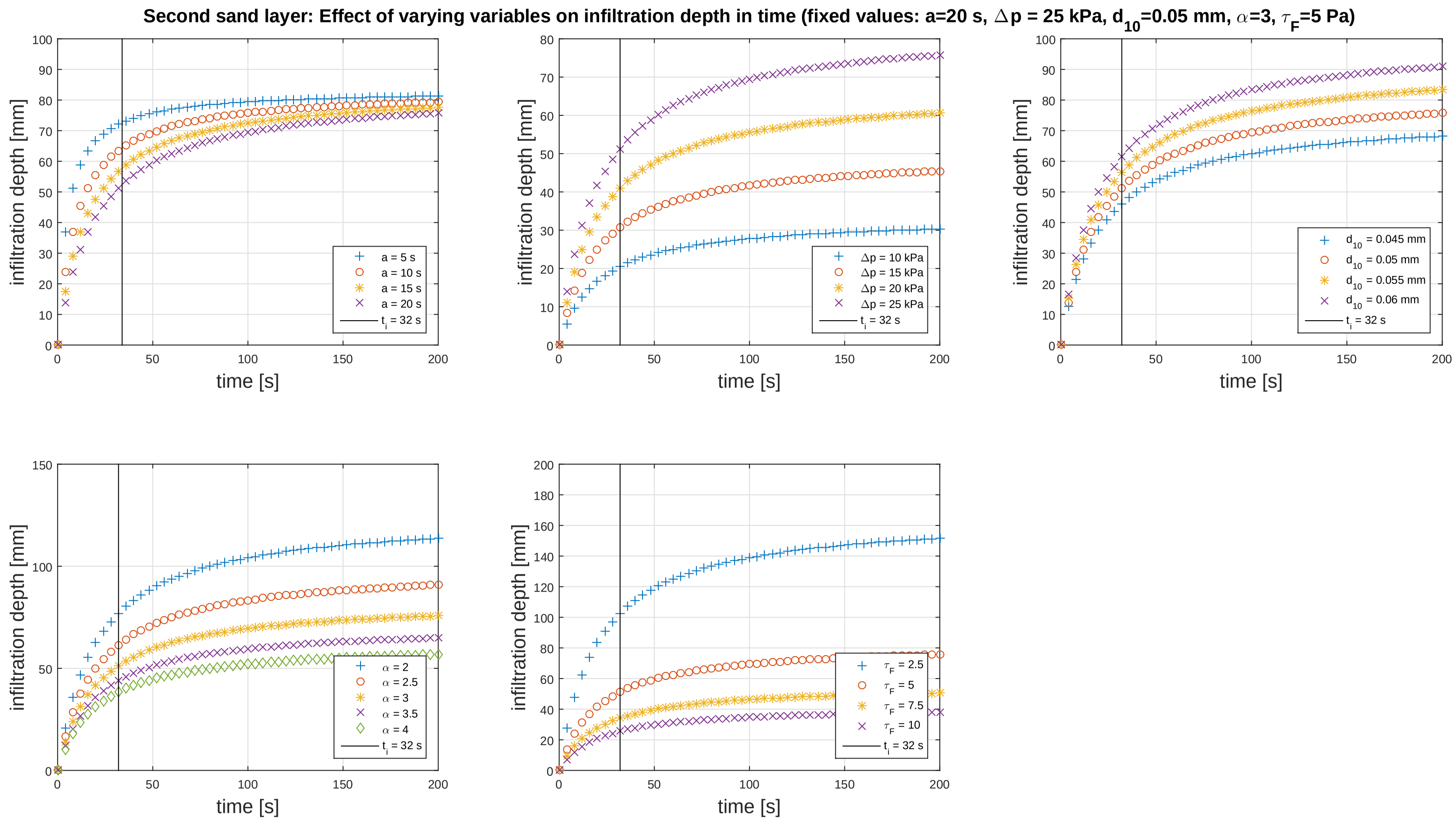

FIGURE B.3: Sensitivity analysis of parameters on the slurry infiltration depth in time for the Second Sand Layer.

B.2 Sieve curves and bentonite fact sheet

Due to the absence of in-situ sand from the North/South (N/S) line project, manually composed sand is used in the laboratory experiments. Since the 404 East tunnel crosses Birdge 404 through the Second Sand Layer, it would be preferred to use sand that represents the Seconds Sand Layer. Unfortunately, this sand is too fine to compile with dry sieves and there were no filters available at the laboratory that could withhold this fine fraction of flowing through the filter. It was approved by the committee to use the third sand layer for this laboratory experiment. Sieve curves of both sands are shown in figure B.4.

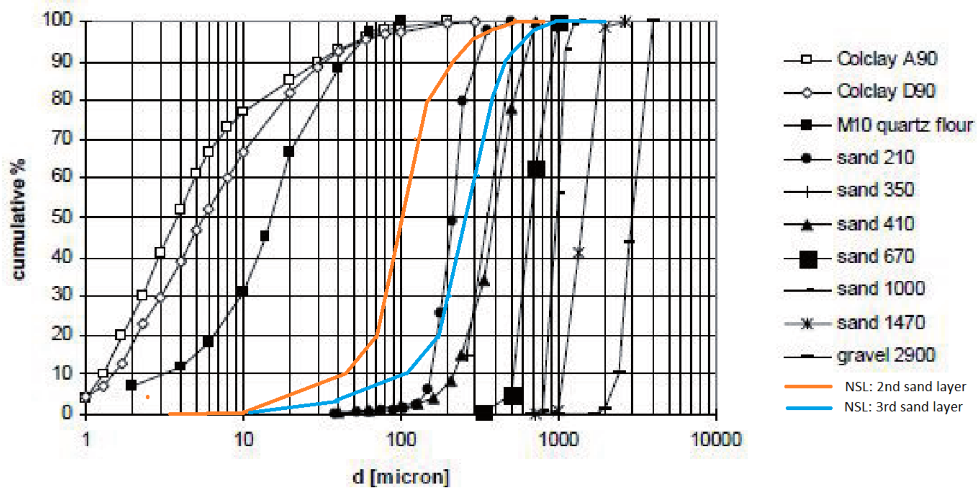

FIGURE B.4: Sieve curves of the Second and Third Sand Layer close to the project site, adopted from [36, 39].

In total five different kind of sands were used to compose the representative sand sample for the Third Sand Layer, see figure B.5. Approximately 50 kilograms of artificial sand is compiled. To achieve a homogeneous sand mixture 1 kilogram of sand is compiled and decanted at least ten times between different buckets. This is repeated until the total amount of 50 kilograms is reached. During this procedure the sand is sufficiently mixed, but also some white dust was fluttered into the air. The mixed sand sample is sieved and figure B.6 shows the result.

Figure B.7 shows the sand used in the column infiltration tests conducted by Krause [30]. The artificial sand used in this research is similar to Boden 2.

The bentonite used in this laboratory experiment is IBECO B1 active sodium bentonite. This is the same bentonite as used in the N/S line project. During boring of the tunnels, 40-50 kg per m^3 water is used when boring through the sand layers. For the laboratory experiments 50 $gram$ of bentonite per liter of water is used. Different mixing and stiffen configurations are used, which are elaborated in more detail in section B.3.4. The bentonite and water are mixed in a *Hobort mixer*, in a 10 liter bowl with stainless steel mixer, see figure B.8. A fact sheet of IBECO B1 active bentonite is presented in table B.2.

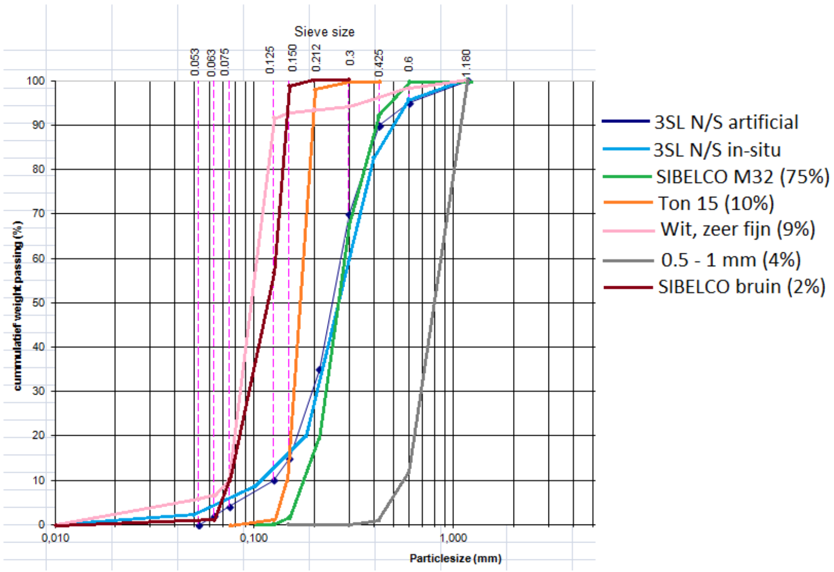

FIGURE B.5: Plot of different sieve curves of the sands used to compose the manually composed Third Sand Layer.

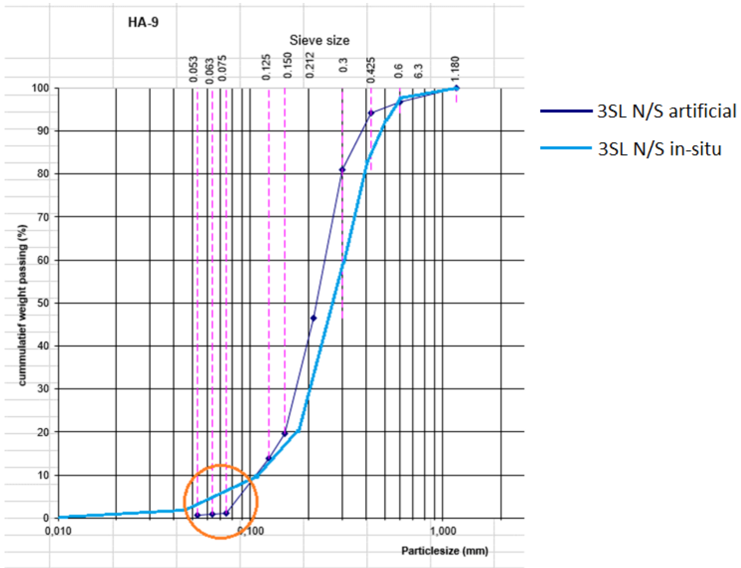

FIGURE B.6: Sieve curve of the manually composed Third Sand Layer after mixing compared to the original sieve curve [39].

TABLE B.2: Bentonite fact sheet.

Technical parameters	Value
Water content [%]	11 ± 3
Specific density [g/cm^3]	2.65
Bulk density [g/l]	800
Screen residu on 0.063 mm [%]	20 ± 5
Slurry at 50 kg/m^3, after 24 hours	
Slurry density [t/m^3]	1.028
Marsh viscosity [s/l]	40
Liquid limit (ball) [N/m^2]	30 (6)
Filtrate volume [ml]	12

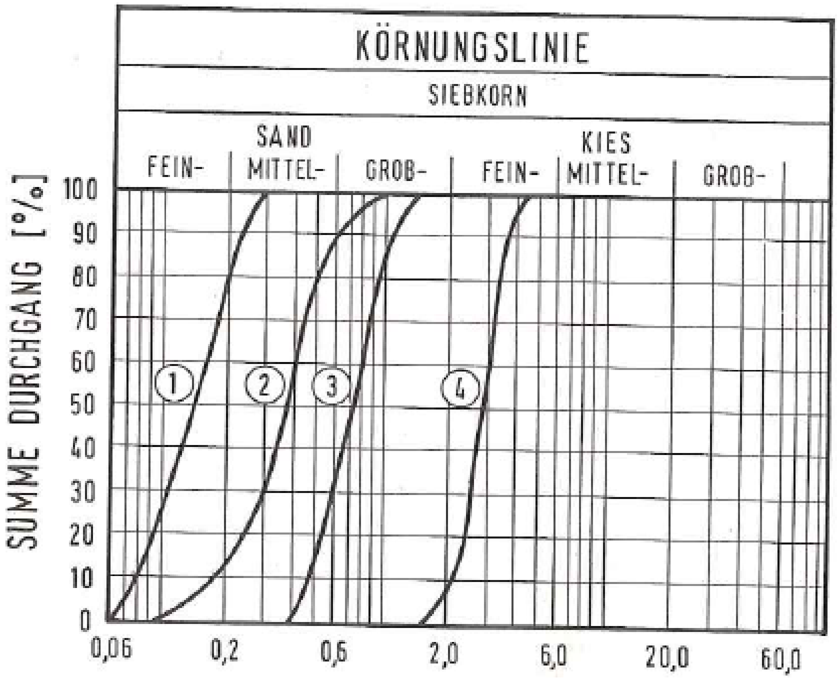

FIGURE B.7: Particle size distribution of the sands used in the laboratory experiments of Krause [30]

FIGURE B.8: Mixing of bentonite and water in a Hobort mixer.

B.3 Test procedures and preliminary tests

The laboratory experiments that are conducted in this research are in agreement with existing literature [30, 36]. This similarities increase the likelihood of the results obtained to be accurate. Both authors describe the outline of the experiment, but not very accurately. In this section a detailed overview is given of the different steps during the column infiltration tests.

B.3.1 Equipment and testing manual

This section aims to provide a manual for conducting column infiltration tests with a saturated sand and a bentonite slurry.

Required equipment:

- A transparent perspex infiltration column (IC) with a valve at the bottom and connection for a pressure hose at the top;
- Hoses for air and water supply;
- Air pressure and water tank as a supply source;
- Scales (preferably connected to a computer);
- Pore pressure sensors (preferably accurate at low pore pressures);
- Software to record the pore water pressures at an accurate interval;
- Manometers to measure the piezometric head in a permeability determination;
- Sieves (BS or ASTM) to conduct sieve tests;
- Fann viscometer to conduct viscosity tests for the slurry;
- Mixer the bentonite and water (preferably high shear mixer);
- Funnel to equally distribute the sand into the IC;
- Filters for the bottom of the infiltration column and the pore pressure sensors.

Prior to the actual testing, make sure that the infiltration column is water tight, the pore pressure sensors and scales are calibrated and the software works properly. A list of the different steps to follow in conducting the column infiltration test is given below:

1. Place a coarse and a fine filter at the bottom of the infiltration column (IC). Please note that the permeability of the filter should be greater than the permeability of the sand sample to prevent that the filter is the retarding factor of the water flow through the sample;
2. Weigh the amount of sand to calculate the porosity;
3. Use a (small) funnel to equally distribute the sand into the IC to the required sample height. For equally distribution the funnel should be moved across the surface of the IC. For pore pressure measurements in the mud spurt zone, the sensors should be close (in the order of 1 to 2 centimeters) to the infiltration front;
4. Calculate the porosity, see B.3.2;
5. Close the IC and make sure that the screws (when used) are sufficiently tightened to prevent leakage;
6. Attach the water hose to the valve at the bottom of the IC and *slowly* let water flow into the sample. In this research the whole IC is put onto a scale and approximately 1 gram of water per second is added into the IC. The reason for this is that the sand should not be pushed up in the IC and to fully saturate the column of sand;
7. Let the water fill up the IC up to 30 to 40 centimeters above the infiltration front. With the IC still on the scale the permeability of the sand sample is measured, see section B.3.3;
8. After the permeability test, open de valve at the bottom of the IC and let the water flow out until the level reaches the infiltration front. Please note that a tiny layer (couple of millimeters) of water should still be present above the infiltration front to make sure the sand column is fully saturated. Since the density of slurry is higher than water, the water flows on top of the slurry when it is poured on the infiltration front;
9. Place the IC from the scale onto a platform which is a bit higher than the scale;
10. Use the Fann viscometer to measure the yield point (YP) of the slurry, see section B.3.4. How to mix the slurry is also described in this section;

11. Detach the upper part of the IC and pour the slurry onto the infiltration front. Please note that this should be done in a delicate way, since the infiltration front should not be damaged. In this research approximately 700 milliliters of slurry is put onto the infiltration front. The amount of slurry needed depends on the sand and on the excess pressure used;
12. Attach the upper part of the IC;
13. Place some sort of collector onto the scale. A hose connects the valve of the IC to the collector. This collector is used to measure the weight of the water that is pushed out of the IC. It is preferred that the scale is connected to a computer and can measure the displaced water in time in a proper time interval;
14. Attach the air pressure hose to the top of the IC;
15. Some checks need to be done before adding air pressure to the IC:
    - Clearly mark the location of the infiltration front and the height of the slurry;
    - Make sure the column does not leak. When it does, tighten the screws or start over if the leakage is too severe;
    - Start the measuring software. The recording interval could be altered with the software used in this experiment, which provided the opportunity to change the interval of recording during the test.
16. Add air pressure to the IC by closing the air valve on top of the IC and increasing the air pressure to the required pressure. In this experiment an air pressure of 25 kPa is used, because at higher pressures severe leakage of the IC occurred. Make sure that you know what air pressures the IC can withstand to prevent accidents;
17. Check whether the applied air pressure is also given by the pressure sensors. In the case that the sensors give a lower value than the applied air pressure, it could be the case that the sample is not completely saturated or the sensors are not fully in contact with water;
18. Change the recording interval of the software to the required interval;
19. Make sure the scale measurement is running before starting the test. Please note that a camera to film the display of the scale is used in this experiment. It is preferred to have a scale connected to the computer which measures the weight of the displaced water in time at a certain interval;
20. Open the bottom valve to start the infiltration process;
21. After approximately 2 minutes of testing it is possible to change the recording interval, since the pore pressure drop occurs in the first minute of testing;
22. Close the valve when testing time is reached. Please note that the tests ran for a minimum of 30 minutes in this research. This way both the mud spurt (slurry infiltration) and the external filter cake formation (consolidation) are captured;
23. Open the air pressure valve to release the pressure in the IC. Also make sure that the air pressure in the hose is back to atmospheric pressure;
24. Mark the height of the slurry in the IC;
25. Detach the top part of the IC;
26. Detach the sensor part of the IC and pour the slurry into a collector. After that, put the infiltrated sand column with the filter cake in another collector and make sure you keep some samples from the first couple of centimeters of the infiltration front. It is important to keep the sample, because the infiltrated slurry becomes visible very clearly when the sample has dried out. When the sample has dried out, the infiltration depth of the slurry is measured with a ruler and is compared with the calculated infiltration depth;
27. Clean all the different components of the IC. Also make sure you dry every single part very carefully, otherwise leakage in the next test is inevitable.

B.3.2 Porosity measurements

The porosity is defined as the ratio of the volume of pore space and the total volume of the sample,

$$n = \frac{V_p}{V_t} \quad \text{(B.1)} \qquad V_p = V_t - V_s \quad \text{(B.2)}$$

in which V_p is the pore volume in m^3, V_s the volume of the solids in m^3, V_t the total volume in m^3 and n the porosity [37]. The volume of the solids is calculated using the mass of the sand added to the infiltration column in kg divided by the density of the sand, $\rho_{sand} = 2,650\ kg/m^3$. The total volume is calculated with the height of the sand sample in the infiltration column in m and the radius of the infiltration column in m,

$$V_s = \frac{m_{sand}}{\rho_{sand}} \quad \text{(B.3)} \qquad V_t = h_{sand}\pi r_{IC}^2 \quad \text{(B.4)}$$

B.3.3 Permeability measurements

To calculate the permeability of the sand sample the discharge is measured every 5 seconds for a period of 2 minutes. Before this measurement, the bottom valve is connected to a manometer and the hydraulic head is measured. Then, the valve is connected to a bucket and the discharge is measured at the stated interval. After that, the valve is connected to the manometer again to determine the head for the second time. Now, the hydraulic gradient i $(-)$ is calculated. The twenty four discharge measurements are used to calculate an average discharge per second, and the permeability is calculated with,

$$i = \frac{\Delta h}{L} \quad \text{(B.5)} \qquad k = \frac{Q}{A_{IC} i} \quad \text{(B.6)}$$

In which Δh is the head difference in the manometers before and after discharge measurement in cm piezometric head, L is the distance between the points in cm, k is the permeability of the sample in m/s, Q is the averaged discharge in m^3/s and A_{IC} is the surface area of the infiltration column in m^2. It has to be noted that the discharge remained quite constant over the change in head, therefore the averaging of the discharge seems reasonable.

B.3.4 Slurry yield strength measurements

During discussion with engineers from Witteveen+Bos (W+B), Deltares and supervisors from the Delft University of Technology (DUT) several ways of composing slurry are presented;

- Mixing slurry for approximately 16 hours, no stiffening (Deltares);
- Mixing slurry for a couple of hours, stiffen for approximately 24 hours (DUT);
- Mixing slurry for 30 minutes, stiffen between 6 and 24 hours (W+B);

For the infiltration tests conducted in this research all the above are used for different tests, which led to a difference in yield strength of the slurries, see tables B.3. It is recommended to keep the mixing configuration consistent to get slurries with consistent yield strengths.

The apparatus used to calculate the yield strength of the slurry is the Fann viscometer, model 35SA. The model type is important for the calculation of the yield strength. In the manual two equations are provided with which the plastic viscosity (PV) in cP and the yield point (YP) $lb/100\ ft^2$ is calculated with,

$$PV = \theta_{600} - \theta_{300} \qquad \text{(B.7)} \qquad\qquad YP = \theta_{300} - PV \qquad \text{(B.8)}$$

In which θ_{600} and θ_{300} represent the display value on the Fann viscometer at 600 and 300 rpm, respectively [20]. The unit $lb/100\ ft^2$ can be converted into Pa by dividing by 0.51 [32].

B.4 Overview of laboratory test results

Table B.3 provides an overview of the measured and calculated parameters for the conducted laboratory tests. The formulas used to determine porosity n, permeability k, yield point of the slurry YP and the penetration depth of the pore water fluid h_{pw} are presented in Appendix B.3.2. It is seen that Δh_{sl} increases as h_{pw} increases. This makes sense, since more pore fluid is displaced.

TABLE B.3: Measured and calculated parameters from all column infiltration tests.

Test	h_{sample}	x_{sensor}	n	k	YP	V_{pw}	h_{pw}	Δh_{sl}
Unit	cm	cm	$-$	m/s	Pa	ml	cm	cm
7-8$_m$	32.5	2	0.29	N/A	6.9	70^a	3.4	N/A
7-8$_a$	33	2.5	0.36	N/A	8.1	59^a	2.4	N/A
13-8$_m$	27.5	2	0.30	N/A	9.9	105	5.0	0.9
14-8$_m$	27	1.5	0.30	N/A	11.6	79	3.7	0.8
17-8$_m$	27.5	2	0.31	2.71E-04	11.6	53	2.4	0.4
17-8$_a$	27.3	1.8	0.30	2.19E-04	7.1	119	5.7	1.3
18-8$_m$	26	0.5	0.30	5.80E-04	10.4	129^b	6.3	1.7
19-8$_m$	26.3	0.8	0.30	2.32E-04	8.5	118	5.7	1.4^c
19-8$_a$	27	1.5	0.31	2.59E-04	9.0	104	4.9	1.1^c
20-8$_m$	26.8	1.3	0.30	2.73E-04	7.1	109	5.2	1.3
24-8$_m$	27	1.5	0.30	2.98E-04	5.8	55^d	2.6	0.4
24-8$_a$	27	1.5	0.30	2.54E-04	4.8	79^e	3.7	0.7
25-8$_m$	27	1.5	0.30	2.79E-04	4.3	41^d	2.0	0.3

a: runtime 10 minutes. b: runtime 110 minutes. c: slurry in the sensor C. d: runtime 6 seconds. e: runtime 12 seconds.

The volume of displaced pore water in time is visualized for all test results in figure B.9. Not all the tests results can be used, because in some tests errors occurred during sample preparation. In tests 7-8$_{m/a}$ the packing density was increased. This is the reason that the volume of displaced fluid is below average. During test 14-8$_m$ leakage occurred and the yield strength of the slurry was 3.5 Pa ($\pm$30%) higher than the average. During the preparation of test 17-8$_m$ the air pressure hose was installed to the bottom valve instead of the water hose by accident. This resulted in heavy disturbance of the sample.

The results of test 19-8$_m$ and 19-8$_a$ show an increase in pore pressure after twenty and seven seconds, respectively. The increase of pore pressure resulted from slurry infiltrating the sensors during the test, visualized in figure B.10. For all the tests, except 19-8$_{m/a}$, it is concluded that after 30 seconds all the excess pressure is transferred to the soil skeleton, since no pore pressure is recorded beyond this time. But, there is still water flowing through the infiltration column, see figure B.9.

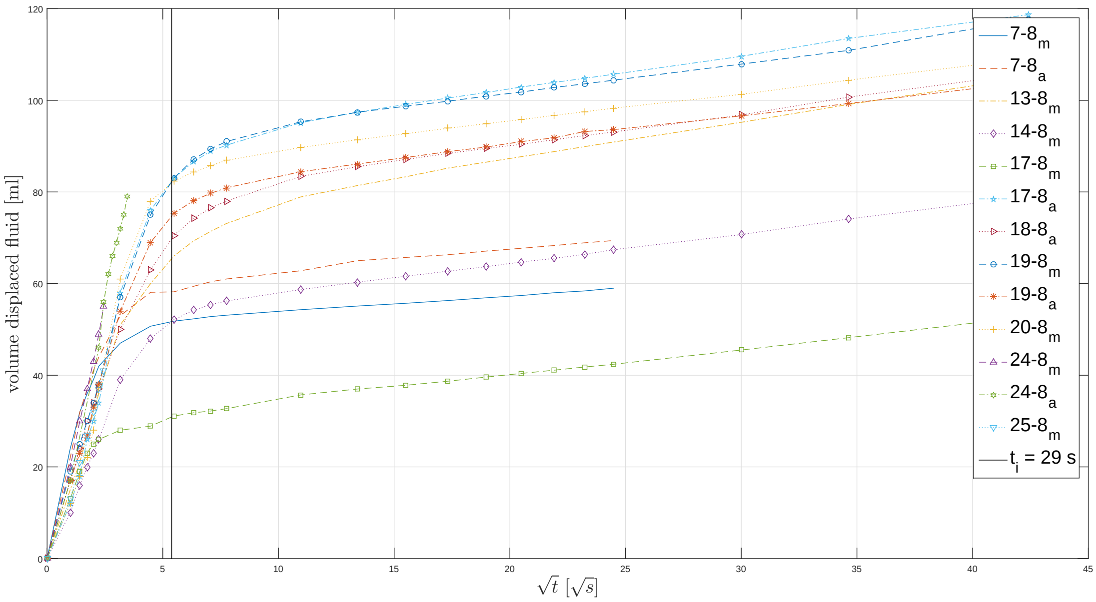

FIGURE B.9: Volume of displaced fluid for all column infiltration tests.

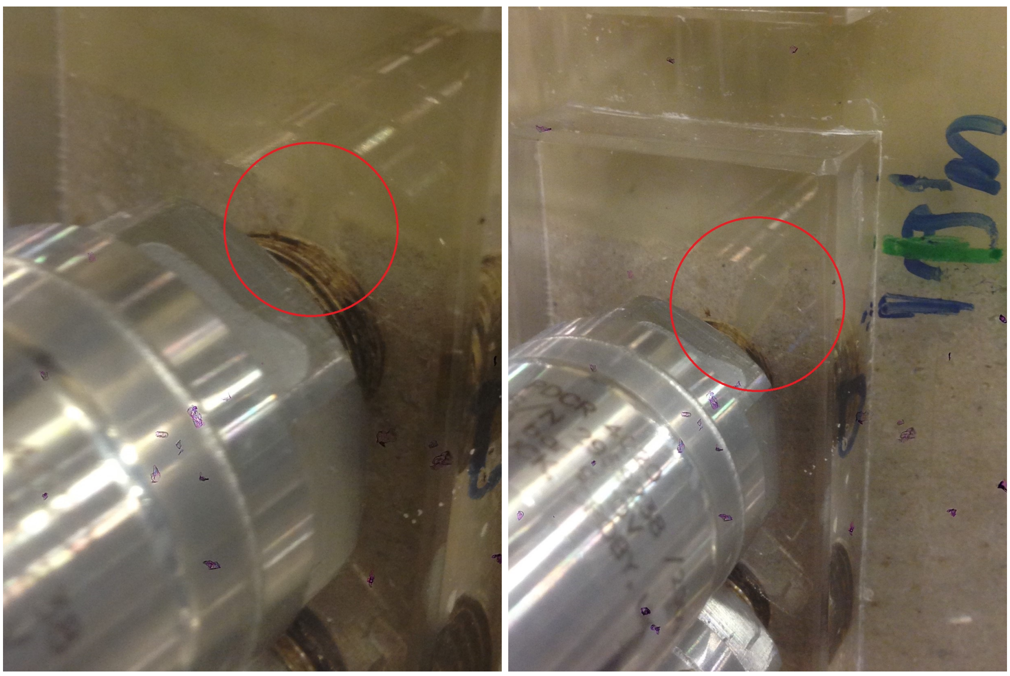

(A) (B)

FIGURE B.10: Pressence of slurry in pore pressure sensor during testing of 19-8$_m$ (A) and 19-8$_a$ (B).

Bibliography

[1] R. Aime et al. "15m Diameter Tunnelling under Netherlands Polders". In: *AITES Singapore* (2004), pp. 1–8.

[2] Municipality Amsterdam. *Trajectory North South line*. Apr. 2015. URL: http://www.amsterdam.nl/noordzuidlijn/informatie/trajectkaart/.

[3] G. Anagnostou. "The contribution of horizontal arching to tunnel face stability". In: *Geotechnik* 35.1 (2012), pp. 34–44. ISSN: 01726145. DOI: 10.1002/gete.201100024.

[4] G. Anagnostou. "The face stability of slurry-shield-driven tunnels". In: *Tunnelling and Underground Space Technology* 9.2 (1994), 165—174.

[5] K.J. Bakker, J.W. Huijben, and J.K. Vrijling. *Bored and Immersed Tunnel (course at the Delft University of Technology)*. 2012.

[6] V. Batu. *Aquifer Hydraulics: A comprehensive guide to Hydrogeologic Data Analysis.* 1998, p. 727.

[7] DIN 4085 Baugrund. "Berechnung des Erddrucks – Berechnungsgrundlagen". In: *BeuthVerlag GmbH, Berlin* (1987).

[8] A. Bezuijen. "Blow-out pressures measured in a centrifuge model and in the field". In: *Tunnelling. A Decade of Progress. GeoDelft 1995-2005* 1 (2006), pp. 143–148.

[9] A. Bezuijen. "Influence of pore pressure at tunnel face". In: *Tunnelling. A Decade of Progress. GeoDelft 1995-2005* (2006), pp. 27–33.

[10] A. Bezuijen. "The influence of soil permeability on the properties of a foam mixture in a TBM". In: *Tunnelling. A Decade of Progress. GeoDelft 1995-2005* (2006), pp. 35–41.

[11] A. Bezuijen. "The stability of a tunnel face in soft clay". In: *Tunnelling. A Decade of Progress. GeoDelft 1995-2005* (2006), pp. 149–155.

[12] A. Bezuijen and M. Huisman. *Afpleistering en mudspurt tijdens boren (BTL report 27 in Dutch)*. 1997.

[13] A. Bezuijen, J. P. Pruiksma, and H. H. van Meerten. "Pore pressures in front of tunnel , measurements , calculations and consequences for stability of tunnel face". In: *Tunnelling. A Decade of Progress. GeoDelft 1995-2005* (2006), pp. 27–33.

[14] A. Bezuijen and A.M. Talmon. "Processes around a TBM". In: *Geotechnical Aspects of Underground Construction in Soft Ground* (2008).

[15] W. Broere. "Influence of excess pore pressures on the stability of the tunnel face". In: *Geotechnical Aspects of Underground Construction in Soft Ground* (2002), pp. 179–184.

[16] W. Broere. "Influence of Infiltration and Groundwater Flow on Tunnel Face Stability". In: *Geotechnical Aspects of Underground Construction in Soft Ground* (2000), pp. 339–344.

[17] W. Broere. "On the face support of microtunnelling TBMs". In: *Tunnelling and Underground Space Technology incorporating Trenchless Technology Research* 46 (2015), pp. 12–17.

[18] W. Broere. *Tunnel Face Stability & New CPT Applications (PhD thesis)*. 2001, p. 208. ISBN: 9040722153.

[19] G.A. Bruggeman. *Analytical Solutions in Geohydrological Problems, Elsevier*. 1999.

[20] Fann Instrument Company. *Model 35 Viscometer Instruction Manual*. 2013.

[21] D. Festa, W. Broere, and J. W. Bosch. "An investigation into the forces acting on a TBM during driving - Mining the TBM logged data". In: *Tunnelling and Underground Space Technology* 32 (2012), pp. 143–157.

[22] P. Fritz. "Slurry Shield Tunneling in Highly Permeable Ground". In: *12th Panamerican Conference on Soil Mechanics and Geotechnical Engineering* (2003), pp. 1–8.

[23] P. Fritz, R. Hermanns Stengele, and A. Heinz. "Modified Bentonite Slurries for Slurry Shields in Highly Permeable Soils". In: *Proceedings of the Third International Symposium on Geotechnical Aspects of Underground Construction in Soft Ground - Toulouse* (2002).

[24] H.A. Greve, M.W.P. van Lange, and H. van Muijen. "Prevaluatie onderzoek boortunnels". In: *K100* (1996).

[25] N Horn. "Horizontaler Erddruck auf senkrechte Abslussflächen von Tunnelrören". In: *Landeskonferenz der Ungarischen Tiefbauindustri* (1961), pp. 7–16.

[26] M. Huisman. "Theorie en Proeven Statische Afpleistering (in Dutch)". In: *BTL-rapport 34* (1998).

[27] S. Jancsecz and W. Steiner. "Face support for a large Mix- shield in heterogeneous ground conditions". In: *Tunneling* (1994), pp. 531–550.

[28] F.J. Kaalberg, R.E.P. De Nijs, and J.A.T. Ruigrok. "TBM face stability & excess pore pressures in close proximity of piled bridge foundations controlled with 3D FEM". In: *Geotechnical Aspects of Underground Construction in Soft Ground* (2014), pp. 555–560.

[29] Seung Han Kim and Fulvio Tonon. "Face stability and required support pressure for TBM driven tunnels with ideal face membrane – Drained case". In: *Tunnelling and Underground Space Technology incorporating Trenchless Technology Research* 25.5 (2010), pp. 526–542.

[30] T. Krause. *Schildvortriebmit flüssigkeits- und erdgestützter Ortsbrust (PhD thesis)*. 1987.

[31] M.K. Kreuk and C.A. Messemaeckers van de Graaff. *Alternatieven voor boorvloeistoffen (in Dutch)*. 1998.

[32] C. Lam and S.A. Jefferis. "Interpretation of Viscometer Test Results for Polymer Support Fluids". In: *Tunneling and Underground Construction* (2014), pp. 439–449.

[33] F. Min, W. Zhu, and X Han. "Filter cake formation for slurry shield tunneling in highly permeable sand". In: *Tunnelling and Underground Space Technology incorporating Trenchless Technology Research* 38 (2013), pp. 423–430.

[34] M. Mohkam and C. Bouyat. "Research studies for slurry shield tunneling". In: *4th International Conference of the Institution of Mining and Metallurgy* (1955), pp. 235–241.

[35] R.E.P. De Nijs, F. Kaalberg, and J.A.T. Ruigrok. "Monitoring and analysis of pore water pressure increase during two TBM passages". In: *Proceedings of the XVI ECSMGE - Geotechnical Engineering for Infrastructure and Development* (2014).

[36] A. M. Talmon, D. R. Mastbergen, and M. Huisman. "Invasion of pressurized clay suspensions into granular soil". In: *Journal of Porous Media* 16 (2013), pp. 351–365.

[37] A Verruijt. *Soil mechanics*. 2001.

[38] A. Verruijt. *Theory of Groundwater Flow*. 1970.

[39] Witteveen+Bos. *Internal documents*. 2015.